

2014-12-15

# Succinate-binding site of succinyl-CoA synthetase

Huang, Ji

---

Huang, J. (2014). Succinate-binding site of succinyl-CoA synthetase (Master's thesis, University of Calgary, Calgary, Canada). Retrieved from <https://prism.ucalgary.ca>. doi:10.11575/PRISM/27933  
<http://hdl.handle.net/11023/1962>

*Downloaded from PRISM Repository, University of Calgary*

UNIVERSITY OF CALGARY

Succinate-binding site of succinyl-CoA synthetase

by

Ji Huang

A THESIS

SUBMITTED TO THE FACULTY OF GRADUATE STUDIES  
IN PARTIAL FULFILMENT OF THE REQUIREMENTS FOR THE  
DEGREE OF MASTER OF SCIENCE

GRADUATE PROGRAM IN BIOLOGICAL SCIENCES

CALGARY, ALBERTA

DECEMBER, 2014

© Ji Huang 2014

## Abstract

Succinyl-CoA synthetase (SCS) is an essential enzyme that catalyzes substrate-level phosphorylation in the citric acid cycle. In my study, the pig GTP-specific SCS (GTPSCS) was overproduced in *E. coli* BL21(DE3), and purified through three different columns: Ni-NTA affinity, Superdex-200 prep grade size exclusion and Hitrap Blue High Performance affinity. A crystal of GTPSCS in complex with coenzyme A (CoA) diffracted to 2.1 Å. The CoA-binding site was determined to be located in the N-terminal domain of the  $\alpha$ -subunit of the enzyme. A crystal of GTPSCS in complex with  $Mg^{2+}$ -succinate and CoA was grown in polyethylene glycol 3350, ammonium succinate and Hepes (pH 7.0) and diffracted to 2.2 Å. The succinate-binding site of GTPSCS was determined to be located in the C-terminal domain of the  $\beta$ -subunit of the enzyme. The discovery of the succinate-binding site of SCS supports the view that the succinyl-phosphate complex can be formed during the catalytic reaction.

## **Acknowledgements**

First, I would like to thank my supervisor, Dr. Marie Fraser, who gave me this opportunity to study in this crystallography lab. Dr. Fraser gave me a lot useful advice in the two and a half years' Master study not only in doing experiments, but also in building critical thinking. As an international student in Canada, I have to use my second language, which is English to communicate, study and live. Dr. Fraser really gave me a lot of help in overcoming the language difficulty. The wonderful time for pursuing my Master's degree in Dr. Fraser's lab is a precious memory in my life.

I would like to thank Koto Hayakawa, who offered me a lot of constructive suggestions for growing crystals. I also thank my committee members Dr. Steve Zimmerly and Dr. Greg Moorhead for their help and advice for my research project, and other committee member Dr. David Schriemer for reading my thesis and questioning me about my research.

In addition, I would like to thank the funding agency the Natural Sciences and Engineering Research Council of Canada (NSERC) for supporting my research during the two and a half years, and the Canadian Light Source, Saskatoon, Saskatchewan, Canada for providing the facilities for me to collect diffraction data.

## Table of Contents

Acknowledgements.....	ii
Table of Contents.....	iii
List of Tables.....	v
List of Figures and Illustrations.....	vi
List of Symbols, Abbreviations and Nomenclature.....	ix
CHAPTER ONE: INTRODUCTION.....	1
1.1 Succinyl-CoA synthetase.....	1
1.2 The proposed catalytic mechanism of SCS.....	6
1.3 Proposed succinate-binding site of GTPSCS.....	9
1.4 The goal of my research.....	11
CHAPTER TWO: METHODS.....	20
2.1 Calibration of Superdex-200 prep grade column (16 mm/62 cm).....	20
2.2 Purification of wild type GTPSCS.....	20
2.2.1 Plasmid purification.....	20
2.2.2 Transformation.....	21
2.2.3 Protein expression.....	22
2.2.4 Cell lysis.....	22
2.2.5 Ni-NTA affinity column.....	22
2.2.6 Superdex-200 pg column.....	23
2.2.7 Hitrap Blue High Performance affinity column.....	24
2.2.8 Bradford assay.....	25
2.2.9 SDS-PAGE.....	25
2.2.10 Enzyme assay.....	26
2.3 Crystallization.....	27
2.4 Data collection and refinement.....	28
2.5 Site-directed mutagenesis of GTPSCS.....	29
2.6 Kinetic studies of formate inhibition of wild type GTPSCS.....	30
CHAPTER THREE: RESULTS.....	33
3.1 Calibration of Superdex-200 prep grade column (16 mm/62 cm).....	33
3.2 Purification of wild type GTPSCS.....	36
3.2.1 Ni-NTA affinity column.....	37
3.2.2 Superdex-200 pg column.....	37
3.2.3 Hitrap Blue High Performance affinity column.....	38
3.2.4 Bradford assay.....	40
3.2.5 Purification table for wild type GTPSCS.....	41
3.3 Protein crystallization.....	42
3.4 X-ray diffraction data.....	45
3.4.1 Data collection for GTPSCS/CoA complex.....	45
3.4.2 Data collection for GTPSCS/succinate/CoA complex.....	46
3.5 Structures.....	48

3.5.1 CoA-binding site of GTPSCS .....	48
3.5.2 Succinate-binding site of GTPSCS .....	53
3.6 Site-directed mutagenesis of C332 $\beta$ A GTPSCS.....	58
3.6.1 Purification of C332 $\beta$ A GTPSCS.....	58
3.6.1.1 Ni-NTA affinity column .....	58
3.6.1.2 Superdex-200 pg column .....	59
3.6.1.3 Hitrap Blue High Performance affinity column .....	60
3.7 Kinetic studies of formate inhibition of wild type GTPSCS .....	62
CHAPTER FOUR: DISCUSSION .....	64
4.1 Purification of GTPSCS.....	64
4.2 CoA-binding site of GTPSCS.....	65
4.3 Succinate-binding site of SCS .....	73
4.3.1 Comparison of the structure of succinate-bound GTPSCS with CoA-bound GTPSCS.....	73
4.3.2 The magnesium ion stabilizing succinate-bound GTPSCS.....	78
4.3.3 Analysis of succinate-binding sites of GTPSCS and ATPSCS.....	79
4.3.4 Comparison of the structures of succinate-bound GTPSCS with citrate-bound hACLY .....	81
4.4 Verification of the proposed catalytic mechanism based on analysis of the structure .....	83
4.5 The formate inhibition on GTPSCS.....	85
CHAPTER FIVE: CONCLUSIONS AND FUTURE STUDIES.....	87
5.1 Conclusions.....	87
5.2 Future studies .....	88
REFERENCES .....	91

## List of Tables

Table 1.1 Organic acids tested with succinyl-CoA synthetase .....	18
Table 2.1 The sense and antisense primers for mutating cysteine to alanine at residue 332 in the $\beta$ -subunit of GTPSCS.....	31
Table 3.1 Molecular weight and elution volumes of the calibration kit proteins and blue dextran 2000 used for calibrating Superdex-200 pg column .....	35
Table 3.2 Quantity, activity and yield of wild type GTPSCS subsequent to each step of purification .....	41
Table 3.3 Crystallization conditions in which the GTPSCS/succinate/CoA complex nucleates .	43
Table 3.4 X-ray diffraction data collection and processing of GTPSCS/CoA complex .....	52
Table 3.5 Structure refinement of GTPSCS/CoA complex .....	52
Table 3.6 X-ray diffraction data collection and processing of GTPSCS/succinate/CoA complex .....	57
Table 3.7 Structure refinement of GTPSCS/succinate/CoA complex .....	57
Table 3.8 Statistical results from kinetic studies of formate inhibition .....	63
Table 4.1 The comparison of the interactions of CoA with GTPSCS and <i>E. coli</i> SCS.....	67

## List of Figures and Illustrations

Figure 1.1 The reaction that catalyzed by SCS in the Krebs cycle.....	13
Figure 1.2 Sequence alignment of the $\alpha$ -subunit of pig GTPSCS and residues 487-820 of truncated human ACLY .....	14
Figure 1.3 Sequence alignment of the $\beta$ -subunit of pig GTPSCS and residues 2-425 of truncated human ACLY .....	15
Figure 1.4 Sequence alignment of the citrate-binding domain of human ATP-citrate lyase with homologous domains of GTP-specific succinyl-CoA synthetase, <i>Methylobacterium extorquens</i> AM1 malyl-CoA synthetase and <i>H. thermophilus</i> TK-6 citryl-CoA synthetase.....	16
Figure 1.5 Sequence alignment of $\beta$ -subunits of pig GTPSCS, human ATPSCS and <i>E. coli</i> SCS .....	17
Figure 2.1 T7-7 plasmid containing genes for coding $\alpha$ and $\beta$ subunits of GTPSCS.....	32
Figure 3.1 Chromatogram showing the elution profile of calibration kit proteins (aldolase, ovalbumin, carbonic anhydrase, ribonuclease A) and blue dextran 2000 .....	34
Figure 3.2 Calibration curve of Superdex-200 pg column .....	36
Figure 3.3 9% SDS-PAGE gel showing the Ni-NTA column purification of wild type GTPSCS .....	37
Figure 3.4 Chromatogram of Superdex-200 pg column showing UV absorbance at 280 nm versus elution volume .....	38
Figure 3.5 Chromatogram of Hitrap Blue High Performance affinity column showing UV absorbance at 280 nm versus elution volume .....	39
Figure 3.6 Standard curve of the Bradford assay showing absorbance at 595 nm versus protein concentration (mg/mL).....	40
Figure 3.7 Crystals of the GTPSCS/succinate/CoA complex.....	44
Figure 3.8 9% SDS-PAGE gel showing the proteins in the crystals .....	45
Figure 3.9 Diffraction image of GTPSCS in complex with CoA.....	46
Figure 3.10 Diffraction image of GTPSCS in complex with succinate and CoA .....	47
Figure 3.11 The electron density around CoA in GTPSCS obtained from X-ray diffraction.....	49



Figure 3.12 The overall structure of GTPSCS in complex with CoA .....	50
Figure 3.13 The interactions between CoA and GTPSCS .....	51
Figure 3.14 The electron density around succinate in GTPSCS obtained from X-ray diffraction .....	54
Figure 3.15 The overall structure of GTPSCS in complex with succinate and CoA.....	55
Figure 3.16 The interactions between succinate and GTPSCS.....	56
Figure 3.17 Alignment of the mutated plasmid sequence (Sbjct) with the wild type plasmid (Query) .....	58
Figure 3.18 9% SDS-PAGE gel showing Ni-NTA column purification of C332βA GTPSCS ...	59
Figure 3.19 Chromatogram of Superdex-200 pg column showing UV absorbance at 280 nm versus elution volume for C332βA GTPSCS .....	60
Figure 3.20 Chromatogram of Hitrap Blue HP affinity column showing UV absorbance at 280 nm versus elution volume for C332βA GTPSCS .....	61
Figure 3.21 The Michaelis-Menten plots showing the initial rate (μmol/min) of GTPSCS as a function of various succinate concentrations (mM).....	62
Figure 4.1 Superposition of the N-terminal domains from α-subunits of the GTPSCS/CoA complex and the <i>E. coli</i> SCS/CoA complex (PDB code 2SCU) in viewing 3'-phosphoadenosines of CoA.....	68
Figure 4.2 Superposition of the N-terminal domains from α-subunits of the GTPSCS/CoA complex and the <i>E. coli</i> SCS/CoA complex (PDB code 2SCU) in viewing 5' diphosphates of CoA.....	69
Figure 4.3 Superposition of the N-terminal domains from the α-subunits of the GTPSCS/CoA complex and the <i>E. coli</i> SCS/CoA complex (PDB code 2SCU) in viewing pantetheine moiety of CoA.....	70
Figure 4.4 Superposition of the N-terminal domains (residues 2-131) from α-subunits of GTPSCS/CoA complex and dephosphorylated GTPSCS (PDB code 1EUC).....	72
Figure 4.5 Superposition of the GTPSCS/succinate/CoA complex and GTPSCS/CoA complex.....	74
Figure 4.6 Superposition of the succinate-binding domains of the GTPSCS/succinate/CoA complex and the GTPSCS/CoA complex .....	75

Figure 4.7 Superposition of the succinate-binding sites of the GTPSCS/succinate/CoA complex and the GTPSCS/CoA complex .....	76
Figure 4.8 Surface representations of the GTPSCS in complex with CoA (left) and the GTPSCS in complex with succinate and CoA (right) .....	77
Figure 4.9 Interactions of the magnesium ion with inorganic phosphate, water molecules and succinate in the GTPSCS/succinate/CoA complex.....	80
Figure 4.10 Superposition of the succinate-binding domain of succinate-bound GTPSCS with the citrate-binding domain of citrate-bound ACLY (PDB code 3MWD) .....	82
Figure 4.11 Superposition of the C-terminal domains from $\alpha$ -subunits of the GTPSCS/succinate/CoA complex and phosphorylated GTPSCS (PDB code 2FP4).....	84
Figure 5.1 The proposed site of phosphohistidine loop in ACLY .....	90

## List of Symbols, Abbreviations and Nomenclature

<b>Abbreviation</b>	<b>Definition</b>
ATP	Adenosine triphosphate
ADP	Adenosine diphosphate
ATPSCS	ATP-specific succinyl-CoA synthetase
ACLY	ATP-citrate lyase
CoA	Coenzyme A
CLS	Canadian Light Source
C332 $\beta$ A	Cys 332 $\beta$ mutated to Ala 332 $\beta$
<i>E. coli</i>	<i>Escherichia coli</i>
FPLC	Fast protein liquid chromatography
GTP	Guanosine triphosphate
GDP	Guanosine diphosphate
GTPSCS	GTP-specific succinyl-CoA synthetase
GTPSCS/CoA complex	GTPSCS in complex with CoA
GTPSCS/succinate/CoA complex	GTPSCS in complex with Mg <sup>2+</sup> -succinate and CoA
g	gram
hACLY	Human ATP-citrate lyase
IPTG	Isopropyl $\beta$ -D-1-thiogalactopyranoside
kDa	kilo dalton
min	minute
mM	millimole per liter

**Abbreviation****Definition**

M

mole per liter

Ni-NTA

Nickel-nitrilotriacetic acid

PEG 3350

Polyethylene glycol 3350

PDB

Protein data bank

r.m.s.d.

Root-mean-square deviation

rpm

Revolutions per minute

SDS-PAGE

Sodium dodecyl sulfate polyacrylamide gel electrophoresis

s

second

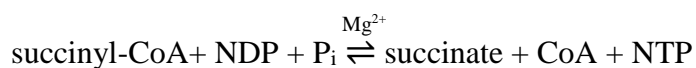
2-ME

2-mercaptoethanol

## Chapter One: Introduction

### 1.1 Succinyl-CoA synthetase

Succinyl-CoA synthetase (SCS), also known as succinate thiokinase or succinate-CoA ligase, is an essential enzyme that catalyzes substrate-level phosphorylation in the citric acid cycle (Figure 1.1). SCS is responsible for breaking down succinyl-CoA to succinate and CoA, accompanied by the phosphorylation of NDP (ADP or GDP) to NTP (ATP or GTP) <sup>1</sup>.

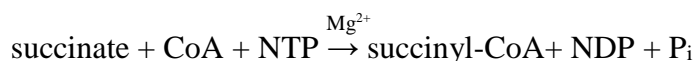


The reaction catalyzed by SCS is reversible and the direction depends on the relative concentrations of substrates and products. The reverse direction to that occurring in the citric acid cycle produces succinyl-CoA, which may be used for activating ketone bodies <sup>2</sup> and heme biosynthesis <sup>3</sup>. SCS is phosphorylated on a histidine residue by succinyl-CoA and inorganic phosphate or by nucleotide triphosphate as part of the catalytic reaction. Some SCSs can use either ATP or GTP to catalyze the reaction, but there are also more specific SCSs, ATP-specific SCS (ATPSCS) and GTP-specific SCS (GTPSCS), which would only use the specific nucleotide to catalyze the reaction.

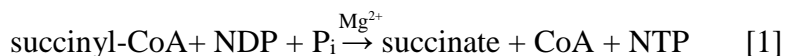
SCS has high specificity for the substrate succinate and does not use the other organic acids from the citric acid cycle that have similar structures to succinate. Robinson *et al.* tested succinate and other organic acids (Table 1.1) as substrates by measuring the dephosphorylation of SCS phosphorylated on the active site histidine residue <sup>4</sup>, because succinate was proposed to attack phosphorylated SCS during the catalytic reaction. Phosphorylated SCS, CoA, magnesium chloride and the selected organic acid were mixed and the quantity of phosphorylated SCS remaining after a period of time was observed. This indicated the utilization of each organic acid listed in Table 1.1. The organic acids that can promote the enzyme dephosphorylation were then

compared with succinate in the absence of CoA. A similar percentage of phosphorylated SCS remaining was only detected when malate was used. However, the turnover rate for malate was only one-fifth that of succinate. In addition, a relatively high concentration of malate, 91 mM, had only a 3% rate of thiol ester bond formation with CoA as compared to using succinate <sup>4</sup>. Therefore, even though an organic acid might have a similar structure to succinate in one portion (Table 1.1), SCS was shown not to be able to use that organic acid to be specific for succinate.

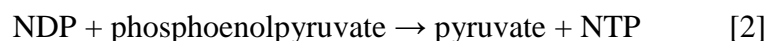
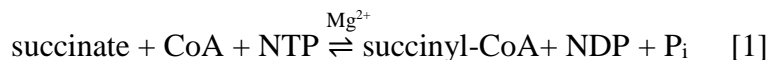
It is important to know the enzymatic activity of SCS, because it can help us to understand the biological role of the enzyme in particular cells of the body. There are three major ways to measure the activity of SCS. Two are single enzyme assays, and one is a coupled enzyme assay. The first way to measure the activity is by measuring the increase in absorbance at 235 nm due to the formation of the thioester bond of succinyl-CoA <sup>5</sup>:



The second way to measure the activity is by measuring the increase in absorbance at 412 nm due to the formation of yellow TNB<sup>2-</sup> dianion <sup>6</sup>:



The third way to measure the activity is by measuring the decreasing absorbance at 340 nm due to the disappearance of NADH in a coupled enzyme assay with pyruvate kinase and lactate dehydrogenase. The coupled reactions are <sup>5</sup>:



The first way has been used as the standard assay during the purification of GTPSCS or *E. coli* SCS, because it is convenient and fast. The second way to measure enzyme activity is more sensitive since TNB<sup>2-</sup> has a much larger molar absorbance at 412 nm than that of the thiol ester bond at 235 nm, however, DTNB can inhibit enzyme activity<sup>6</sup>. The third way is mainly used when measuring the enzyme activity of ATPSCS, because the high concentration of ATP needed by this enzyme absorbs significantly at 235 nm, leading to inaccurate results when attempting to measure the production of succinyl-CoA at 235 nm.

The nucleotide specificity of SCS varies in different species. Bacterial SCSs tend to be less specific for the nucleotide as they can use either ATP/ADP or GTP/GDP to catalyze the reaction. *E. coli*. SCS prefers adenine to guanine nucleotides<sup>7</sup>, while *Thermus aquaticus* SCS prefers guanine to adenine nucleotides<sup>8</sup>. For eukaryotic SCS, spinach SCS is specific for ATP<sup>9</sup>. However, in vertebrates, there are two different isoforms of SCS, and both of them are heterodimers: one is ATP-specific SCS (ATPSCS, EC 6.2.1.5), and the other one is GTP-specific SCS (GTPSCS, EC 6.2.1.4). These two isoforms have the same  $\alpha$ -subunit, but different  $\beta$ -subunits, and the  $\beta$ -subunit determines the nucleotide specificity of SCS<sup>10</sup>.

SCSs have different binding affinities for each substrate. In general, the binding affinity of an enzyme for its substrate is comparable to the concentration of that substrate in the cell when the enzyme is needed. Baccanari *et al.* determined that the apparent  $K_m$  of different isoforms of pig GTP-specific SCS (GTPSCS) for succinate is 0.39-0.45 mM, for GTP is 0.009-0.011 mM and for CoA is 0.004-0.007 mM<sup>11</sup>. Johnson *et al.* determined the apparent  $K_m$ s of pigeon SCS (GTPSCS and ATPSCS) for succinate, nucleotide and CoA. Johnson *et al.* found that ATPSCS has about 10 times higher apparent  $K_m$  for succinate than GTPSCS does, and about 30 times higher apparent  $K_m$  for ADP than GTPSCS has for GDP; while CoA and NTP have

almost the same apparent  $K_m$  for both isoforms<sup>10</sup>. In addition, Lambeth *et al.* mentioned that GTPSCS mainly serves the anabolic role in tissues<sup>12</sup>. This may be related to the lower apparent  $K_m$  of succinate for GTPSCS when compared with the ATPSCS.

SCS is a multimeric enzyme in both prokaryotes and eukaryotes. In the prokaryote *E.coli*, SCS has two  $\alpha\beta$ -heterodimers that link together to form an  $\alpha_2\beta_2$  heterotetrameric structure<sup>13</sup>. In eukaryotes, for example, mammals and birds, SCS is an  $\alpha\beta$ -heterodimer. Despite different quaternary structures, the mature  $\alpha$ -subunit from rat shows 70% sequence identity to the corresponding portion of *E.coli* SCS and 90% similarity if conservative replacements are considered<sup>14</sup>. The mature  $\beta$ -subunit from pig is around 45% identical to the corresponding portion of *E. coli* SCS<sup>15</sup>, and 64% similar if conservative replacements are considered. It is obvious that the  $\beta$ -subunit does not show as high sequence identity and similarity as the  $\alpha$ -subunit, and this is may be because the nucleotide specificity of SCS is determined by  $\beta$ -subunit.

In humans, the amount of ATPSCS and GTPSCS varies in different tissues. ATPSCS is much more highly expressed in catabolic tissues like heart, brain and skeletal muscle tissues, while GTPSCS is more expressed in anabolic tissues, such as kidney and liver<sup>12</sup>. It was proposed that the succinyl-CoA used in ketone body activation is produced by GTPSCS. The GTP/GDP ratio is much greater than ATP/ADP ratio in the mitochondria<sup>2</sup>, meaning GTPSCS can drive the reverse reaction to produce succinyl-CoA under conditions where ATPSCS cannot. This is consistent with an anabolic role for GTPSCS. In contrast, ATPSCS could use succinyl-CoA to produce nucleotide triphosphate because of the lower ATP/ADP ratio in the mitochondria. This catabolic role of ATPSCS would be the reason for the prevalence of ATPSCS in catabolic tissues<sup>12</sup>. However, it was found that human  $\delta$ -aminolevulinate synthase (ALAS-E,



erythroid-specific isoform) participates in an interaction with the  $\beta$ -subunit of human ATPSCS<sup>16</sup>. ALAS-E is a mitochondrial enzyme utilizing succinyl-CoA and glycine to synthesize  $\delta$ -aminolevulinic acid in the first step of heme biosynthesis. The interaction between these two enzymes was thought to allow succinyl-CoA to be efficiently transferred to ALAS-E<sup>16</sup>, indicating that ATPSCS can also play an anabolic role in mammals.

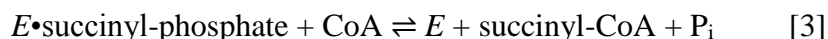
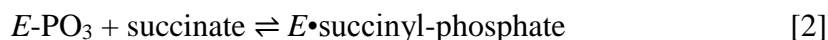
SCS deficiency can be caused by mutations in the genes coding for SCS. Gene *SUCLG1* codes for the  $\alpha$ -subunits of GTPSCS and ATPSCS, and genes *SUCLG2* and *SUCLA2* code for the  $\beta$ -subunits of GTPSCS and ATPSCS, respectively. A mutation in *SUCLA2* leading to encephalomyopathy and mitochondrial DNA depletion was first identified by Elpeleg *et al.*<sup>17</sup>. Subsequent identification of deleterious mutations in the *SUCLA2* gene<sup>18, 19, 20, 21, 22, 23, 24</sup> and the *SUCLG1* gene<sup>19, 25, 26, 27, 28, 29, 30, 31, 32</sup> showed that patients with these mutations had elevated levels of methylmalonic acid. The absence of SCS to catalyze the conversion of succinyl-CoA to succinate would inhibit the conversion of methylmalonyl-CoA to succinyl-CoA. The subsequent reduction in the conversion of methylmalonic acid to methylmalonyl-CoA would lead to the elevated levels of methylmalonic acid. However, it is still difficult to understand the relationship between deleterious mutations in SCS and mitochondrial DNA (mtDNA) depletion. Elpeleg *et al.* proposed that the disruption between SCS and nucleoside diphosphate kinase (NDPK) Nm23-H4 (mitochondrial isoform) might lead to mtDNA depletion, because the disruption might affect the ability of NDPK to phosphorylate mitochondrial deoxyribonucleotide diphosphates to deoxyribonucleotide triphosphates<sup>17</sup>. However, the existence of an SCS/NDPK complex seems impossible. This is because the two enzymes have different localizations in the mitochondria. SCS is located in the matrix, while NDPK is in the mitochondrial intermembrane space<sup>33</sup>. In

addition, the activity of NDPK is much lower than the activity of SCS, so it seems impossible for NDPK to alter nucleotide ratios<sup>34</sup>.

SCS is related to mitochondrial glucose-stimulated insulin secretion (GSIS). It was reported that mitochondrial GTP (mtGTP) synthesized by GTPSCS is involved in GSIS<sup>35</sup>. In beta-cells of the pancreas, the mitochondrial isoform of phosphoenolpyruvate carboxykinase (PEPCK-M) hydrolyzes mtGTP during the synthesis of mitochondrial phosphoenolpyruvate (mtPEP). This mtPEP can escape to the cytosol and be involved in the metabolic pathways that generate a signal for insulin secretion<sup>34</sup>. Therefore, mtGTP produced by GTPSCS was considered to be able to regulate GSIS<sup>35</sup>.

## 1.2 The proposed catalytic mechanism of SCS

It was proposed that the reaction catalyzed by SCS takes place by a three-step mechanism as reviewed by Wolodko *et al.*<sup>36</sup>. The three-step mechanism is as follows:



where E represents SCS,  $P_i$  denotes inorganic phosphate, a dot indicates noncovalent binding and a hyphen indicates a covalent bond. Magnesium ions were proposed to be critically important in the catalytic reaction for both the phosphorylation and dephosphorylation steps<sup>37</sup>. The importance of the magnesium ion in the catalytic reaction was also supported by Robinson *et al* in their study of the succinate-specificity of SCS<sup>4</sup>.

In partial step [1], SCS is phosphorylated by the high-energy carrier nucleoside triphosphate and nucleoside diphosphate is released. Kaufman *et al.* were first to propose that

SCS is a phosphorylating enzyme<sup>38</sup>. This was because SCS was involved in the phosphorylation step that accompanied the oxidation of  $\alpha$ -ketoglutarate. Kreil and Boyer then suggested that phosphohistidine existed as an intermediate in the catalytic reaction, since the phosphohistidine was detected in highly purified *E. coli* SCS<sup>39</sup>. The localization of this histidine residue was first identified in the  $\alpha$ -subunit of *E. coli* SCS<sup>40,41</sup>. Based on the primary sequences of both *E. coli* SCS<sup>42</sup> and the tryptic peptide containing the phosphohistidine from *E. coli* SCS<sup>43</sup>, His 246 $\alpha$  of *E. coli* SCS was identified as the active site histidine residue. Phosphohistidine was first seen in the crystal structure of *E. coli* SCS, identified by the PDB code 1SCU<sup>36</sup>. The phosphohistidine was located in the C-terminal domain of the  $\alpha$ -subunit and stabilized by two “power” helices, one from the  $\alpha$ -subunit and one from the  $\beta$ -subunit<sup>36</sup>. The corresponding active site residue in GTPSCS is His 259 $\alpha$ . Phosphorylated His 259 $\alpha$  was first seen in the crystal structure of GTPSCS, identified by the PDB code 1EUD.

The nucleotide-binding site of SCS was originally proposed to be localized in the  $\alpha$ -subunit<sup>40</sup>, an interpretation which contrasted with the view that the  $\beta$ -subunit determines the nucleotide specificity. The original proposal was based on the realization that the  $\alpha$ -subunit was able to catalyze its own phosphorylation. As well, it was proposed that the  $\alpha$ -subunit had to contain both the phosphohistidine residue and the nucleotide-binding site for the two to be located close to each other. The crystal structures of the complexes of ADP bound to *E. coli* SCS<sup>44</sup> and GTP bound to GTPSCS<sup>45</sup> revealed the nucleotide-binding site in the crevice of the ATP-grasp domain of the  $\beta$ -subunit. This was consistent with Johnson *et al.*'s realization that the  $\beta$ -subunit of SCS determined the nucleotide specificity.

A huge distance exists between the nucleotide-binding site and the active site histidine residue. In *E. coli* SCS, this distance is 35 Å<sup>44</sup>. Because of the huge distance between the two

catalytic sites, a phosphohistidine shuttling theory was proposed <sup>46</sup>. It was hypothesized that the active site histidine loop in the  $\alpha$ -subunit swings to shuttle the phosphoryl group between the two catalytic sites. Unfortunately, only one conformation of the histidine loop has ever been observed in any of the crystal structures.

In partial step [2], the phosphorylated histidine residue is thought to be attacked by the reactive carboxyl group of succinate, leading to the formation of enzyme-bound succinyl-phosphate. Two other possibilities were also considered as reviewed by Nishimura and Meister <sup>47</sup>. One was the formation of an enzyme-bound phosphoryl-CoA intermediate, meaning that CoA would attack the phosphorylated histidine instead of succinate. The other possibility is that no discrete intermediates are formed in this step, with steps [2] and [3] combined for a concerted reaction <sup>4</sup>. The formation of succinyl-phosphate in the second step was supported by Nishimura and Meister <sup>47</sup>. Nishimura and Meister found that [<sup>32</sup>P] succinyl-phosphate was formed when [ $\gamma$ -<sup>32</sup>P] ATP and succinate were mixed with SCS. Incubation of SCS with [<sup>14</sup>C] succinyl-phosphate and CoA led to the formation of [<sup>14</sup>C] succinyl-CoA. In addition, the incubation of SCS with [<sup>32</sup>P] succinyl-phosphate and ADP led to the formation of [<sup>32</sup>P] ATP. These discoveries provide substantial evidence to support the succinyl-phosphate pathway as the partial step [2].

In partial step [3], CoA was proposed to attack the SCS-bound succinyl-phosphate intermediate, forming succinyl-CoA and releasing inorganic phosphate. The CoA-binding site was originally suggested to be located in the  $\beta$ -subunit of *E. coli* SCS <sup>42</sup>. However, the crystal structure of the *E. coli* SCS/CoA complex, identified by the PDB code 1SCU, revealed that the CoA-binding site is in the  $\alpha$ -subunit <sup>36</sup>. CoA is non-covalently bound to the nucleotide-binding motif in the N-terminal domain of the  $\alpha$ -subunit. Both hydrophobic and hydrophilic interactions

are involved between CoA and SCS. It was not surprising to discover that the sulfhydryl group of CoA extended toward to the C-terminal domain of the  $\alpha$ -subunit. This positioned the sulfur atom about 5 Å away from phosphorylated His 246 $\alpha$ . The close distance allows CoA to attack the enzyme-bound succinyl-phosphate intermediate to form succinyl-CoA, assuming that the phosphate of the succinyl-phosphate is located near the phosphoryl group of the phosphohistidine. The inorganic phosphate-binding site, identified in the crystal structure of *E. coli* SCS, was located about 3 Å away from the active site histidine <sup>44</sup>.

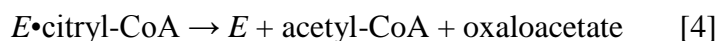
To date, the succinate-binding site has not been determined. This information is needed for us to fully understand the catalytic mechanism of SCS. This can be seen by comparing the current knowledge of partial reaction [1] with partial reactions [2] and [3]. Since the succinate binding site of SCS is not known, it is difficult to judge whether the enzyme-bound succinyl-phosphate intermediate can be formed in partial reaction [2]. It is also difficult to predict how CoA can attack the enzyme-bound succinyl-phosphate intermediate to produce succinyl-CoA. Only when all the substrate-binding sites are revealed, can we interpret the catalytic mechanism of SCS.

### **1.3 Proposed succinate-binding site of GTPSCS**

Although the succinate-binding site of SCS is not known, the binding site for the organic acid, citrate, is known for the related enzyme, ATP-citrate lyase (ACLY, EC 4.1.3.8). ACLY is another member of the acyl-CoA synthetase (NDP-forming) superfamily <sup>48</sup>. In addition to SCS and ACLY, the acyl-CoA synthetase (NDP-forming) superfamily includes citryl-CoA synthetase and malyl-CoA synthetase <sup>49</sup>. The discovery of the citrate-binding site of ACLY is significant,

because it can be used to predict the organic acid substrate-binding sites of other members of this superfamily, such as the succinate-binding site of SCS.

ACLY is the primary enzyme responsible for synthesizing cytosolic acetyl-CoA, an important precursor for fatty acid synthesis, in the cells of humans. In the cytoplasm, ACLY utilizes ATP, citrate and CoA to produce acetyl-CoA<sup>50</sup>. The proposed four-step catalytic mechanism<sup>51</sup> is as follows:



where E represents ACLY, P<sub>i</sub> denotes inorganic phosphate, a dot indicates a noncovalent bond and a hyphen indicates a covalent bond. Wells proposed that enzyme-bound citryl-phosphate was formed in the second partial step of the ACLY catalyzed reaction<sup>51</sup>. This enzyme-bound intermediate is similar to the proposed SCS-bound succinyl-phosphate. The citrate-binding site was determined in truncated human ACLY (hACLY) by Sun *et al.*<sup>48</sup>. The truncated hACLY is the N-terminal portion of a single polypeptide chain. Five different domains (labelled domains 3, 4, 5, 1, 2 from the amino- to the carboxyl-terminus) were defined in this truncated hACLY. Sun *et al.* pointed out that domains 3, 4 and 5 (residues 2–425) in truncated hACLY are homologous to the β-subunit of SCS, and domains 1 and 2 (residues 487–820) are homologous to the α-subunit of SCS<sup>48</sup>. Alignment of the primary sequences (Figure 1.2 and Figure 1.3) of truncated hACLY and GTPSCS shows 48% similarity between residues 487-820 of hACLY and the α-subunit of GTPSCS, and 40% similarity between residues 2-425 of hACLY and the β-subunit of GTPSCS<sup>52</sup>. The citrate-binding site is located in domain 5 of truncated hACLY

(PDB code 3MWD). This domain 5 is homologous to the C-terminal domain of the  $\beta$ -subunit of SCS. A sequence alignment of the citrate-binding domain of truncated hACLY with the homologous domains of SCS, citryl-CoA synthetase and malyl-CoA synthetase is shown in Figure 1.4. According to this alignment, the succinate binding site is predicted to be Gly 327 $\beta$ , Gly 328 $\beta$ , Ile 329 $\beta$  and Val 330 $\beta$ . This predicted succinate-binding site is supported by the superposition of the citrate-binding domain of ACLY with the homologous domain of GTPSCS. According to the superposition, the reactive carboxyl group of succinate would be expected to interact with the amide groups of Gly 328 $\beta$  and Val 330 $\beta$  of GTPSCS, because citrate interacts with the corresponding residues of ACLY, Asn 346 and Thr 348. It was proposed that the hydrophobic residue Ile 329 $\beta$  of GTPSCS serves the same role as the corresponding residue Phe 347 of ACLY. The site-directed mutagenesis study in which Ile 332 $\beta$  of *E. coli* SCS was mutated to alanine showed an increased apparent  $K_m$  of the mutant for succinate<sup>53</sup>. This indicated that the corresponding residue Ile 329 $\beta$  in GTPSCS is important for succinate-binding. In addition, a sequence alignment of ATPSCS, GTPSCS and *E. coli* SCS shows that the residues in this predicted succinate-binding site are well conserved (Figure 1.5). Due to these reasons, we hypothesize that the sequence of Gly 327 $\beta$  - Gly 328 $\beta$  - Ile 329 $\beta$  - Val 330 $\beta$  in the C-terminal domain of the  $\beta$ -subunit would be the succinate-binding site of GTPSCS.

#### **1.4 The goal of my research**

In order to understand fully how SCS catalyzes the reaction and to verify the proposed mechanism, it is worthwhile to discover the succinate-binding site of SCS. The enzyme used in my research is pig GTPSCS. The most important reason to select GTPSCS is that crystals of this enzyme diffract to high resolution. The high resolution data can help to build protein models

with high accuracy. X-ray crystallography is a major way to obtain protein structures and it has many advantages when compared with other techniques. In addition, X-ray crystallography has been used to solve all the SCS structures that have been published. Since the structures are similar, the succinate-binding site in any other form of SCS will be similar to that found in GTPSCS.

My research project will be composed of five major steps, overproduction of the protein, purification of the protein, co-crystallization of GTPSCS with succinate and CoA, collection of the X-ray diffraction data and determination and analysis of the structure. While working out the purification of GTPSCS, I collected data from a crystal of the complex of GTPSCS with CoA that was grown by Manpreet Malhi when he was a project student. I solved and refined this structure and used it as a model to solve the structure of the GTPSCS/succinate/CoA complex. The structure of the GTPSCS/succinate/CoA complex revealed the succinate-binding site and the structure of GTPSCS and CoA was useful for judging the structural changes on succinate binding.



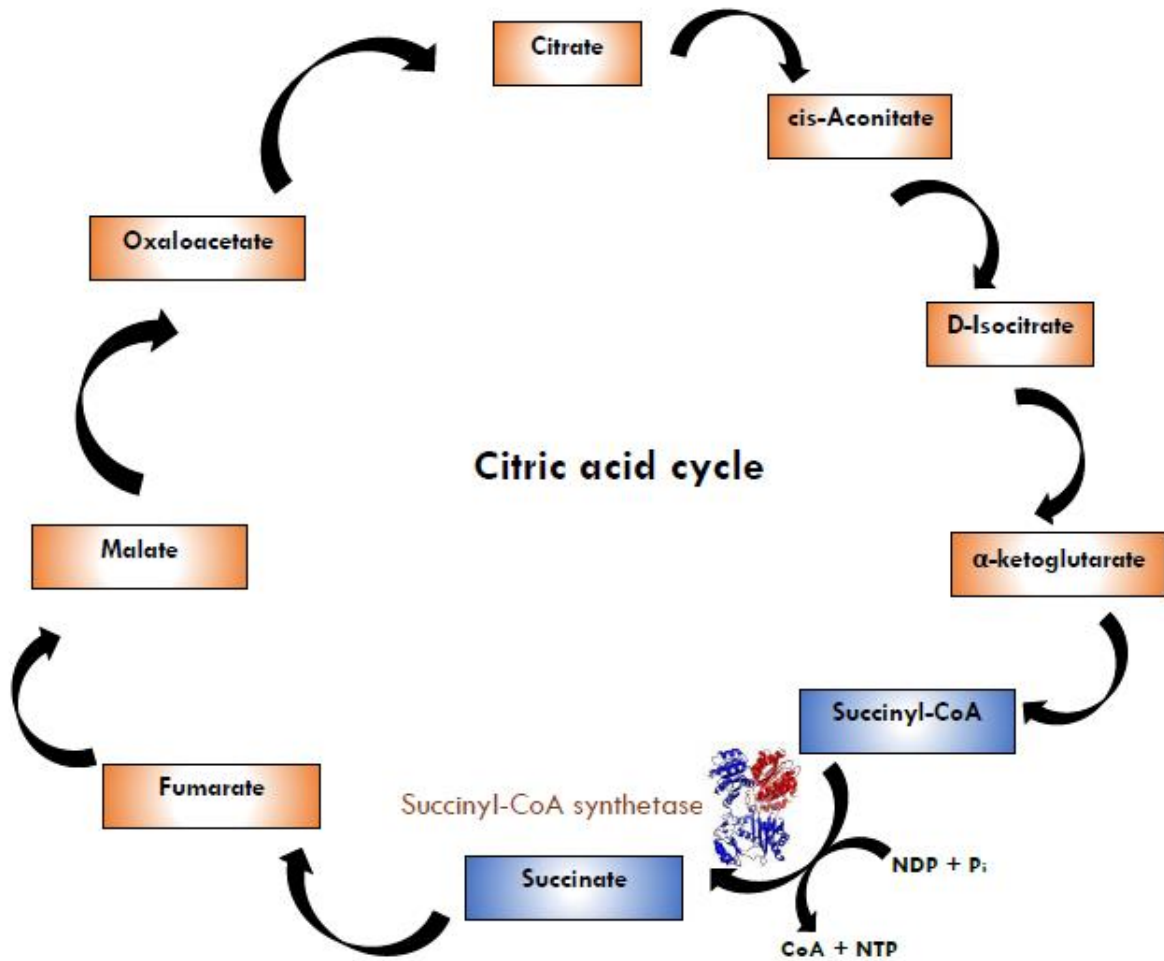


**Figure 1.1** The reaction that catalyzed by SCS in the Krebs cycle. The heterodimeric structure of SCS is displayed as ribbon, the  $\alpha$ -subunit is in red, while the  $\beta$ -subunit is in blue. NTP refers to either ATP or GTP, while NDP refers to either ADP or GDP.

```

GTPSCS_α-subunit  -----SYTASRKHLYVDKNTKVICQGFTGKQGTFFHSQQALEYGTNLVGGT 45
hACLY             GKSTTLFSRHTKAIIVWGMQTRAVQGMLDFDYVCSRDEPSVAAMVYPFTGD 50
                  :: * : .:*:: : . : : : . . *

GTPSCS_α-subunit  TPGKG--GKTHLGLPVFNTVKEAKEQTGATASVIYVP--PPFAAAAINEA 91
hACLY             HKQKFYWGHEKILIPVFKNMADAMRKHPEVDVLINFASLRSAYDSTMETM 100
                  * *::: :***:: :* .: . :* .. . ::::

GTPSCS_α-subunit  IDAEVPLVVCITEGIPOQDMVRVKHRLLRQGKTRLIGPNCPGVINPGECK 141
hACLY             NYAQIRTI AIIAEGIPEALTRKLIKADQKG-VTIIGPATVGGIKPGCFK 149
                  *:: :. *:*::: : : : : : * . :*** * *:* *

GTPSCS_α-subunit  IG-----IMPGHIHKKGRIGIVSRSGTLTYEAVHQTTQVGLGQSLCV 183
hACLY             IGNTGGMLDNI LASKLYRPGSVAYVSRSGGMSNELNNII SRITDGVYEGV 199
                  ** *::: : : * . ***** : : * : : : . * *

GTPSCS_α-subunit  GIGGDPFNGTDFTDCL EIFLNDPATEGIILIGEIGGNAEENAAEFLKQHN 233
hACLY             AIGGDRYPGSTFMDHVLRYQDTPGVKMIIVVLGEIGGTEEYKICRGIKE-- 247
                  .**** : * : * * : : : *:: :***. * : .. :*:

GTPSCS_α-subunit  SGPKSKPVVSFIAGLTAPPGR---RMGHAGAI IAGGKGGAKEKITALQSA 280
hACLY             -GRLTKPIVCWCIGTCATMFSSEVQFGHAGACANQASETAVAKNQALKEA 296
                  * :***: : * *. :***** .. * * **:. *

GTPSCS_α-subunit  GVVVSMSPAQLGTTIYKEFEKRKML----- 305
hACLY             GVFVPRSFDELGEIIQSVYEDLVANGVIVPAQEVPPT 334
                  **. * . * :** * . :*.

```

**Figure 1.2 Sequence alignment of the  $\alpha$ -subunit of pig GTPSCS and residues 487-820 of truncated human ACLY. The asterisk (\*) indicates that the residues in the column are identical in both sequences; the colon (: ) indicates a conserved substitution between the two sequences; while the period (.) indicates the presence of a semi-conserved substitution. A hyphen (-) within the sequence means that there is no residue in that position. The sequences were aligned by using ClustalW2.**

```

GTPSCS_β-subunit      ---MNLQEYQSKKLMSD---NGVKVQRFFVADTANEALEAAKRLNAKEIV 44
hACLY                 -SAKAISEQTGKELLYKFICTTSAIQNRFKYARVTPDTDWARLLQDHPWL 50
                       :.*  .*:.*: . . . :*. * .. : *: * : : :
GTPSCS_β-subunit      LKAQILAGGRGKGVFSSGLKGGVHLTKDPEVVGQLAKQMIGYNLATKQTP 94
hACLY                 LSQNLVVK-PDQLIKRRGKLGVLGVNLTLDGVKSWLKPRLGQEATVGKAT 99
                       *. :.:. . : : * * * :. : * . * : * : . : . : .
GTPSCS_β-subunit      KEGVKVNKVMVAEALDISRETYLAILMDRSCNGPVLVGSPPQGGVDIEEVA 144
hACLY                 G---FLKNFLIEPFVPHSQAEFFVCIYATREGDYVLFHHEGGVDVGDVD 146
                       :.:.:. : * : : : : : * : : : * : : * : * : *
GTPSCS_β-subunit      ASNPELIFKEQIDIIEG-IKDSQAQRMAENLGFGLPQNQAADQIKKLYN 193
hACLY                 AKAQKLLVGVDEKLNPEDIKKHLVHAPEDK-----KEILASFISGLFN 190
                       *. :*: . : : ** . : .*: : : * . * . * : *
GTPSCS_β-subunit      LFLKIDATQVEVNPFGETPEGQVVCFDAKINFDDNAEFRQKD----- 235
hACLY                 FYEDLYFTYLEINPLVVTKDG-VYVLDLAAKVDATADYICKVKWGDIEFP 239
                       : : . : * :*:** : * : * * : * : . * .*: : *
GTPSCS_β-subunit      -IFAMDDKSENEPIEENAAKY----DLKYIGLDGNIACFVNGAGLAMATC 280
hACLY                 PPFGREAYPEEAYIADLDAKSGASLKLTLNPKGRIWTMVAGGGASVVYS 289
                       * . : .*: * : ** . * . : . * . * : * * . * : . .
GTPSCS_β-subunit      DIIFLNGGK--PANFLDLGGGVKESQVYQAFK----LLTADPKVEAILVN 324
hACLY                 DTICDLGGVNELANYGEYSGAPSEQQTYDYAKTILSLMTREKHPDGKILI 339
                       * * ** * : : . * . * . * : * * : * : : . : .
GTPSCS_β-subunit      IFGGIVNCAIIAN---GITKACRELE-----LKVPLVVRLEGTVNHEAQN 366
hACLY                 IGGSIANFTNVAATFKGIVRAIRDYQGPLKEHEVTIFVRRGGPNYQEGLR 389
                       * * . * . * : : * ** : * * : : : * . : . * * * . * : * .
GTPSCS_β-subunit      ILTNSGLPITSAVDLEDAAKKAVASVTKK----- 395
hACLY                 VMGEVGGKTTGIPIHVFGTETHMTAIVGMALGHRPIP 425
                       : : : * . . : : . : . : * *

```

**Figure 1.3 Sequence alignment of the β-subunit of pig GTPSCS and residues 2-425 of truncated human ACLY. The sequences were aligned by using ClustalW2.**

```

GTP_succinyl-CoA Synthetase  --NEPIENEAAKYD-----LKYIGLDGNIACFVNGAGLAMATCDIIF
Malyl-CoA Ligase             --GDPREAQAAEHN-----LSYIGLEGEIGCIVNGAGLAMATMDMIK
Citryl-CoA Synthetase       RPPTEREIEASLIDRDDHRGKAGSYVEVDGDIAMMTFSGGGSTVTIETTY
Human ATP-Citrate Lyase     REAYPEEAYIADLDAKSGASLKLTLNPKGRIWTMVAGGGASVVYSDTIC
                               *   :   :           . :  .* *  :. *. *  : .   :

GTP_succinyl-CoA Synthetase  LNG--GKPANFLDLGGGVKESQVYQAFKLLTADPK-----VEAILVN--I
Malyl-CoA Ligase             HAG--GEPANFLDVGGGASPD RVATAFRLVLSDRN-----VKAILVN--I
Citryl-CoA Synthetase       AIG--LKPANFTDIGGNPPAEKMYKITKIILSKPG-----IRGVLVCGGT
Human ATP-Citrate Lyase     DLGGVNELANYGEYS GAPSEQQTYDYAKTILSLMTREKHPDGKILIIIGGS
                               *   :  ** :  : .*   .:           :  : :           :*:

                               ▼▼▼
GTP_succinyl-CoA Synthetase  FGGIVNCAIIANGITKACRELELKVPL-----VVRLEGTNVHEAQNILT
Malyl-CoA Ligase             FAGINRCDWVAEGVVKAAAREVKIDVPL-----IVRLAGTNVDEGKKILA
Citryl-CoA Synthetase       ANNTRIDVTLGEGVANAI RDLYKEGKLNPDWIWVVRNGPEAEKGLRMLY
Human ATP-Citrate Lyase     IANFTNVAATFKGIVRAIRDYQGPLKEHEVT-IFVRRGGPNYQEGLRVMG
                               .           :*:. .* * :           .** *:. :. . :. :

GTP_succinyl-CoA Synthetase  NSGLPITSAVDLEDAAKKAVASVTKK-----
Malyl-CoA Ligase             ESGLDLITADTLTEAARKAVEACHGAKH-----
Citryl-CoA Synthetase       EAFKECKVKGEIYDSSLPLTEAPIRLKELLDI-
Human ATP-Citrate Lyase     EVGKTTGIPIHVFGTETHMTAIVGMALGHRPIP
                               :           :           :

```

**Figure 1.4 Sequence alignment of the citrate-binding domain of human ATP-citrate lyase with homologous domains of GTP-specific succinyl-CoA synthetase, *Methylobacterium extorquens* AM1 malyl-CoA synthetase and *H. thermophilus* TK-6 citryl-CoA synthetase. The residues in the citrate-binding site are highlighted in red, and the predicted succinate-binding site residues are also highlighted in red and indicated with *arrowheads*. The sequences were aligned by using ClustalW2.**

```

GTPSCS      MNLQEQYSKKLMSDNGVKVQRFFVADTANEALEAAKRLNAKEIVLKAQIL 50
ATPSCS      MSLHEYMSMELLQEAGVSVPKGYVAKSPDEAYAIAKKLGSKDVKVKAQVL 50
E. coli SCS  MNLHEYQAKQLFARYGLPAPVGYACTTPREAEAAASKIGAGPWVVKQVH 50
              :.*:** : :*: * : . :.. :. ** * :.: : * :.*:

GTPSCS      AGGRGKGVFSSGLKGGVHLTKDPEVVGQLAKQMIGYNLATKQTPKEGVKV 100
ATPSCS      AGGRGKGTFFESGLKGGVKIVFSPEEAKAVSSQMIGKKLFTKQTGEKGRIC 100
E. coli SCS  AGGRGK-----AGGVKVVNSKEDIRAFANWLGKRLVTYQTDANGQPV 93
              *****      ***:.. . * :.: :* .* * ** :*

GTPSCS      NKVMVAEALDISRETYLAILMDRSCNGPVLVGGSPQGGVDIEEVAASNPEL 150
ATPSCS      NQVLVCERKYPREYYFAITMERSFQGPVLIGSSHGGVNIEDVAAESPEA 150
E. coli SCS  NQILVEAATDIAKELYLGAVVDRSSRRVVFMASTEGGVEIEKVAEETPHL 143
              * :.:* :* *.. ::** . * :.:*..**:*.*** ..*

GTPSCS      IFKEQIDIEGIKDSQAQRMAENLGFGLPQNQAADQIKKLYNLFKIDA 200
ATPSCS      I I K E P I D I E E G I K K E Q A L Q L A Q K M G F P P N I V E S A A E N M V K L Y S L F L K Y D A 200
E. coli SCS  I H K V A L D P L T G P M P Y Q G R E L A F K L G L E G K L V Q Q F T K I F M G L A T I F L E R D L 193
              * * :* * * . :.* **: : :. :. : * .*: : *

GTPSCS      TQVEVNPFGETPEGQVVCFDAKINFDDNAEFRQKDI FAMD D K S E N E P I E N 250
ATPSCS      T M I E I N P M V E D S D G A V L C M D A K I N F D S N S A Y R Q K K I F D L Q D W T Q E D E R D K 250
E. coli SCS  A L I E I N P L V I T K Q G D L I C L D G K L G A D G N A L F R Q P D L R E M R D Q S Q E D P R E A 243
              : :.*:** :* :.*.*.*. *.*: **: . : * :.: :

GTPSCS      EAAKYDLKYIGLDGNIACFVNGAGLAMATCDIIFLNGGKPANFLDLGGGV 300
ATPSCS      DAAKANLNYIGLDGNI GCLVNGAGLAMATMDI I K L H G G T P A N F L D V G G G A 300
E. coli SCS  Q A A Q W E L N Y V A L D G N I G C M V N G A G L A M G T M D I V K L H G G E P A N F L D V G G G A 293
              **: :*:*..*****.*:*****.* ** :*:* *****:***.

GTPSCS      KESQVYQAFKLLTADPKVEAILVNIFGGIVNCAIIANGITKACRELELKV 350
ATPSCS      TVHQVTEAFKLITSDKKVLAILVNIFGGIMRCDVIAQGIVMAVKDLEIKI 350
E. coli SCS  T K E R V T E A F K I I L S D D K V K A V L V N I F G G I V R C D L I A D G I G A V A E V G V N V 343
              . :* :***: :* ** * :*****:.* :***:* * :.: :

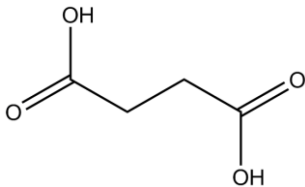
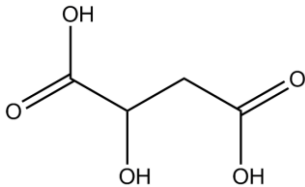
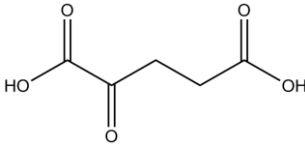
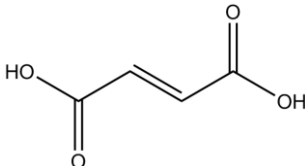
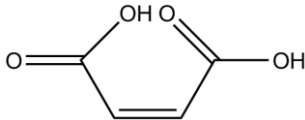
GTPSCS      PLVVRLEGTNVHEAQNILTNSGLPITSAVDLEDAAKKAV----- 389
ATPSCS      P V V V R L Q G T R V D D A K A L I A D S G L K I L A C D D L D E A A R M V V K L S E I V T L A K Q 400
E. coli SCS  P V V V R L E G N N A E L G A K K L A D S G L N I I A A K G L T D A A Q Q V V ----- 382
              * :****:*..... :.:*** * :. . * **: .*

GTPSCS      ASVTKK----- 395
ATPSCS      A H V D V K F Q L P I 411
E. coli SCS  A A V E G K ----- 388
              * * *

```

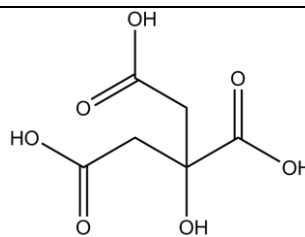
**Figure 1.5** Sequence alignment of  $\beta$ -subunits of pig GTPSCS, human ATPSCS and *E. coli* SCS. Predicted succinate-binding site is highlighted in red with *arrowheads*. The sequences were aligned by using ClustalW2.

**Table 1.1 Organic acids tested with succinyl-CoA synthetase. The structures of each organic acid was drawn using ChemDraw Std 14.0 (Cambridgesoft). The organic acids are shown in the protonated forms.**

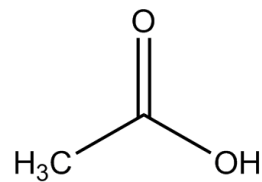
Organic acid	Structure
Succinic acid	
Malic acid	
Alpha-ketoglutaric acid	
Fumaric acid	
Maleic acid	

---

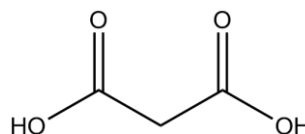
Citric acid



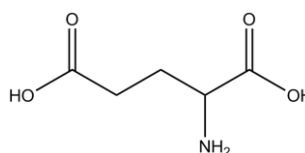
Acetic acid



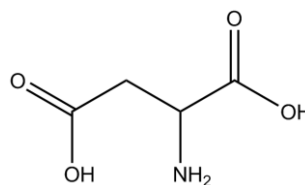
Malonic acid



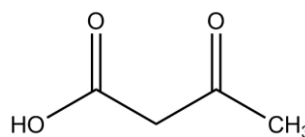
Glutamic acid



Aspartic acid



Acetoacetic acid



## Chapter Two: Methods

### 2.1 Calibration of Superdex-200 prep grade column (16 mm/62 cm)

Superdex-200 prep grade (pg) column (GE Healthcare) is a size exclusion column for separating proteins with molecular weights varying from 10 to 600 kDa. The molecular weight of the protein can be estimated from its elution volume from the size exclusion column. To obtain the molecular weight of GTPSCS, the column had to be calibrated. The Superdex-200 pg column has a diameter 16 mm ( $d=2r$ ) and a length of 62 cm ( $l$ ), so the column volume is 124.6 mL ( $V_c = \pi r^2 l$ ). The gel filtration calibration kit (Pharmacia) contains four proteins (aldolase, ovalbumin, carbonic anhydrase, ribonuclease A) and blue dextran 2000 to be used to calibrate the Superdex-200 pg column using a fast protein liquid chromatography system (FPLC, GE Healthcare Life Science) at a flow rate of 0.5 mL/min. First, the void volume ( $V_o$ ) was determined by running freshly prepared blue dextran 2000 (1.0 mg/mL) through the column. The buffer used in the calibration process was 50 mM phosphate, 150 mM NaCl, pH 7.2. All buffers used in FPLC are filtered and degassed. Then the elution volume ( $V_e$ ) of each protein in the calibration kit was determined. The four proteins were dissolved together in less than 2 mL buffer at a concentration of 3.0 mg/ml for each protein and the solution was injected onto the column.

### 2.2 Purification of wild type GTPSCS

#### 2.2.1 Plasmid purification

A T7-7 plasmid (Figure 2.1) containing the genes that encode the  $\alpha$  and  $\beta$  subunits of GTPSCS was already constructed<sup>45</sup> and stored in *E.coli* strain DH5 $\alpha$ . The plasmid also contains the gene for ampicillin resistance and T7 promoters and ribosome-binding sites upstream of each



gene for GTPSCS. The purification of the T7-7 plasmid from *E. coli* cells was started by inoculating agar medium (20 mL containing 0.3 g Agar-Agar Granulated and 0.5 g Luria-Bertani broth) with the DH5 $\alpha$  glycerol stock. The next day a single colony was picked to inoculate 5 mL Luria-Bertani broth (0.125 g, Life Technologies) containing 100  $\mu$ g/mL ampicillin. This was grown overnight at 37 °C with shaking at 225 rpm. 5 mL overnight culture was centrifuged at 14000 rpm in a Fixed-angle rotor F-45-30-11 for 3 min at room temperature to pellet the cells. The plasmid was then purified from the cell pellet using the protocol of the QIA prep<sup>®</sup> spin Miniprep kit. The plasmid concentration was determined by measuring the absorbance of a 1.5  $\mu$ L sample at 260 nm using the NanoDrop<sup>®</sup> ND-1000 UV-Vis Spectrophotometer (Thermo Fisher Scientific).

### **2.2.2 Transformation**

To overproduce GTPSCS, *E. coli* strain BL21 (DE3) was used. For this, BL21(DE3) Inoue competent cells were thawed on ice, and 1.7  $\mu$ L of purified T7-7 plasmid (139.9 ng/ $\mu$ L) and 50  $\mu$ L of BL21 (DE3) competent cells were mixed in a 14 mL tube (BD Falcon) and placed on ice for 30 min. The cells were incubated at 42°C in a water bath for 90 seconds to give a heat-shock, and then cooled on ice for 2 min. After that, 800  $\mu$ L of NZY<sup>+</sup> broth was added and the cells were grown at 37°C with shaking at 225 rpm for 45 min. 200  $\mu$ L of the incubated cell culture was spread onto an agar plate containing 100  $\mu$ g/mL ampicillin and the plate was incubated for 16 h at 37°C.

### ***2.2.3 Protein expression***

100 mL Luria-Bertani broth (2.5 g, Life Technologies) containing 100 µg/mL ampicillin was inoculated with a single colony, and the LB culture was grown overnight at 37°C with shaking at 225 rpm. The next day, 1L Terrific Broth (12 g tryptone, 24 g yeast extract, 4 mL glycerol, 2.31 g KH<sub>2</sub>PO<sub>4</sub>, 12.54 g K<sub>2</sub>HPO<sub>4</sub> per litre) containing 100 µg/mL ampicillin was inoculated with 50 mL overnight culture and the TB culture was grown at 37 °C and 225 rpm to an optical density A<sub>600 nm</sub> of 1.6-2.0 over 6 to 7 h. Protein overproduction was induced with 1.0 mM isopropyl-β-D-1-thiogalactopyranoside (IPTG) and the temperature was dropped to 25°C, then the culture was grown for another 16 h. The following day, cells were harvested by centrifugation for 30 min at 5000 rpm in a Sorvall SLA-3000 rotor at 4°C. Cells were stored at -80°C in lysis buffer (the volume of buffer in mL equals 1.5 times of cell mass in g) containing 20 mM imidazole, 300 mM NaCl, 50 mM NaH<sub>2</sub>PO<sub>4</sub>, 5 mM 2-mercaptoethanol (2-ME), pH 8.0 until needed for protein purification.

### ***2.2.4 Cell lysis***

Frozen cells were thawed on ice, and then sonicated in an ice-water bath for 180 seconds in total, with cycles of 30 s sonication followed by 30 s rest to allow the solution to cool. After centrifugation at 12000 rpm in a Sorvall SS34 rotor at 4°C for 30 min to pellet the cell debris, the soluble cell lysate in the supernatant was separated for protein purification.

### ***2.2.5 Ni-NTA affinity column***

Ni-NTA (nickel-nitrilotriacetic acid) resin is an affinity resin for proteins that contain an affinity tag of six or more histidine residues. A 10 mL Ni-NTA affinity column was prepared,

and connected to a fraction collector. The solution flowed through the column by gravity and the fraction collector counted drops for each fraction. For purification, the soluble cell lysate was loaded onto the pre-equilibrated column. The flow rate for loading the sample was less than 1 mL/min. Each fraction contained 100 drops. Protein bound to the Ni-NTA column was washed with 5 column volumes of wash buffer (same as lysis buffer), then GTPSCS was eluted with buffer containing 100 mM imidazole, 300 mM NaCl, 50 mM NaH<sub>2</sub>PO<sub>4</sub>, 5 mM 2-ME, pH 8.0. A final wash buffer (500 mM imidazole, 300 mM NaCl, 50 mM NaH<sub>2</sub>PO<sub>4</sub>, 5mM 2-ME, pH 8.0) was used to wash tightly bound molecules from the column. Eluted fractions that contained GTPSCS were detected by enzyme assays and SDS-PAGE gels in order to decide which fractions would be pooled for the next purification step. GTPSCS in the pooled fractions was precipitated by ammonium sulfate (0.5 g per 1 ml solution) and stored at 4°C.

### ***2.2.6 Superdex-200 pg column***

The second chromatographic step used the size exclusion column for separating proteins of different molecular weights. The Superdex-200 pg column was connected to the FPLC. The ammonium sulfate precipitate of GTPSCS was collected by centrifugation at 10000 rpm in a Sorvall SS34 rotor at 4°C for 30 min, and then the pellet was re-suspended in less than 2 mL low salt running buffer (50 mM NaH<sub>2</sub>PO<sub>4</sub>, 5 mM 2-ME, pH 8.0 ). After filtering the protein through a 0.45 µm filter (EMD Millipore), the sample was injected onto the column at a flowrate 0.5 mL/min and 2.5 mL fractions were collected. The running buffer used in this step was 50 mM NaH<sub>2</sub>PO<sub>4</sub>, 150 mM NaCl, 5 mM 2-ME, pH 8.0. Based on the enzyme assays and results from SDS-PAGE gel of fractions showing high absorbance at 280 nm, fractions containing GTPSCS were pooled, and the GTPSCS was precipitated with ammonium sulfate (0.5 g per 1 mL

solution) and stored at 4°C.

### ***2.2.7 Hitrap Blue High Performance affinity column***

The last chromatographic step for purification of GTPSCS used a Hitrap Blue HP affinity column. The dye ligand, Cibacron Blue F3G-A in the column has affinity for nucleotide-binding proteins. In this step, a 1 mL Hitrap Blue HP affinity column (GE Healthcare) was connected to the FPLC, and GTPSCS was expected to bind to the column with a low salt buffer. After washing with the low salt buffer, pure GTPSCS would be eluted with a high salt buffer. The ammonium sulfate precipitate of GTPSCS was collected by centrifugation at 10000 rpm in a Sorvall SS34 rotor at 4°C for 30 min, and then the pellet was re-suspended in less than 2 mL low salt binding buffer (20 mM sodium phosphate, 5 mM 2-ME, pH 7.0). First, GTPSCS was desalted to get rid of ammonium sulfate using a Sephadex G25 column (GE Healthcare), and then GTPSCS was bound to the Hitrap Blue HP affinity column at a flowrate 1 mL/min. After that, a gradient with high salt buffer (20 mM sodium phosphate, 1 M NaCl, 5 mM 2-ME, pH 7.0) was used to elute GTPSCS using the same flowrate. 1 mL fractions were collected. Based on the enzyme assays and results from the SDS-PAGE gel of fractions showing high absorbance at 280 nm, fractions containing GTPSCS were pooled.

Pooled fractions were concentrated in a 15 mL ultrafilter (Amicon® Pro, EMD Millipore) at 4000 rpm in a SX4250 rotor at 4°C, and at the same time, a buffer containing 10 mM TrisHCl, 5 mM 2-ME, pH 8.0 was used to decrease the salt concentration in the protein solution to less than 3 mM. The concentration of purified GTPSCS was determined by the absorbance at 280 nm using the absorption coefficient  $0.35 \text{ mg}^{-1} \text{ cm}^{-1}$  <sup>54</sup>. 20 µL aliquots were flash frozen in thin-walled PCR tubes in liquid nitrogen and stored at -80°C <sup>55</sup>.

### **2.2.8 Bradford assay**

The Bradford protein assay is an effective way to measure the concentration of protein in a solution, and was used to determine protein concentration after each purification step. The dye reagent for the assay was prepared by diluting 1 part Dye Reagent Concentrate (BIO-RAD) with 4 parts distilled, deionized H<sub>2</sub>O (ddH<sub>2</sub>O), and filtering the solution using Whatman #1 filter paper to remove the particulates. Five dilutions (0.4 mg/mL, 0.5 mg/mL, 0.6 mg/mL, 0.7 mg/mL, 0.8 mg/mL) of bovine serum albumin (BSA) stock solution were used to make a standard curve. 100 µL of each dilution, a blank using 100 µL dd H<sub>2</sub>O, and samples of GTPSCS were pipetted into clean test tubes, each containing 5 mL dye reagent. The tubes were well mixed by vortexing and left for 6 min at room temperature. The spectrophotometer (CARY 100 Bio UV-Visible) was used to measure the absorbance at 595 nm of each standard solution in order to make the standard curve, then the absorbance of each sample was measured and the standard curve was used to calculate the concentration of the protein.

### **2.2.9 SDS-PAGE**

Sodium dodecyl sulfate polyacrylamide gel electrophoresis (SDS-PAGE) is a useful technique to separate proteins. A Mini-Protean 3 system with 0.75 mm gels and combs that have 10 wells was routinely used. The SDS-PAGE gel consisted of a 4% stacking gel and a 9% separating gel. The solution for the separating gel contained 4.3 mL of ddH<sub>2</sub>O, 3.0 mL 30% (w/v) acrylamide/bisacrylamide (Mix Ratio 37.5:1, Sigma-Aldrich), 2.5 mL 1.5 M Tris-HCl (pH 8.8), 0.1 mL 10% w/v SDS, 0.1 mL fresh 10% w/v ammonium persulfate and 4 µL TEMED (Invitrogen™). The solution for the stacking gel contained 3.0 mL of ddH<sub>2</sub>O, 0.65 mL 30% (w/v) acrylamide/bisacrylamide (Mix Ratio 37.5:1, Sigma-Aldrich), 1.25 mL 0.5 M Tris-HCl (pH6.8),

50  $\mu$ L 10% w/v SDS, 50  $\mu$ L fresh 10% w/v ammonium persulfate and 5  $\mu$ L TEMED (Invitrogen™). After pouring the separating gel, a layer of ethanol was added to isolate the gel from air. After 45 min for the polymerization, the ethanol was removed, and the stacking gel solution was loaded onto the solidified separating gel. The 10 well comb was inserted into the stacking gel, which was then allowed to polymerize for 45 min. 20  $\mu$ L of sample was diluted in a 1:1 ratio with 2 $\times$ sample buffer (0.355 mL ddH<sub>2</sub>O, 0.125 mL 0.5 M Tris-HCl (pH 6.8), 0.25 mL glycerol, 0.2 mL 10% (w/v) SDS and 0.02 mL 0.5% (w/v) bromophenol blue and 0.05 mL 2-ME) and denatured at 95°C for 4 min. The denatured protein samples and 5  $\mu$ L of molecular weight ladder (PAGERuler (BIO BASIC INC) or Blueeye prestained protein ladder (GeneDirex)) were loaded into separate wells. Electrophoresis was conducted at 200 V for about 45 min with 500 mL of 1 $\times$ running buffer (25 mM Tris base, 192 mM glycine and 3.5 mM SDS). The gel was stained for 1 h in the stain solution (2.5 g Coomassie brilliant blue R250 in 1L destain solution), then destained in a solution containing 45% methanol and 10% acetic acid for another 1 h and finally switched to 10% glacial acetic acid.

### ***2.2.10 Enzyme assay***

In order to measure the activity of the enzyme after each purification step, the production of succinyl-CoA was detected at 235 nm in a continuous assay. One enzyme unit of activity (U) for GTPSCS is equal to 1  $\mu$ mol of succinyl-CoA formed per min. For the kinetic assay, 1  $\mu$ L sample solution (diluted to give 5 times or 10 times dilution) was mixed in 1 mL assay solution containing 0.05 M Tris-succinate (pH 7.4), 0.01 M MgCl<sub>2</sub>, 0.1 mM GTP and 0.1 mM CoA<sup>5</sup> and the increase in absorbance at 235 nm was recorded for 60 s at room temperature. In order to get the initial velocity of the reaction, the linear slope of the absorbance curve at the beginning of the

reaction was chosen. The extinction coefficient for the thioester bond of succinyl-CoA at 235 nm was assumed to be  $4500 \text{ M}^{-1}\text{cm}^{-1}$ <sup>56</sup>.

### 2.3 Crystallization

Crystallization is an essential step in determining protein structures by X-ray crystallography, and it can be difficult to obtain protein crystals of good quality. In order to crystallize a protein, a large amount of the protein at high purity can be required. Vapor diffusion is the most commonly used method for protein crystallization. Vapor diffusion can be used with either hanging-drops or sitting-drops. Hanging-drops are most popular and refer to drops of protein solution placed on an inverted cover slip and suspended above a reservoir solution. The drop contains purified protein mixed with reservoir solution in a certain ratio. This drop is equilibrated with the larger reservoir solution containing buffer, salt or other precipitants, and sometimes additives. Since the droplet of protein solution contains a lower concentration of precipitant than the reservoir, as the drop and reservoir solution equilibrate, the precipitant and protein concentrations gradually increase in the drop. The right crystallization conditions, generally with slow equilibration, give the best crystals for the diffraction experiment.

Co-crystallization requires the target protein to be mixed with ligand in order to achieve the complex. In this case, CoA and succinate were added to GTPSCS, then 10 mM Tris buffer (pH 8.0) was used to dilute the protein solution to an appropriate final concentration. The solution was kept on ice for 30 min before setting up crystallization trials. Crystallization was started from the PEG/Ion Screen™ HR2-126 (Hampton Research). Based on the screening results, the concentrations of salt (magnesium formate) and precipitant (Polyethylene glycol (PEG) 3350) were optimized and an appropriate buffer (Hepes) at the optimal pH (pH 7.0) was

selected. The ratio between protein sample and reservoir solution mixed on the coverslip was 1:1 (0.5  $\mu$ L:0.5  $\mu$ L). The temperature for crystals to grow was 21°C.

The other condition that was used to grow crystals of the GTPSCS/succinate/CoA complex had PEG 3350, ammonium succinate and Hepes buffer at pH 7.0. Magnesium chloride was added to the protein sample. The ratio between protein sample and reservoir solution mixed on the coverslip was still 1:1 (0.5  $\mu$ L:0.5  $\mu$ L). The temperature for crystals to grow was 21°C.

In order to make sure the crystals that grew in the crystallization trials contained GTPSCS, crystals from five wells having the same conditions (0.14 M magnesium formate, 20% w/v PEG 3350, Hepes pH 7.0) were harvested into a microcentrifuge tube, and the reservoir solution was used to wash these crystals three times. All the solution in the microcentrifuge tube was removed from the crystals, and 10  $\mu$ L of 2 $\times$  sample buffer was added to dissolve the crystals before denaturing the protein and loading the sample on a 9% SDS-PAGE gel.

## **2.4 Data collection and refinement**

Crystals were mounted onto cryo-loops with cryoprotectant (same concentrations of precipitant, salt and buffer as mother liquor plus 20% glycerol) and cooled in the nitrogen stream at 100 K before shipment to the Canadian Light Source, Saskatoon, Canada at low temperature. Remote data collection at the insertion device beamline (CLS 08ID-1) was used to collect diffraction data from crystals of the GTPSCS/CoA complex with a Rayonix MX300 CCD detector, the crystal to detector distance of 250 mm and the wavelength of 0.97795 Å. The rotation range was 0.5° per image and the total rotation range was 150°. The exposure time was 1 second for each image. Remote data collection at the bending magnet beamline (CLS 08B1-1) was used to collect diffraction data from the crystals of the GTPSCS/succinate/CoA complex



with a Rayonix MX300HE CCD detector, the crystal to detector distance of 290 mm and the wavelength of 0.9794 Å. The rotation range was 0.5° per image and the total rotation range was 180°. The exposure time was 3 seconds for each image. The diffraction data were processed using IMOSFLM<sup>57</sup> and other programs from the CCP4 package<sup>58</sup>. Molecular replacement was used to solve the phase problem. PHENIX<sup>59</sup> and Coot<sup>60</sup> were used to refine and rebuild the structure. For the GTPSCS/CoA complex, the dictionary to restrain the geometry of the ligand CoA was created by the Grade Web Server (<http://grade.globalphasing.org>). The model quality was judged using MolProbity<sup>61</sup>.

## 2.5 Site-directed mutagenesis of GTPSCS

Since the succinate-binding site of GTPSCS was predicted to lie at 327β-330β (Gly-Gly-Ile-Val) and Cys 332β was covalently attached to 2-mercaptoethanol in the structure of the GTPSCS/CoA complex, this residue was mutated to alanine (defined as C332βA). The concern was that the attachment may distort the structure in this area, and affect the binding of succinate to GTPSCS. Mutation to alanine would remove the sulfur atom forming the disulfide bond with 2-ME. The primer sequence was designed to be complementary to the sequence of the target area except for the bases coding for cysteine (Table 2.1). First, the gel purified primers were dissolved in ddH<sub>2</sub>O to give a concentration of 100 pmol/μL. The mutagenesis included two steps, first single strand elongation with plasmid and a single primer in each of two tubes, followed by mixing of the two and a second step for double strand elongation. In the first step, 5 μL 10× Q5 reaction buffer (New England Biolabs), 0.36 μL T7-7 plasmid (139.9 ng/μL) containing the genes that encode the α and β subunits of GTPSCS, 0.12 μL sense primer (100 pmol/μL), 0.33 μL Q5 High-Fidelity (2000 U/mL) DNA polymerase (New England Biolabs), 0.5 μL dNTP (25

mM) and 18.69  $\mu\text{L}$  ddH<sub>2</sub>O were mixed in 200  $\mu\text{L}$  thin-walled PCR tube 1. PCR tube 2 contained the same amount of chemicals and plasmid as tube 1 except 0.12  $\mu\text{L}$  antisense primer (100 pmol/ $\mu\text{L}$ ) instead. The elongation took place after loading two separate PCR tubes in the PCR machine (Biometra) and starting the program. The program included 105°C lid preheating (step 1), then 2 min at 95°C for denaturing (step 2), 20 seconds at 95°C still for denaturing (step 3), 10 seconds at 60°C for primers to anneal to the DNA (step 4), 2.5 min at 68°C for the elongation (step 5), after that, the program repeated from step 2, for a total of 11 cycles of the elongation. The program then paused at 21°C allowing for the solutions in the two PCR tubes to be mixed and 0.33  $\mu\text{L}$  of Q5 polymerase (2000 U/mL) to be added. The second step used the same program but for 17 cycles to produce a larger amount of product. In order to get rid of the original plasmids that were mixed with the replication products, 10  $\mu\text{L}$  of sample was mixed with 0.4  $\mu\text{L}$  of DpnI (20000 U/mL, New England Biolabs) and left for 1 h at 37°C. 2  $\mu\text{L}$  of the digested sample was used to transform 50  $\mu\text{L}$  DH5 $\alpha$  competent cells. The mutated plasmids were purified the following day for sequencing at the UCDNA Services, Faculty of Medicine, University of Calgary. 0.4813  $\mu\text{g}$  (0.1  $\mu\text{g}/1000$  bp) purified plasmid was mixed with 3.2 pmole sequencing primer in a final volume of 12  $\mu\text{L}$ .

## **2.6 Kinetic studies of formate inhibition of wild type GTPSCS**

Since the crystals of the GTPSCS/succinate/CoA complex that were grown with magnesium formate showed that some parts of the structure were disordered, we suspected that formate competed with succinate to bind to GTPSCS. To test whether formate inhibited GTPSCS and, if so, to determine the mode of inhibition, kinetics assays were performed using pure GTPSCS and 0, 100 and 200 mM magnesium formate. 0.1 M sodium succinate was titrated

with 0.1 M succinic acid to get a pH 7.4 solution, which was then diluted with 0.2 M Tris-HCl (pH 7.4) to give various concentrations of succinate. The 1 mL reaction mixture still contained 10 mM MgCl<sub>2</sub>, 0.1 mM GTP and 0.1 mM CoA as in the enzyme assay but various concentrations of succinate were used between 0.1 and 50 mM. The assays were performed at room temperature. 1 μL of pure GTPSCS with a concentration of 0.24 mg/mL was well-mixed with 1 mL of assay mixture and the absorbance at 235 nm was measured for 1 min. The initial velocities for various concentrations of succinate were used to generate Michaelis-Menten plots in the presence or absence of formate. The apparent value of K<sub>m</sub> at different concentrations of formate were determined from the Michaelis-Menten plots in order to plot apparent K<sub>m</sub> as a function of formate concentration. A straight line of best fit was drawn, and the inhibition constant K<sub>i</sub> is the negative value of x-intercept on this plot.

**Table 2.1 The sense and antisense primers for mutating cysteine to alanine at residue 332 in the β-subunit of GTPSCS. The underlined sequences indicate the codon for alanine.**

<b>Primers</b>	<b>Sequences</b>
<b>Sense</b>	5'-GGTGGGAATCGTCAAC <u>GCT</u> GCCATCATTGCCAATGG-3'
<b>Antisense</b>	5'-CCACCTTAGCAGTTG <u>GAC</u> CGGTAGTAACGGTTACC-3'

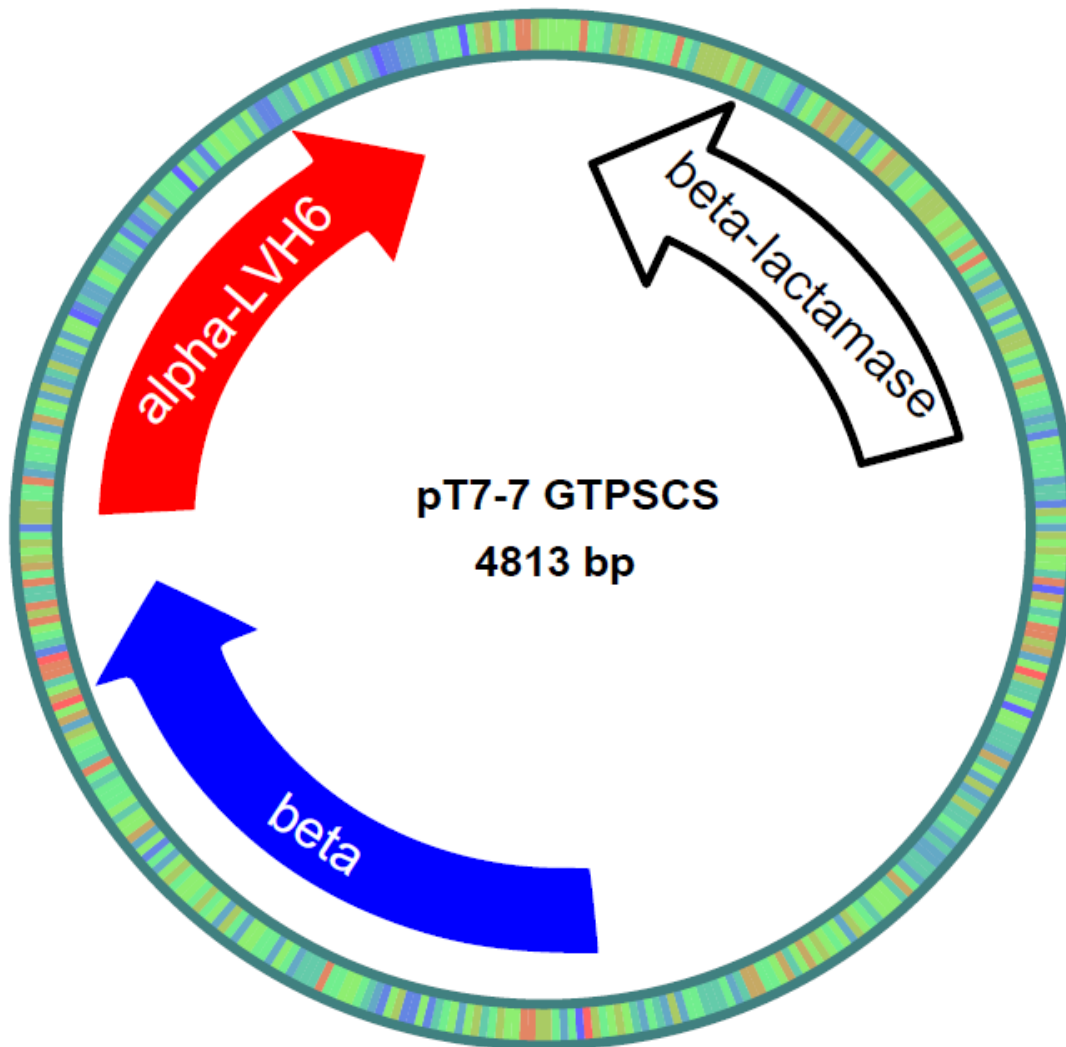


**Figure 2.1 T7-7 plasmid containing genes for coding  $\alpha$  and  $\beta$  subunits of GTPSCS. The length of the plasmid is 4813 bp. A tag LVHHHHHHH has been constructed at the C-terminus of the  $\alpha$ -subunit. The plasmid carries the gene for ampicillin resistance.**

## Chapter Three: Results

### 3.1 Calibration of Superdex-200 prep grade column (16 mm/62 cm)

Superdex-200 prep grade (pg) column is a size exclusion column, which can separate proteins with different sizes (10-600 kDa). Our column volume ( $V_c$ ) is 124.6 mL. The elution volume for blue dextran 2000 is equal to the column void volume ( $V_o=47.02$  mL). The elution volumes ( $V_e$ ) on the chromatogram (Figure 3.1 and Table 3.1) were used to calculate  $K_{av}$  for each calibration kit protein, using the equation  $K_{av} = (V_e - V_o) / (V_c - V_o)$ . The calibration curve of  $K_{av}$  versus log molecular weight is shown in Figure 3.2. The equation for this standard curve is  $y = -2.6662x + 6.0136$  and R squared is 0.9979.

The blue dextran 2000 and the four kit proteins give absorbance peaks at 280 nm, but the chromatogram shows six major peaks. The elution volume of 60.95 mL does not correspond to any of the standard samples. However, the instructions from the kit indicate that aldolase may form a small amount of dimer, which can elute slightly before the standard aldolase. In reality, the 280 nm absorbance peak (70.53 mL) representing monomeric aldolase has a much larger size than the absorbance peak (60.95 mL) for the proposed aldolase dimer. Therefore, a calibration curve derived from the four kit proteins and the blue dextran 2000 was made in order to calculate the molecular weight of the protein that eluted at 60.95 mL. Consistent with the expected result, the molecular weight corresponding to a peak at that elution volume is about twice the molecular weight of monomeric aldolase. Because of this, the dimer of aldolase at 60.95 mL has been included in the final calibration curve for the Superdex-200 pg column.

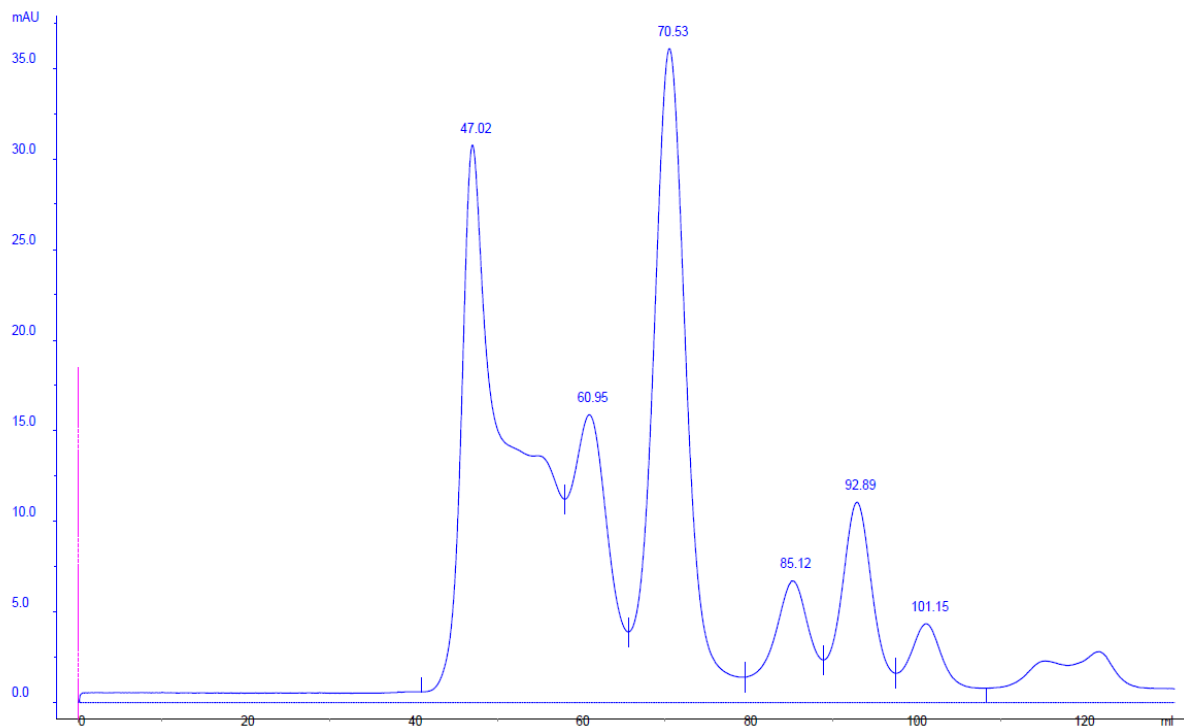


**Figure 3.1 Chromatogram showing the elution profile of calibration kit proteins (aldolase, ovalbumin, carbonic anhydrase, ribonuclease A) and blue dextran 2000. The blue line is the UV absorbance at 280 nm and the pink line marks the injection of the sample.**

**Table 3.1 Molecular weight and elution volumes of the calibration kit proteins and blue dextran 2000 used for calibrating Superdex-200 pg column.**

<b>Standard Protein</b>	<b>Molecular Weight (kDa)</b>	<b>Elution Volume (mL)</b>
Blue dextran 2000	2,000	47.02
Dimer of aldolase	316	60.95
Aldolase	158	70.53
Ovalbumin	45	85.29
Carbonic anhydrase	29	92.93
Ribonuclease A	13.7	101.15

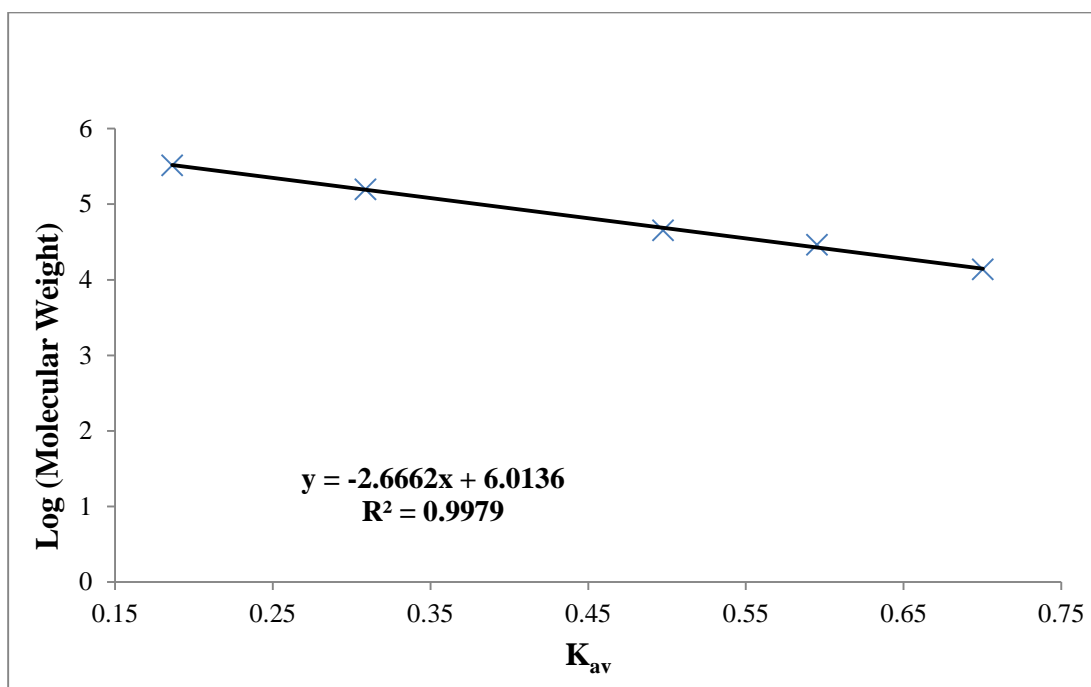


**Figure 3.2 Calibration curve of Superdex-200 pg column. Logarithmic plot of molecular weight (kDa) versus  $K_{av}$  representing the calibration of the Superdex-200 pg column plotted using Microsoft Excel. The range of the  $K_{av}$  is from 0.186 to 0.70 (Molecular weight: 13.7- 328 kDa).**

### **3.2 Purification of wild type GTPSCS**

Since protein crystallization needs high purity protein, a three-step chromatographic purification was designed in order to obtain pure GTPSCS. Due to the 6-His tag at the C-terminus of  $\alpha$ -subunit, a Ni-NTA affinity column was selected to extract GTPSCS from the cell lysate in the first step. Then a Superdex-200 pg gel filtration column was used to separate proteins with different sizes. At the last step, a Hitrap Blue HP affinity column, which binds nucleotide-binding proteins, was used to bind GTPSCS.



### 3.2.1 Ni-NTA affinity column

GTPSCS is able to bind to the nickel resin due to the His tag at the C-terminus of the  $\alpha$ -subunit. The 9% SDS-PAGE gel (Figure 3.3) shows the result after this purification step. Two of the major bands are consistently found between 30-40 kDa and 40-50 kDa from lane 3 to lane 10 on the gel.

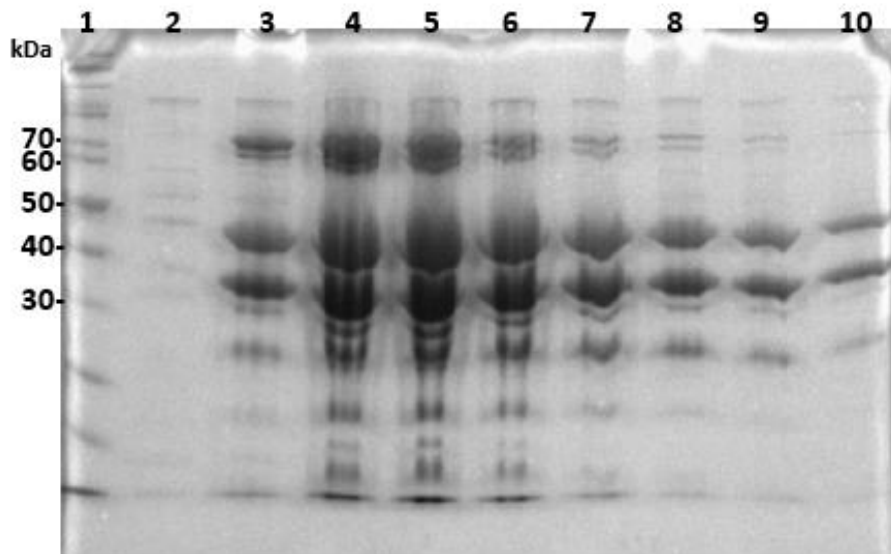


**Figure 3.3 9% SDS-PAGE gel showing the Ni-NTA column purification of wild type GTPSCS. Lane 1 is the Pagenruler ladder (5  $\mu$ L, BIO BASIC INC). Lane 2 refers to the last wash fraction with 20 mM imidazole (20  $\mu$ L). Lanes 3-10 are fractions eluted with 100 mM imidazole (each lane 20  $\mu$ L).**

### 3.2.2 Superdex-200 pg column

The major 280 nm UV absorbance peak on the chromatogram (Figure 3.4) appeared between fractions C4 and C7. The 9% SDS-PAGE gel on the left side of chromatogram shows

that samples from C4, C5, C6 and C7 all have two dense bands between 30-40 kDa and 40-50 kDa.

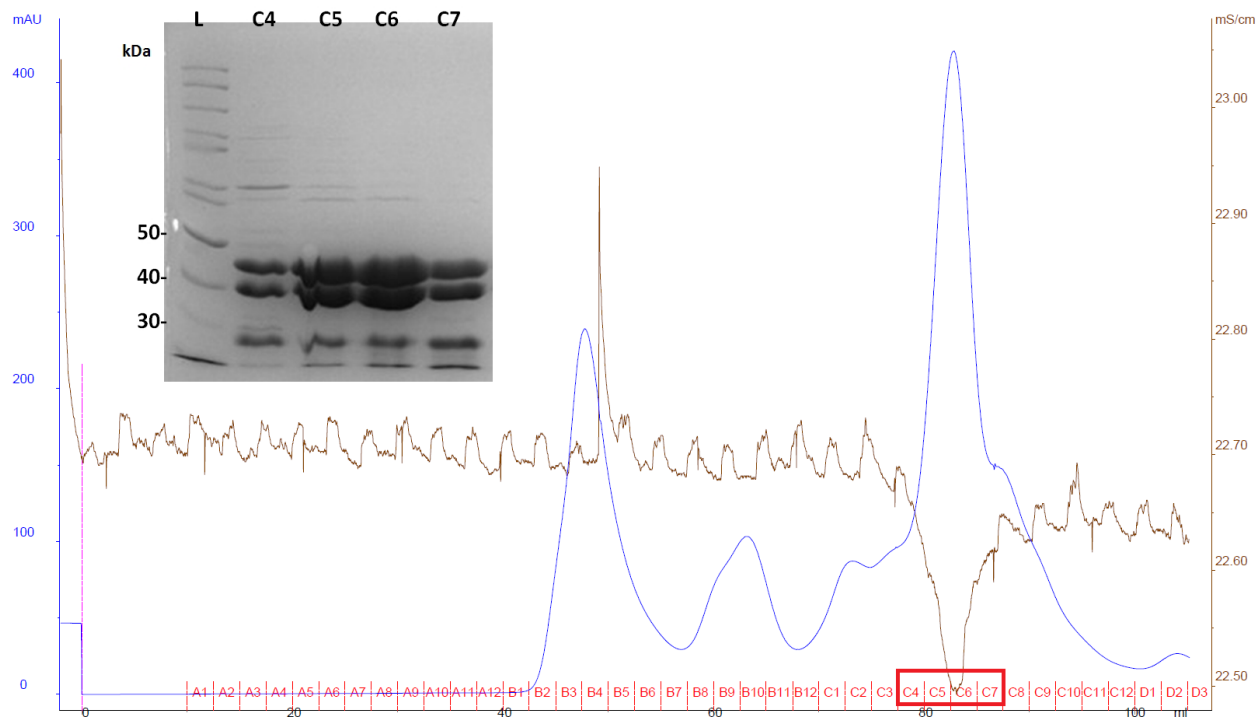


**Figure 3.4 Chromatogram of Superdex-200 pg column showing UV absorbance at 280 nm versus elution volume. The blue line refers to UV absorbance at 280 nm, the brown line is the conductivity and the pink line marks the injection of the sample. SDS-PAGE gel (9%) containing fractions C4, C5, C6 and C7 (20  $\mu$ L sample of each) is shown on the left side of the chromatogram.**

### **3.2.3 Hitrap Blue High Performance affinity column**

The dye ligand, Cibacron Blue F3G-A in the Hitrap Blue HP column is similar in structure to nucleotide cofactors, so this column has affinity for nucleotide-binding proteins. Because of this, under low salt concentration buffer, GTPSCS binds to the column, and a buffer

with higher salt concentration can elute GTPSCS. The chromatogram (Figure 3.5) shows a 280 nm UV absorbance peak when the concentration of salt increases. Only two clean bands (molecular weights are between 30-40 kDa and 40-50 kDa) show on the 9% SDS-PAGE gel from fractions B10-C3.

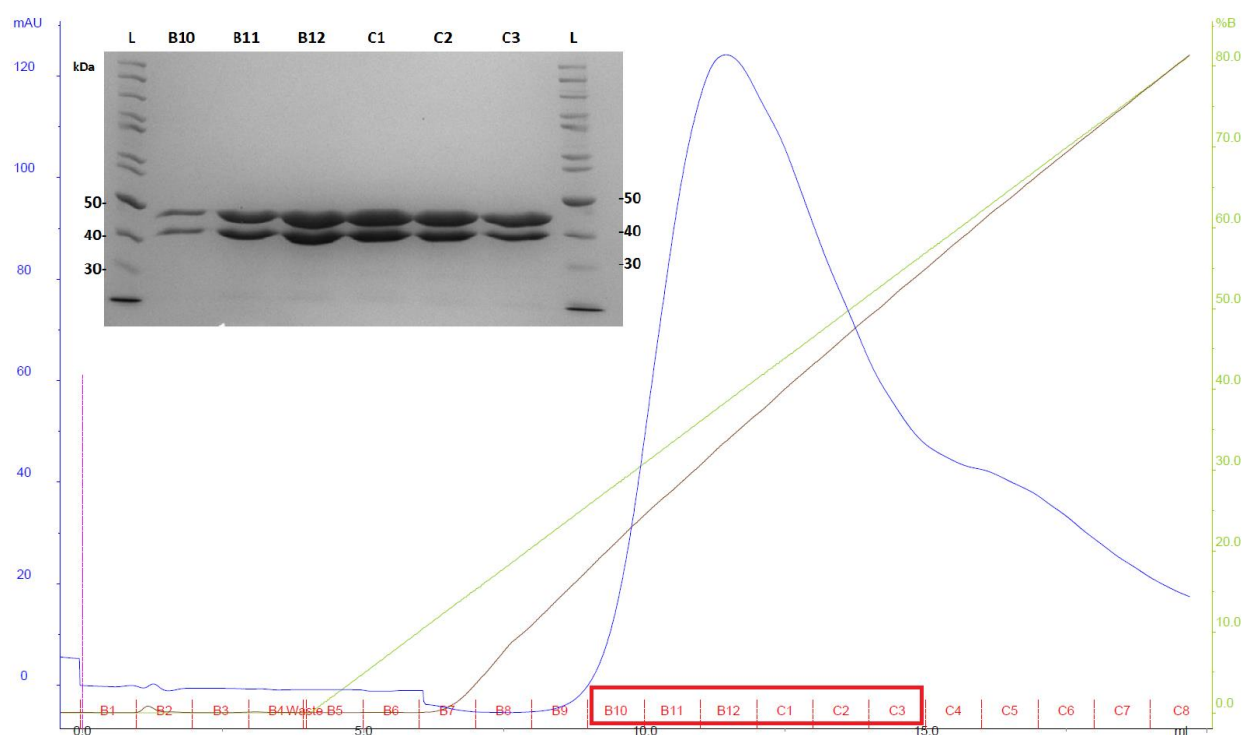


**Figure 3.5 Chromatogram of Hitrap Blue High Performance affinity column showing UV absorbance at 280 nm versus elution volume. The blue line refers to UV absorbance at 280 nm, the brown line is the conductivity, the green line refers to the concentration of salt (NaCl) and the pink line marks the injection of sample. SDS-PAGE gel (9%) containing fractions B10, B11, B12, C1, C2 and C3 (20  $\mu$ L sample of each) is shown on the left side of the chromatogram.**

### 3.2.4 Bradford assay

In order to know the GTPSCS concentration in the pooled fractions after each step of the purification, the Bradford assay was used due to its fast and efficient measurement. Five concentrations of bovine serum albumin (BSA) were used to make the standard curve, which ranges from 0.40 mg/mL to 0.80 mg/mL. Protein solution from each step of the purification was diluted to a concentration within the range of the standard curve. The concentrations determined for GTPSCS were 28.3 mg/mL, 1.6 mg/mL, 0.7 mg/mL and 0.5 mg/mL in the cell lysate, Ni-NTA, Superdex-200 pg and Hitrap Blue HP respectively.

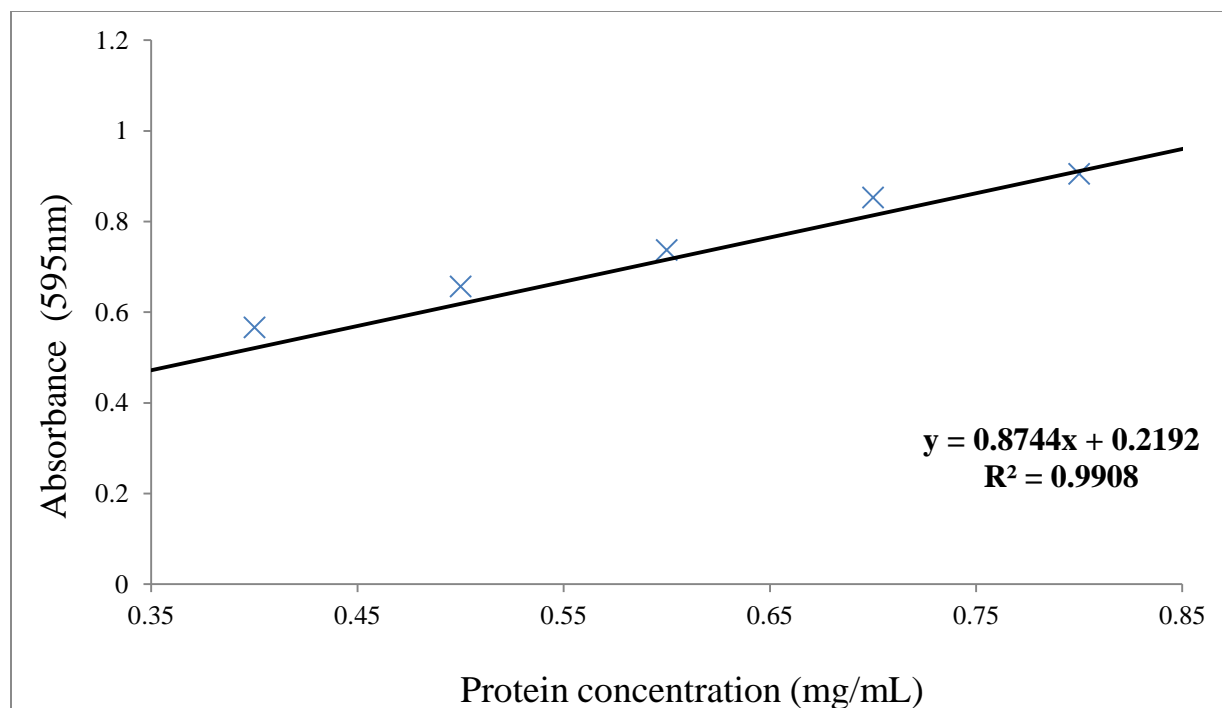


**Figure 3.6 Standard curve of the Bradford assay showing absorbance at 595 nm versus protein concentration (mg/mL). The straight line fit to the five points is shown, and the equation for this line is  $y=0.8744x + 0.2192$  with R squared of 0.9908.**

### 3.2.5 Purification table for wild type GTPSCS

The yield of GTPSCS and increase of GTPSCS specific activity during purification are shown in the purification table (Table 3.2). The protein concentration was determined using the Bradford assay (Figure 3.6), and the activity was measured with the enzyme assay. After the Hitrap Blue HP affinity column, 6 mL of pooled fractions were concentrated to 75  $\mu$ L. The concentration of this protein solution was 22.3 mg/mL.

**Table 3.2 Quantity, activity and yield of wild type GTPSCS subsequent to each step of purification.**

<b>Purification Steps</b>	<b>Volume (mL)</b>	<b>Protein (mg)</b>	<b>Activity (units)</b>	<b>Specific activity (units/mg)</b>	<b>Purification (fold)</b>	<b>Yield (%)</b>
Cell-free extract	32.5	920.7	617.5	0.7	1.00	100.0
Ni-NTA affinity	20	32.4	424.4	13.1	18.7	68.7
Superdex-200 pg	17.5	13.1	178.9	13.7	19.6	29.0
Hitrap Blue HP affinity	6	3.2	49.3	15.4	22.0	8.0

### 3.3 Protein crystallization

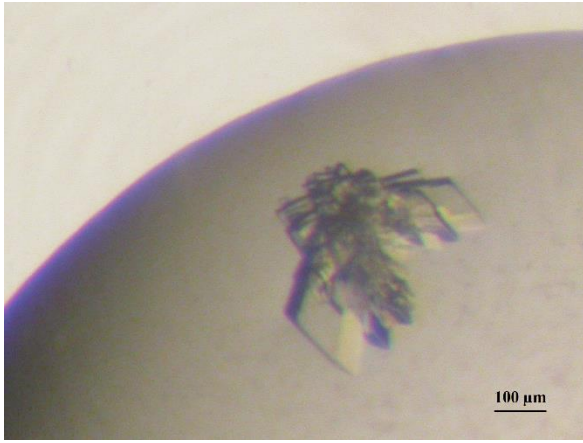
Screening conditions (Table 3.3) showed that crystals of GTPSCS in complex with succinate and CoA can nucleate in several conditions, as clusters of crystals were formed in these conditions. The screening condition 0.2 M magnesium formate, 20% w/v polyethylene glycol 3350, pH 7.0 (Kit: HR2-126, Hampton Research) gave the best crystals (Figure 3.7a), using 0.5  $\mu$ L protein solution (3.9 mg/ml GTPSCS, 5 mM CoA, 50 mM sodium succinate (pH 8.0) and 10 mM Tris buffer pH 7.2) with 0.5  $\mu$ L reservoir solution mixed to form the hanging drop.

After optimizing the concentrations of PEG 3350 and magnesium formate and the pH, relatively good crystals were obtained under the conditions of 0.14-0.15 M magnesium formate, 18-20% w/v PEG 3350, 100 mM Hepes buffer pH 7.0 (Figure 3.7b and 3.7c). The protein sample was mixed with reservoir solution in either a 1:1 (Figure 3.7b) or 2:1 (Figure 3.7c) ratio. The other crystallization conditions that were optimized were around 22% PEG 3350, 125 mM ammonium succinate and 100 mM Hepes buffer pH 7.0 (Figure 3.7d), in which case the protein solution was 4.0 mg/ml GTPSCS, 1.5 mM CoA, 50 mM ammonium succinate (pH 7.0), 50 mM magnesium chloride and 10 mM Tris buffer pH 8.0.

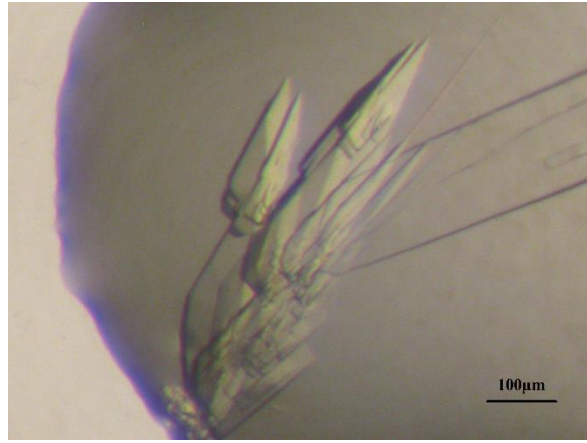
In order to confirm that crystals contained GTPSCS, a SDS-PAGE gel was used to detect the molecular weights of the protein. The 9% SDS-PAGE gel (Figure 3.8) shows two clear bands in lane 2, which can be compared with two different markers in lanes 1 and 3, to demonstrate that the bands lie at 30-40 kDa and 40-50 kDa.

**Table 3.3 Crystallization conditions in which the GTPSCS/succinate/CoA complex nucleates.**

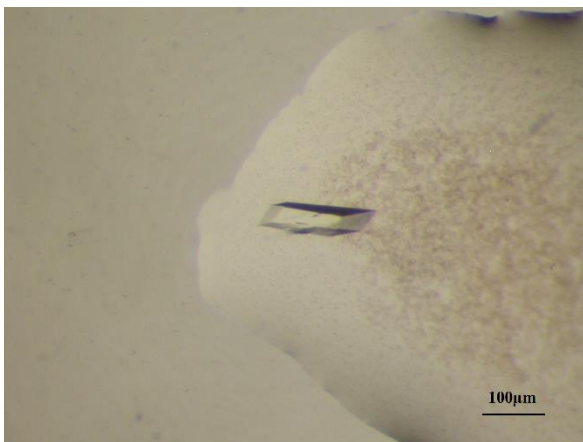
<b>Precipitant</b>	<b>Salt</b>
Polyethylene Glycol 3350	Ammonium acetate
Polyethylene Glycol 3350	Ammonium formate
Polyethylene Glycol 3350	Ammonium succinate
Polyethylene Glycol 3350	Magnesium formate
Polyethylene Glycol 3350	Potassium thiocyanate
Polyethylene Glycol 3350	Potassium formate
Polyethylene Glycol 3350	Sodium thiocyanate
Polyethylene Glycol 3350	Sodium formate



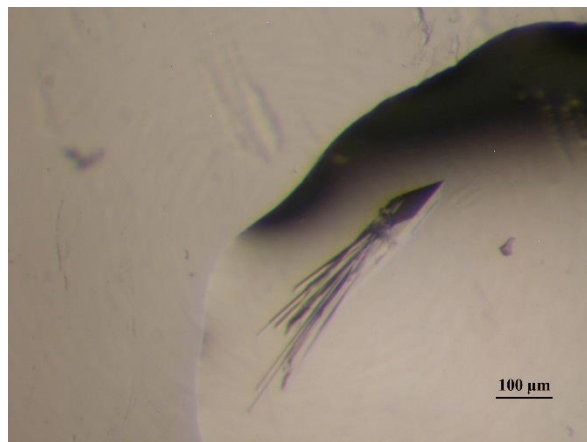
(a)



(b)



(c)



(d)

**Figure 3.7 Crystals of the GTPSCS/succinate/CoA complex. Crystals in (a), (b) and (c) were grown in PEG 3350, magnesium formate and Hepes pH 7.0. Crystals in (d) grew in PEG 3350, ammonium succinate and Hepes pH 7.0. The protein solution used to grow crystals contained GTPSCS, succinate and CoA.**



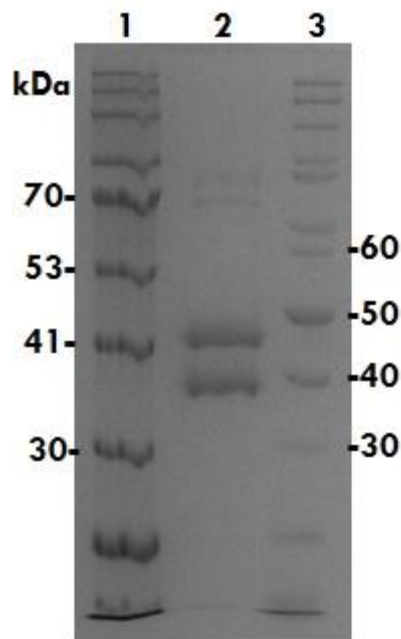


**Figure 3.8 9% SDS-PAGE gel showing the proteins in the crystals. Lane 2 refers to crystals grown in 0.14 M magnesium formate, 20 % w/v polyethylene glycol 3350, Hepes (pH 7.0). Lane 1 is Blueye prestained protein ladder (5  $\mu$ L, GeneDirex), Lane 3 is Pageruler ladder (5  $\mu$ L, BIO BASIC INC).**

### **3.4 X-ray diffraction data**

#### **3.4.1 Data collection for GTPSCS/CoA complex**

The diffraction dataset for GTPSCS/CoA crystals (grown by project student Manpreet Malhi) were collected at the Canadian Light Source (CLS), Saskatoon on beamline 08ID-1 using a MarMosaic Rayonix MX300 CCD X-ray detector. The X-ray wavelength was 0.97795 Å. One of the crystals diffracted to 1.9 Å resolution (Figure 3.9). The statistics resulting from the diffraction data processing are shown in Table 3.3.

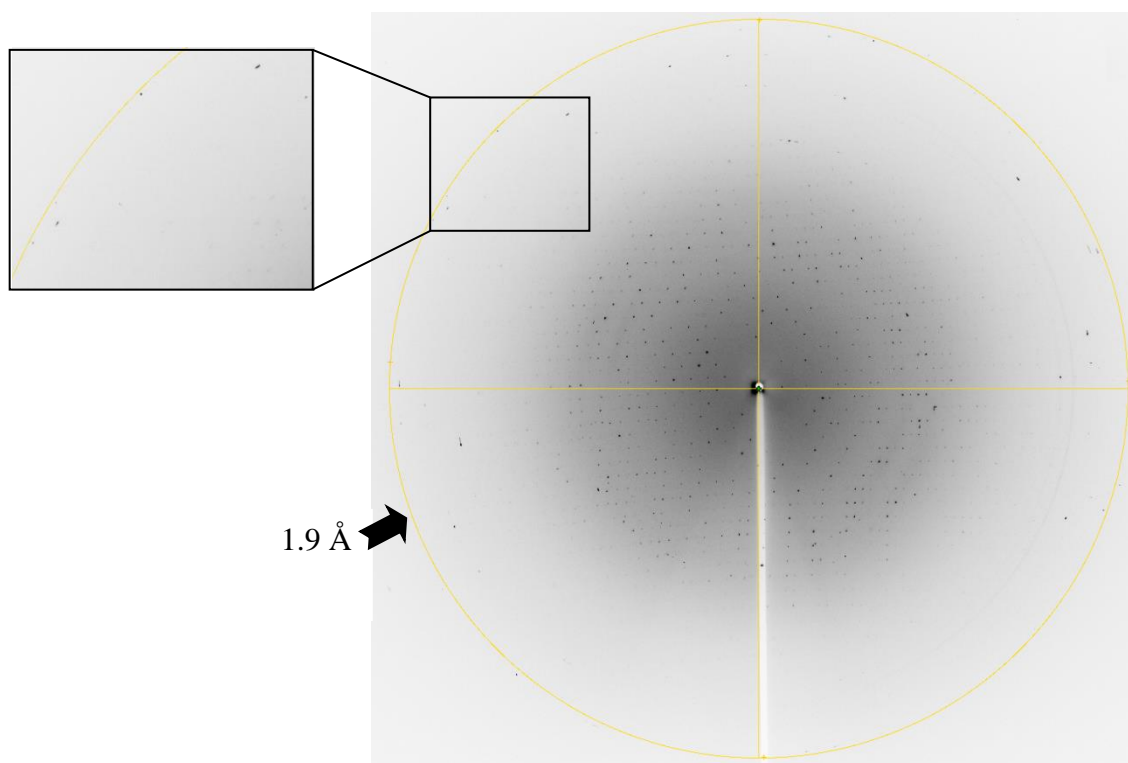


**Figure 3.9** Diffraction image of GTPSCS in complex with CoA. The crystal was shot by X-rays at the Canadian Light Source, SK, Canada. The black dots are X-ray diffraction spots. The resolution limit of 1.9 Å is indicated by the yellow circle. The bright line refers to the beam stop. The image on the left side shows a magnification of the region near the 1.9 Å limit of diffraction.

### **3.4.2 Data collection for GTPSCS/succinate/CoA complex**

The diffraction dataset for GTPSCS/succinate/CoA complex was collected at the Canadian Light Source (CLS), Saskatoon on beamline 08B1-1 beamline using a MarMosaic Rayonix MX300HE CCD X-ray detector. The wavelength was 0.9794 Å. One of the crystals diffracted to 2.1 Å resolution (Figure 3.10). The statistics resulting from the diffraction data processing are shown in Table 3.4.

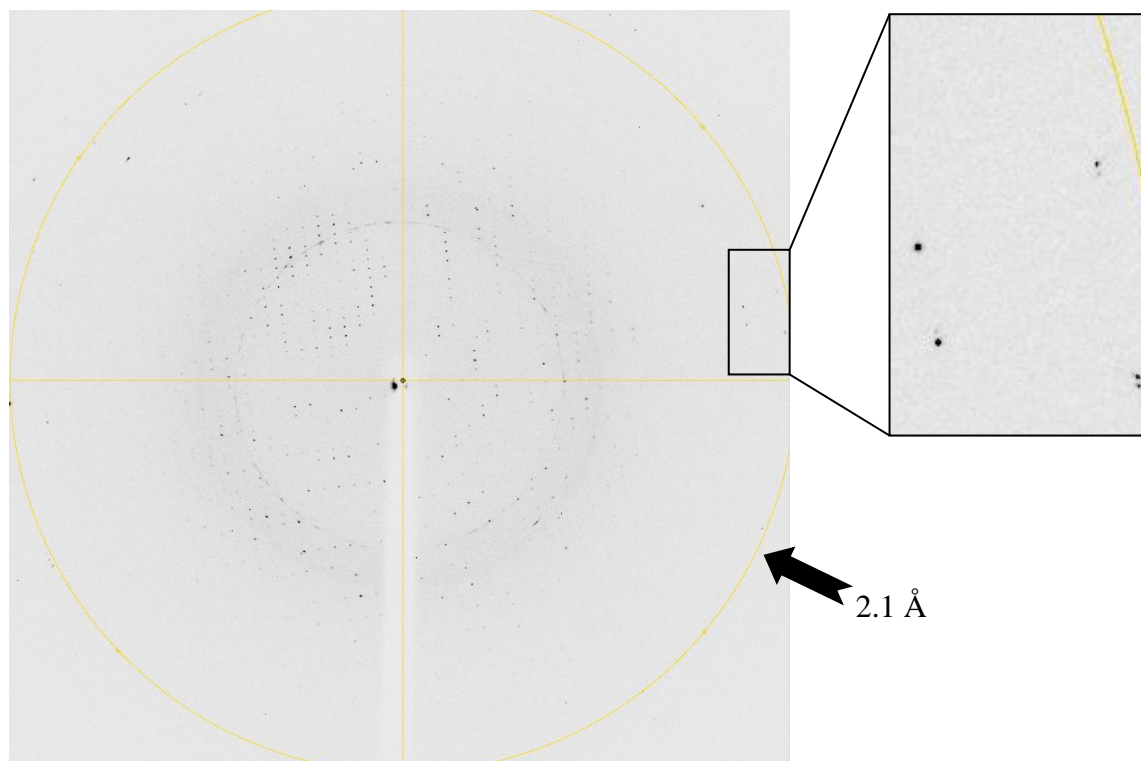


**Figure 3.10** Diffraction image of GTPSCS in complex with succinate and CoA. The crystal was shot by X-rays at the Canadian Light Source, SK, Canada. The black dots are X-ray diffraction spots. The resolution limit of 2.1 Å is indicated by the yellow circle. The bright line refers to the beam stop. The image on the right side shows magnification of the region near the 2.1 Å limit of diffraction.

## 3.5 Structures

### 3.5.1 CoA-binding site of GTPSCS

The X-ray diffraction result shows green electron density ( $F_o-F_c$  map) located in the N-terminal domain of the  $\alpha$ -subunit of GTPSCS (Figure 3.11), which was identified as the CoA-binding site (Figure 3.12). The CoA-bound GTPSCS crystal structure was solved by using molecular replacement with dephosphorylated GTPSCS as the model (PDB code 1EUC). The data processing and refinement results are listed in Table 3.4 and Table 3.5. Five residues of the  $\alpha$ -subunit and seven water molecules interact with CoA. The hydrogen bonds (yellow dashed lines) between residues of GTPSCS or water molecules and CoA are shown in Figure 3.13 (two hydrogen-bonded atoms are within 3.2 Å of each other). The adenine ring of CoA is stabilized by two water molecules with strong interactions indicated by the 2.6 Å distance from one water molecule to the N1A atom and 2.8 Å from the other water molecule to the N6A atom. The phosphoryl group on the ribose moiety interacts with Thr 24 and Lys 50. The  $\epsilon$ -amino group of Lys 50 has a weaker interaction with the O8A atom (3.2 Å) and the O9A atom (3.0 Å), while the hydroxyl group of Thr 24 has a strong interaction with the O8A atom (2.5 Å). The two phosphates between adenosine and pantetheine are stabilized by residues Lys 26, Gln 27 and two water molecules. The amide group of Lys 26 interacts with the O2A atom (3.1 Å) in one phosphate, while the other phosphate interacts with water molecules (2.7 Å to O5A, 2.9 Å to O4A) and amide group of Gln 27 (2.9 Å to O4A). In the pantetheine moiety of CoA, one hydroxyl atom, OAP forms weak hydrogen bonds with two water molecules (2.9 Å and 3.0 Å), the other hydroxyl atom O9P forms hydrogen bond with amide group of Glu 105, and the N8P atom is stabilized by a water molecule with a weak hydrogen bond (3.1 Å). The pantetheine part

of CoA shows no electron density ( $F_o-F_c$  map) for atoms C5P, C6P, C7P and O5P and does not display any hydrogen bonds with GTPSCS, suggesting disorder for this part of CoA.

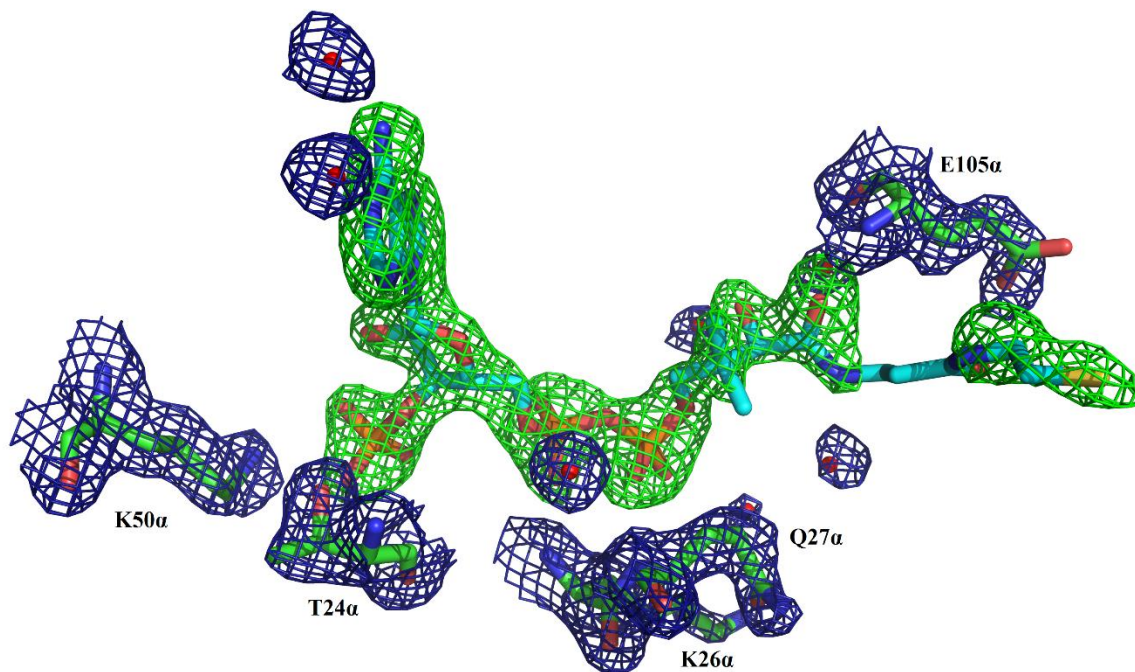


**Figure 3.11** The electron density around CoA in GTPSCS obtained from X-ray diffraction. The green electron density refers to the  $F_o-F_c$  map, which has a contour level of 3.0 r.m.s.d. This map shows electron density for the ligand, CoA (cyan carbon atoms). The blue electron density refers to the  $2F_o-F_c$  map, which has a contour level of 1.0 r.m.s.d. The  $2F_o-F_c$  map shows GTPSCS residues (green carbon atoms) and water molecules (red spheres) that interact with CoA. Nitrogen atoms are colored blue, oxygen atoms are colored red, phosphorus atoms are colored orange and sulfur atom is colored gold.

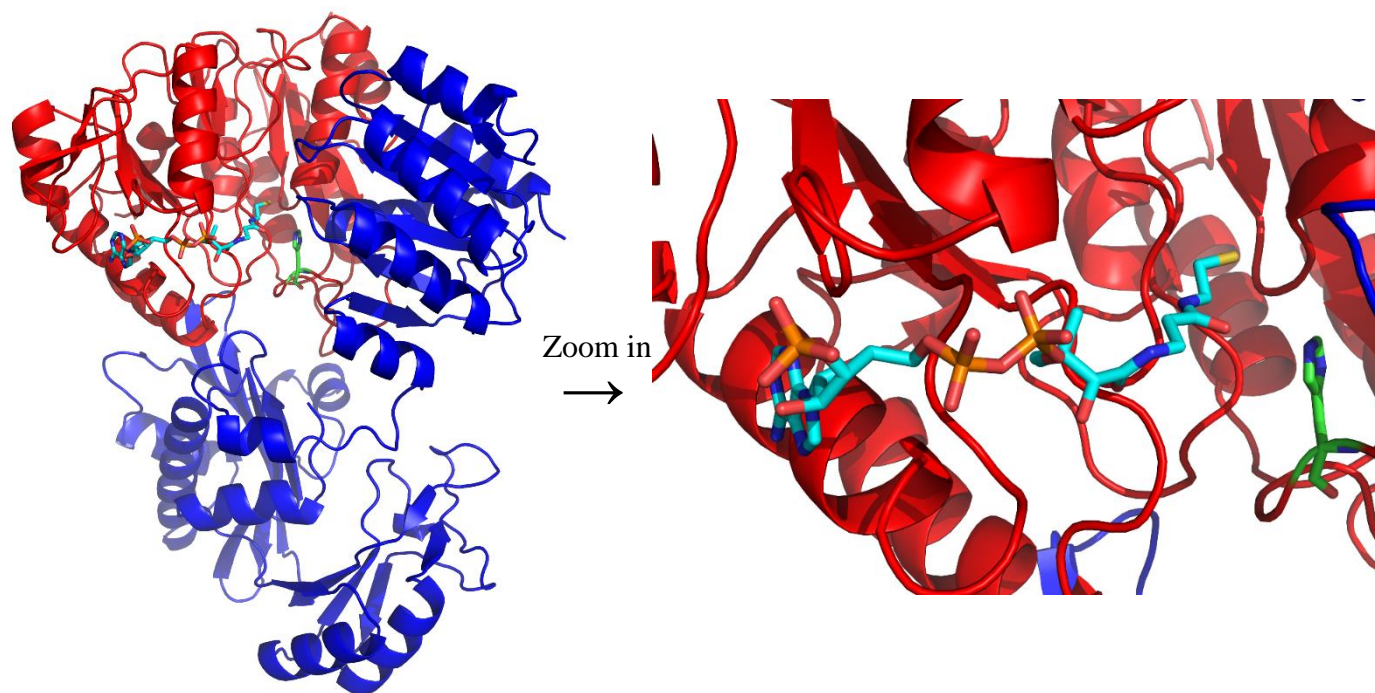


**Figure 3.12** The overall structure of GTPSCS in complex with CoA. The  $\alpha$ -subunit is drawn in red and the  $\beta$ -subunit is blue. GTPSCS is displayed as a ribbon diagram, while CoA and the active site histidine residue of GTPSCS are displayed as sticks. Carbon atoms are coloured cyan for CoA and green for the histidine residue, nitrogen atoms are blue, oxygen atoms are red, phosphorus atoms are orange and the sulfur atom is gold. The figure on the right shows a close-up view of the CoA-binding site.

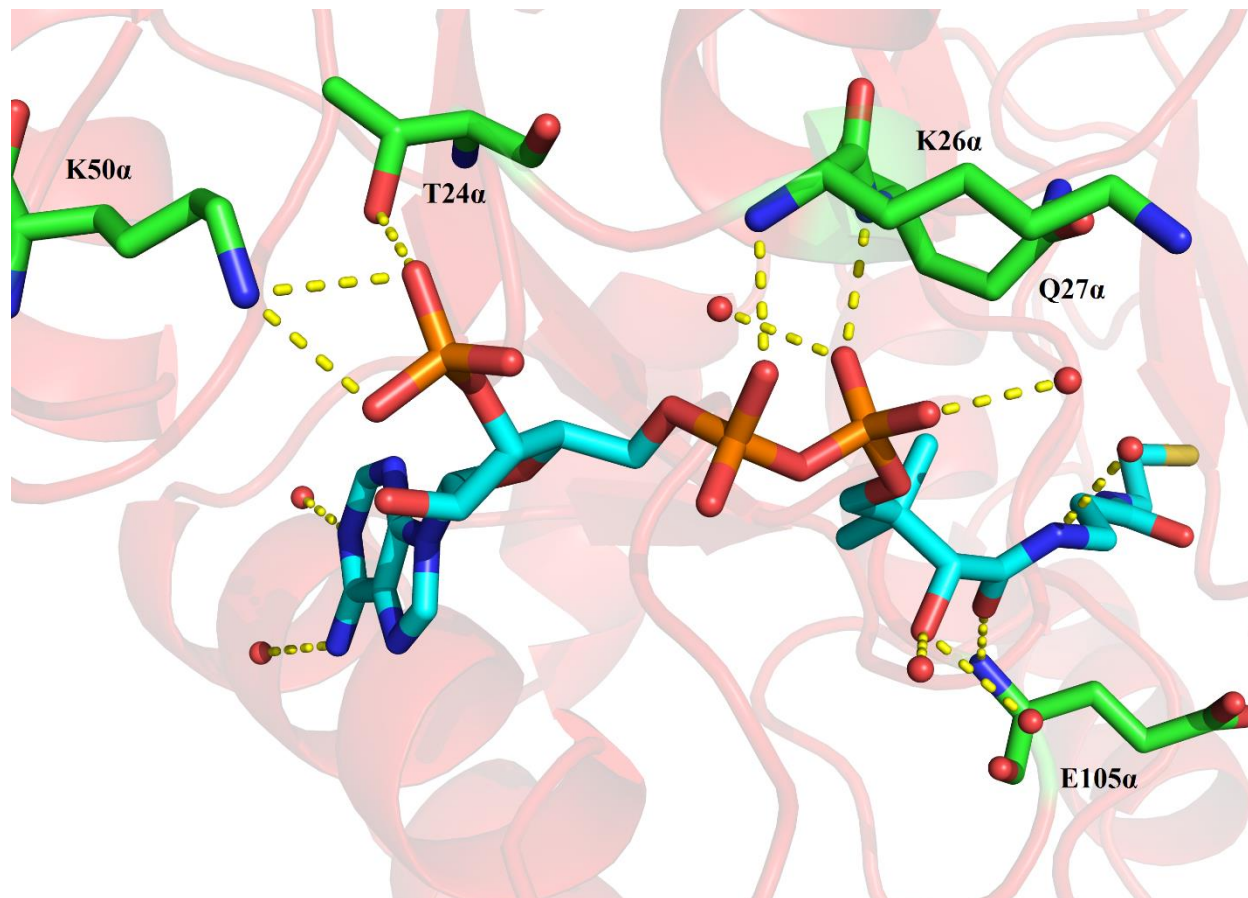


**Figure 3.13** The interactions between CoA and GTPSCS. The  $\alpha$ -subunit is drawn in red and displayed as a ribbon diagram, while CoA and specific GTPSCS residues are displayed as sticks. Carbon atoms are coloured cyan for CoA and green for GTPSCS residues, nitrogen atoms are colored blue, oxygen atoms are colored red, phosphorus atoms are colored orange and the sulfur atom is colored gold. Red spheres represent water molecules. The hydrogen bonds between CoA and GTPSCS residues or water molecules are indicated with yellow dashed lines.

**Table 3.4 X-ray diffraction data collection and processing of GTPSCS/CoA complex.**

Diffraction source	Canadian Light Source 08ID-1 beamline
Wavelength (Å)	0.97795
Temperature (K)	100 K
Detector	Rayonix MX300 CCD
Crystal-detector distance (mm)	250
Roatation range per image (°)	0.5
Exposure time per image (s)	1
Total rotation range (°)	150
Space group	P2 <sub>1</sub>
<i>a, b, c</i> (Å)	86.34, 82.50, 49.38
<i>α, β, γ</i> (°)	90.00, 104.25, 90.00
Mosaicity (°)	1.21
Resolution range (Å)	41.25-2.10 (2.21-2.10)
Total number of reflections	114697 (15619)
Number of unique reflections	36903 (5192)
Completeness (%)	94.6 (91.6)
Mean <I/σ(I)>	5.9 (2.6)
<i>R</i> <sub>merge</sub> (%)	11.5 (45.4)
Mn (I) half set-correlation CC (1/2)	98.6 (79.2)

Note: values for the outer shell are given in parentheses.

**Table 3.5 Structure refinement of GTPSCS/CoA complex.**

Final <i>R</i> <sub>work</sub> (%)	0.1836
Final <i>R</i> <sub>free</sub> (%)	0.2336
r.m.s.d. bond lengths (Å)	0.003
r.m.s.d. bond angles(°)	0.797
Ramachandran favored (%)	97.5



### 3.5.2 Succinate-binding site of GTPSCS

The X-ray diffraction result shows green electron density ( $F_o-F_c$  map) near the active site residue His 259 $\alpha$ . This electron density can be fitted with succinate, water molecules and a magnesium ion (Figure 3.14). The data processing and refinement results are listed in Table 3.6 and Table 3.7. Based on the  $F_o-F_c$  map, we identified that the succinate-binding site of GTPSCS is located in the C-terminal domain of  $\beta$ -subunit (Figure 3.15). The non-reactive carboxyl group of succinate interacts with Tyr 167 of the  $\alpha$ -subunit and Asn 271, Gly 328, Ile 329, Val 330 of the  $\beta$ -subunit. The reactive carboxyl group of succinate is stabilized by three water molecules, one magnesium ion and residue Gly 298 from the  $\beta$ -subunit (Figure 3.16). Hydrogen bonds are formed between residues of GTPSCS or water molecules and succinate (two hydrogen-bonded atoms are within 3.2 Å of each other), while an electrostatic interaction exists between the magnesium ion and succinate (Figure 3.16). Residues Asn 271 $\beta$ , Gly 328 $\beta$  and Val330 $\beta$  interact with one oxygen atom in non-reactive carboxyl group. Gly 328 $\beta$  has the strongest interaction (2.6 Å) while Asn 271 $\beta$  has the weakest (3.1 Å). Residues Tyr 167 $\alpha$  and Ile 329 $\beta$  interact with the other oxygen atom in non-reactive carboxyl group. They both have a similar distance to the oxygen atom (2.7 Å and 2.8 Å). Gly 298 $\beta$  is the only residue in GTPSCS that interacts with the reactive carboxyl group of succinate. The magnesium ion has octahedral coordination with four water molecules and oxygen atom from each of the one inorganic phosphate and the succinate. The distance between this magnesium ion and the succinate oxygen is 2.2 Å.

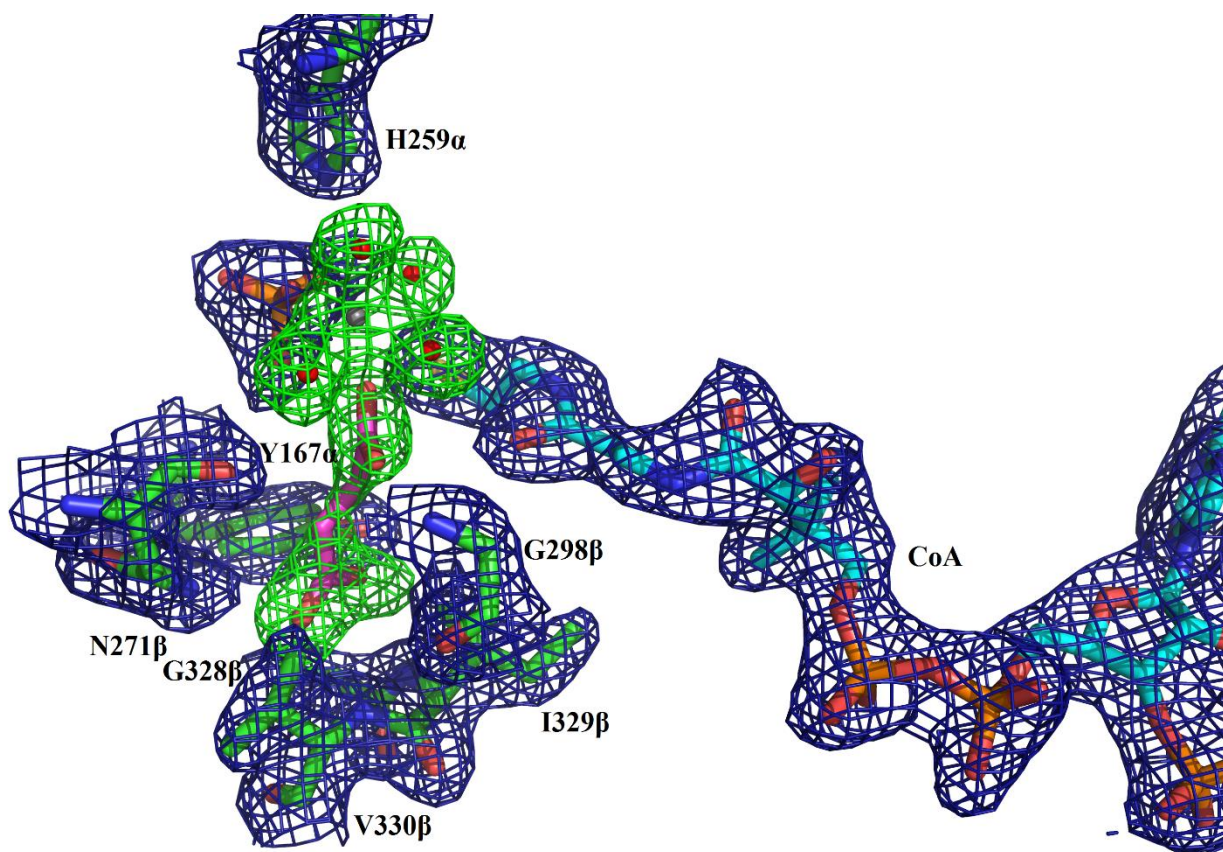


**Figure 3.14** The electron density around succinate in GTPSCS obtained from X-ray diffraction. The green electron density refers to the  $F_o-F_c$  map, which has a contour level of 3.0 r.m.s.d. The  $F_o-F_c$  map shows the ligand, succinate (magenta carbon atoms), water molecules (red spheres) and a magnesium ion (grey sphere). The blue electron density refers to the  $2F_o-F_c$  map, which has a contour level of 1.0 r.m.s.d. The  $2F_o-F_c$  map shows CoA (cyan carbon atoms), His 259 $\alpha$  and other GTPSCS residues interacting with succinate (green carbon atoms). Nitrogen atoms are colored blue, oxygen atoms are colored red, phosphorus atoms are colored orange and sulfur atom is colored gold.

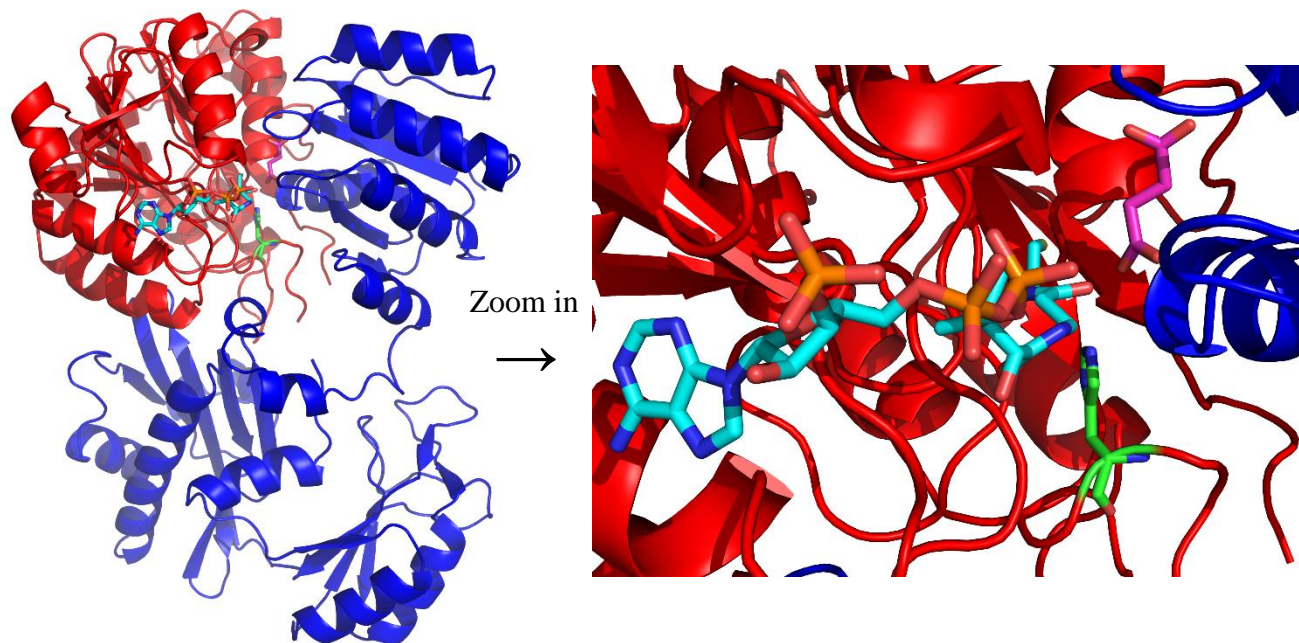


**Figure 3.15** The overall structure of GTPSCS in complex with succinate and CoA. The  $\alpha$ -subunit is drawn in red and the  $\beta$ -subunit is blue. GTPSCS is displayed as a ribbon diagram, while succinate, CoA and the active site histidine residue of GTPSCS are displayed as sticks. Carbon atoms are coloured magenta for succinate (shown in sticks), cyan for CoA (shown in sticks) and green for the His 259 $\alpha$ . Nitrogen atoms are blue, oxygen atoms are red, phosphorus atoms are orange and the sulfur atom is gold. The figure on the right shows a close-up view of the succinate-binding site.

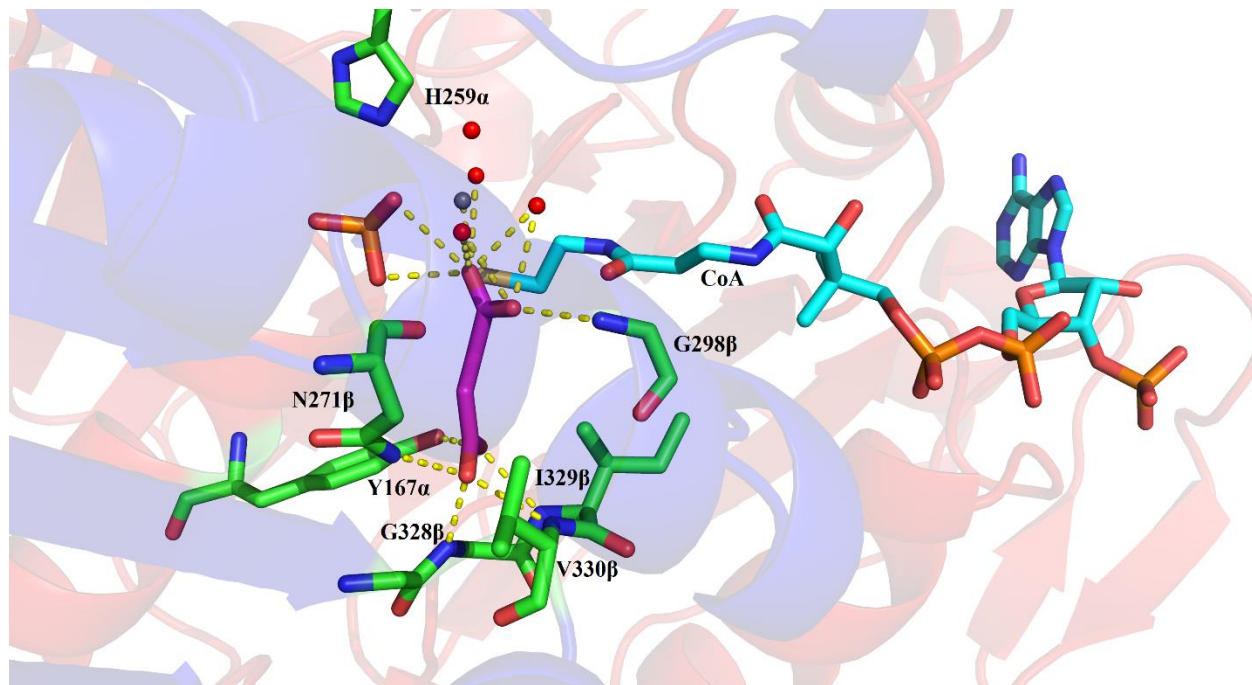


**Figure 3.16** The interactions between succinate and GTPSCS. The  $\alpha$ -subunit is drawn in red and the  $\beta$ -subunit is blue. GTPSCS is displayed as a ribbon diagram, while succinate, CoA and specific GTPSCS residues are displayed as sticks. Carbon atoms are coloured magenta for succinate, cyan for CoA and green for GTPSCS residues. Nitrogen atoms are colored blue, oxygen atoms are colored red, phosphorus atoms are colored orange and the sulfur atom is colored gold. Red spheres represent water molecules and the grey sphere is the magnesium ion. The hydrogen bonds and electrostatic interactions are indicated with yellow dashed lines.

**Table 3.6 X-ray diffraction data collection and processing of GTPSCS/succinate/CoA complex.**

Diffraction source	Canadian Light Source 08B1-1 beamline
Wavelength (Å)	0.9794
Temperature (K)	100 K
Detector	Rayonix MX300HE CCD
Crystal-detector distance (mm)	290
Roatation range per image (°)	0.5
Exposure time per image (s)	3
Total rotation range (°)	180
Space group	P2 <sub>1</sub>
<i>a, b, c</i> (Å)	86.67, 81.02, 50.78
<i>α, β, γ</i> (°)	90.0, 104.9, 90.0
Mosaicity (°)	1.54
Resolution range (Å)	58.23-2.20 (2.32-2.20)
Total number of reflections	122021 (16605)
Number of unique reflections	33544 (4750)
Completeness (%)	97.0 (94.6)
Mean $\langle I/\sigma(I) \rangle$	9.3 (2.6)
$R_{merge}$ (%)	9.6 (46.6)
Mn (I) half set-correlation CC (1/2)	99.5 (78.1)

Note: values for the outer shell are given in parentheses.

**Table 3.7 Structure refinement of GTPSCS/succinate/CoA complex.**

Final $R_{work}$ (%)	0.1680
Final $R_{free}$ (%)	0.2252
r.m.s.d. bond lengths (Å)	0.009
r.m.s.d. bond angles(°)	1.096
Ramachandran favored (%)	97.7

### 3.6 Site-directed mutagenesis of C332 $\beta$ A GTPSCS

In the structure of CoA-bound GTPSCS, 2-mercaptoethanol, which was used as the reducing agent, was covalently attached to Cys 332 of the  $\beta$ -subunit. This residue lies close to the predicted succinate-binding site (Gly 327 $\beta$  - Val 330 $\beta$ ). Because of this, Cys 332 $\beta$  was mutated to Ala 332 $\beta$  to prevent disruption of the binding site by a disulfide bond. Sequencing of the genes for the two subunits of GTPSCS showed only the codon for Cys 332 $\beta$  had been changed and it was correctly changed to that for Ala 332 $\beta$  (Figure 3.17).

```

                                Cys
Query  3366  TTGGTGGAAATCGTCAACTGTGCCATCATTGCCAATGGGATCACCAAAGCATGCCGGGAGC  3425
                   |||
Sbjct  469   TTGGTGGAAATCGTCAACGCTGCCATCATTGCCAATGGGATCACCAAAGCATGCCGGGAGC  528
                   |||
                                Ala
```

**Figure 3.17 Alignment of the mutated plasmid sequence (Sbjct) with the wild type plasmid (Query). Only Cys 332 $\beta$  of GTPSCS has been mutated to alanine.**

#### 3.6.1 Purification of C332 $\beta$ A GTPSCS

##### 3.6.1.1 Ni-NTA affinity column

The 9% SDS-PAGE gel (Figure 3.18) shows the result after this purification step. Two major bands are seen from lanes 3 to 9. These lanes contained samples from the fractions eluted with 100 mM imidazole. Compared with the PAGERuler ladder in lane 1, these two major bands are between 30-40 kDa and 40-50 kDa on the gel.

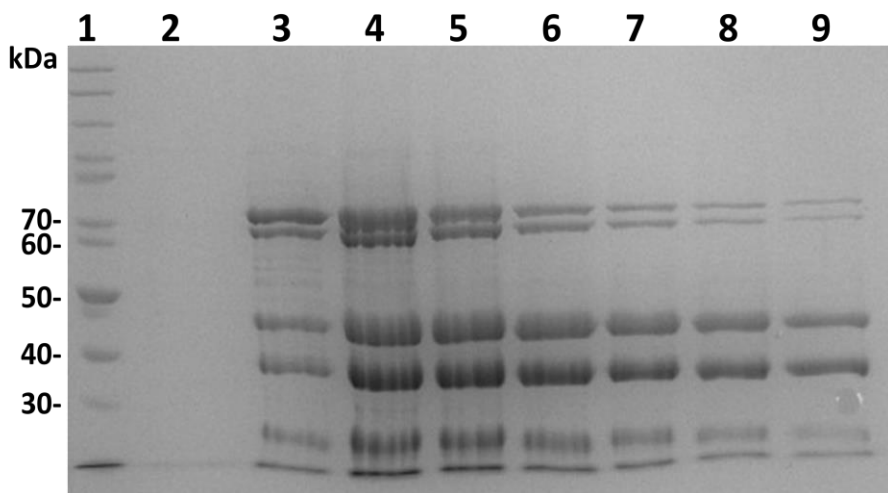


**Figure 3.18 9% SDS-PAGE gel showing Ni-NTA column purification of C332 $\beta$ A GTPSCS. Lane 1 is Pageruler ladder (5  $\mu$ L, BIO BASIC INC). Lane 2 refers to the last wash fraction using 30 mM imidazole (20  $\mu$ L). Lanes 3-9 are fractions eluted with 100 mM imidazole (each lane 20  $\mu$ L).**

### ***3.6.1.2 Superdex-200 pg column***

The major peak (UV absorbance at 280 nm) on the chromatogram (Figure 3.19) appeared between fractions C4 and C6. The 9% SDS-PAGE gel shows the result from fractions B3, B4, B8, B10, C2, C4, C5, C6 and C7. Only fractions C4, C5 and C6 have two dense bands located between 30-40 kDa and 40-50 kDa, which are the expected molecular weights for the subunits of GTPSCS.

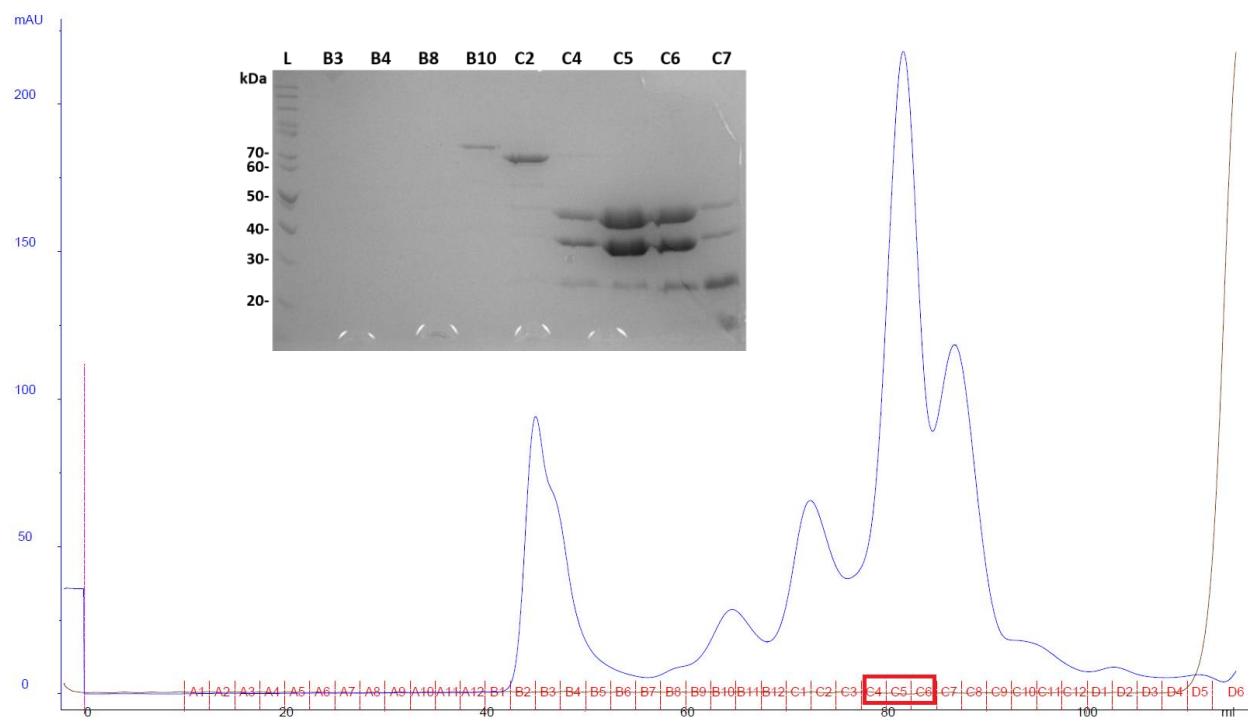


**Figure 3.19 Chromatogram of Superdex-200 pg column showing UV absorbance at 280 nm versus elution volume for C332βA GTPSCS. The blue line refers to UV absorbance at 280 nm, the brown line is the conductivity and the pink line marks the sample injection. The SDS-PAGE gel (9%) displayed on the chromatogram shows the result of fractions B3, B4, B8, B10, C2, C4, C5, C6 and C7 (20 μL each sample) in comparison with the Pageruler ladder (5 μL, BIO BASIC INC) in lane L.**

### ***3.6.1.3 Hitrap Blue High Performance affinity column***

The chromatogram for the elution of the Hitrap Blue HP affinity column shows a peak in the absorbance at 280 nm, which appears when the concentration of salt, and hence the conductivity, is gradually increased (Figure 3.20). The 9% SDS-PAGE gel shows only two bands



in the lanes corresponding to the fractions B12 to C5. Compared with the PAGERuler ladder (Lane L), the molecular weights of these two bands are between 30-40 kDa and 40-50 kDa, which are consistent with the molecular weights of the  $\alpha$  and  $\beta$  subunits.

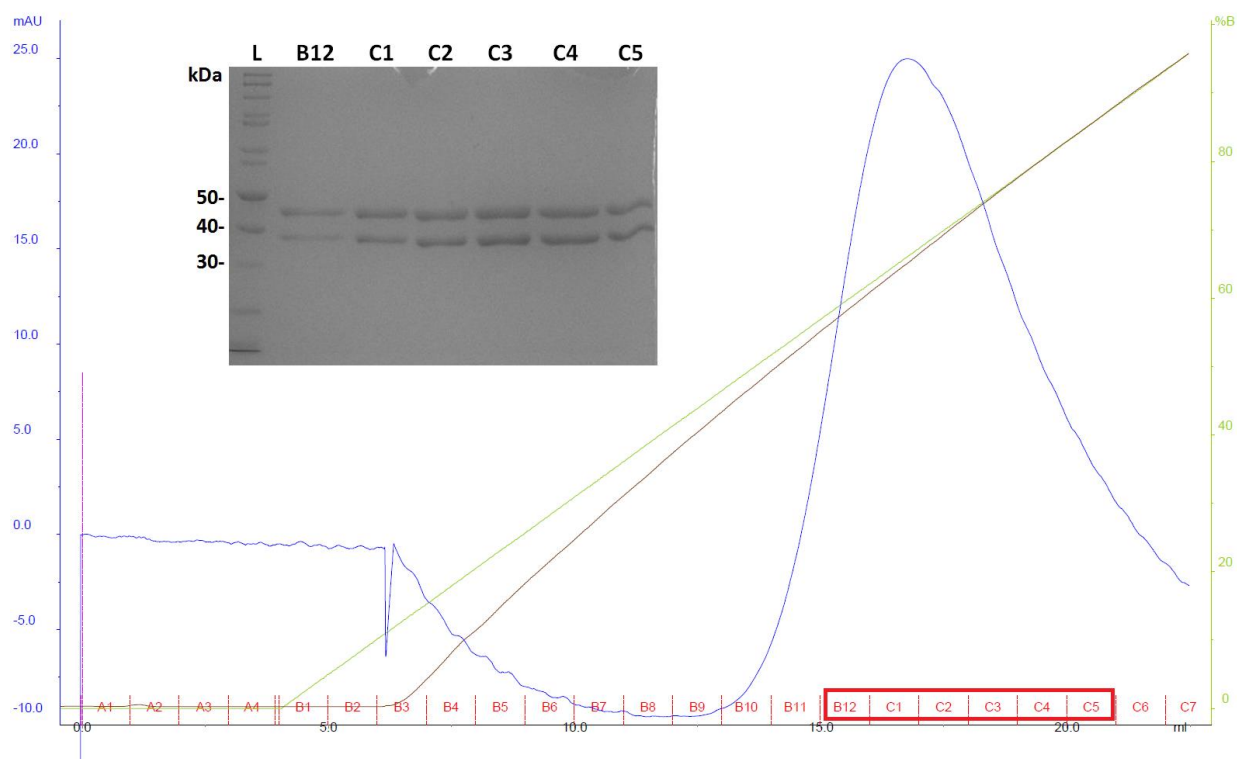


**Figure 3.20 Chromatogram of Hitrap Blue HP affinity column showing UV absorbance at 280 nm versus elution volume for C332 $\beta$ A GTPSCS. The blue line refers to UV absorbance at 280 nm, the brown line is the conductivity, the green line refers to the concentration of salt (NaCl) and the pink line marks the sample injection. The SDS-PAGE gel (9%) displayed on the chromatogram shows the result of fractions B12, C1, C2, C3, C4 and C5 (20  $\mu$ L each sample) in comparison with the PAGERuler ladder (5  $\mu$ L, BIO BASIC INC) in lane L.**

### 3.7 Kinetic studies of formate inhibition of wild type GTPSCS

The initial velocities for various concentrations of succinate with different concentrations of formate were used to calculate three Michaelis-Menten plots (Figure 3.21) in order to know whether formate would compete with succinate to bind to GTPSCS. Statistical results calculated using the program Graphpad Prism 5 are presented in Table 3.8. The R squared representing the goodness of fit are all above 0.99. The maximum velocity at each concentration of formate are slightly different, but overlapping at the 95% confidence interval. The value of the apparent  $K_m$  increased about 5 times and 17 times when formate concentration increased from 0 mM to 100 mM and 200 mM respectively.

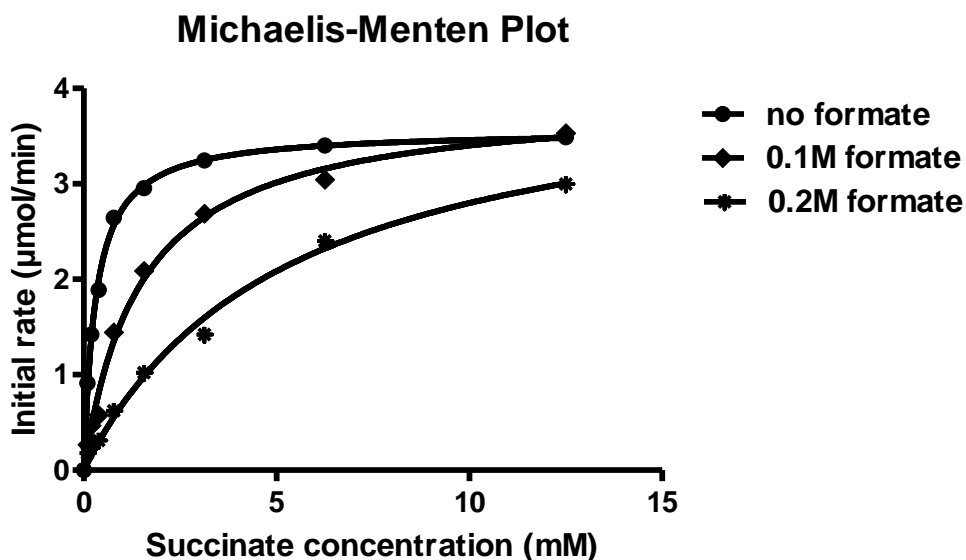


Figure 3.21 The Michaelis-Menten plots showing the initial rate ( $\mu\text{mol}/\text{min}$ ) of GTPSCS as a function of various succinate concentrations (mM). Three curves were obtained in the presence of 0 mM, 100 mM and 200 mM formate.

**Table 3.8 Statistical results from kinetic studies of formate inhibition.**

	0 mM formate	100 mM formate	200 mM formate
Apparent $K_m$ (mM)	0.30	1.48	5.21
Apparent $V_{max}$ ( $\mu\text{mol}/\text{min}$ )	3.56	3.90	4.26
R squared	0.9981	0.9936	0.9920
95% Confidence Intervals			
Apparent $K_m$ (mM)	0.27-0.34	1.11-1.84	3.40-7.03
Apparent $V_{max}$ ( $\mu\text{mol}/\text{min}$ )	3.48-3.65	3.60-4.21	3.58-4.93

## Chapter Four: Discussion

### 4.1 Purification of GTPSCS

Wild type GTPSCS with high purity was obtained through a three-column purification. Three SDS-PAGE gels show the progress of the purification, achieving the goal of two clean bands between 30-40 kDa and 40-50 kDa. These two clean bands correspond to the  $\alpha$  and  $\beta$  subunits of GTPSCS. The conclusion that these samples contained GTPSCS was supported by the enzyme activity measured using the kinetic assay. The chromatogram resulting from the Superdex-200 pg column showed a major 280 nm absorbance peak at the elution volume of 82 mL, whose molecular weight has been estimated around 63 kDa using the Superdex-200 pg column calibration curve. The Bradford assay and kinetic assay were used to measure protein concentration and enzyme activity after each column purification step. Specific activity increased 22-fold from the cell lysate to the high purity protein, which is a reasonable result compared with Fraser *et al*<sup>45</sup>.

The C332 $\beta$ A mutant GTPSCS was not successfully obtained at high purity in significant quantity through a three-column purification. After the last step, two faint bands representing the  $\alpha$  and  $\beta$  subunits were seen on the SDS-PAGE gel, the chromatogram showed only a low value for the 280 nm absorbance and the sample had low enzyme activity. These all indicate that very little target protein had been obtained. The total activity of the mutant enzyme in the cell lysate was only half the value found with wild type GTPSCS. However, Mann *et al.* determined that mutation of the comparable residue, Cys 325 $\beta$  in *E. coli* SCS, did not affect enzyme activity. This is why they concluded that Cys 325 $\beta$  was not an essential residue in the active site of *E. coli* SCS<sup>62</sup>. Therefore, my interpretation is that the mutant GTPSCS was not correctly folded when

produced in *E. coli*. The conditions for protein overproduction in *E. coli* may not have been optimal.

## 4.2 CoA-binding site of GTPSCS

Succinyl-CoA synthetase is composed of  $\alpha$  and  $\beta$  subunits. The  $\alpha$ -subunit contains domain 1, the N-terminal domain, and domain 2, the C-terminal domain, while the  $\beta$  subunit contains domain 3 and 4, which together form the N-terminal domain, and domain 5, the C-terminal domain.

In the crystal structure, the CoA-binding site was located in the N-terminal domain of the  $\alpha$ -subunit of GTPSCS. CoA binds to GTPSCS in much the same way that it binds to *E. coli* SCS. Comparison of the structure of CoA-bound GTPSCS with CoA-bound *E. coli* SCS can give a better understanding of how CoA interacts with different SCSs. Superposition of the N-terminal domains of the  $\alpha$ -subunits of *E. coli* SCS/CoA complex (PDB code 2SCU) and GTPSCS/CoA complex gives a root-mean-square deviation (r.m.s.d.) of 0.70 Å based on 112 C $\alpha$  atoms. The interactions between CoA and the two different SCSs are very similar, except one residue Ser 18 $\alpha$  in *E. coli* SCS is substituted by Lys 26 $\alpha$  in GTPSCS (Table 4.1). However, CoA interacts with the amide groups of Ser 18 $\alpha$  or Lys 26 $\alpha$  (Figure 4.2), so the different side chains do not have a negative impact on the interaction. In both structures, hydrophobic interactions exist between the adenine ring of CoA and two hydrophobic residues, Pro 40 $\alpha$  and Val 72 $\alpha$  of *E. coli* SCS, and Pro 48 $\alpha$  and Val 80 $\alpha$  of GTPSCS, on either face of the adenine ring (Figure 4.1). However, the adenine ring of CoA is stabilized by two water molecules in GTPSCS/CoA complex, while only one water molecule interacts with the adenine ring of CoA in *E. coli* SCS/CoA complex (Figure 4.1). This is probably because of the difference in resolution between these two

structures. At higher resolution, more water molecules can be fitted in the electron density. The 3'-phosphoryl group of ribose of the two CoA molecules is stabilized by Thr 24 $\alpha$  and Lys 50 $\alpha$  in GTPSCS, and the corresponding residues, Thr 16 $\alpha$  and Lys 42 $\alpha$ , in *E. coli* SCS. However, the side chain conformation of Lys 50 $\alpha$  in GTPSCS is different from that of Lys 42 $\alpha$  in *E. coli* SCS (Figure 4.1). This slight conformational change of Lys 50 $\alpha$  leads to weak hydrogen bonds with the 3'-phosphoryl group. The 5'-diphosphate of CoA has interactions with Lys 26 $\alpha$ , Gln 27 $\alpha$  and two water molecules in GTPSCS, and with the corresponding residues, Ser 18 $\alpha$ , Gln 19 $\alpha$  and three water molecules, instead in *E. coli* SCS (Figure 4.2). This difference suggests a stronger interaction between the 5'-diphosphate and *E. coli* SCS. The pantetheine moiety of CoA shows interactions with Glu 105 $\alpha$  and three water molecules in GTPSCS, and with Ile 95 $\alpha$ , Glu 97 $\alpha$  and two water molecules in *E. coli* SCS (Figure 4.3). The additional residue Ile 95 $\alpha$  forms a hydrogen bond with *E. coli* SCS, while the corresponding residue Ile 103 $\alpha$  does not interact in GTPSCS. This may be due to the disorder in the free thiol end of CoA.

Disorder of the CoA is indicated by the absence of continuous electron density from C7P to the terminal thiol. This disorder may be due to the formation of a disulfide bond between the sulfhydryl group of CoA and Cys 132 $\alpha$ . This residue corresponds to Cys 123 $\alpha$  in *E. coli* SCS. It was reported that the side chain of Cys 123 $\alpha$  in *E. coli* SCS can flip to the other side to form a disulfide bond with the sulfhydryl group of CoA<sup>44</sup>. This leads to an alternative conformation of the sulfhydryl end of CoA in *E. coli* SCS. Similarly, extra electron density in the F<sub>o</sub>-F<sub>c</sub> map (Figure 3.11) is observed for residue Cys 132 $\alpha$  in GTPSCS, suggesting that an alternative conformation of Cys 132 $\alpha$  exists. Therefore, an alternative conformation of the sulfhydryl end of CoA maybe forming a disulfide bond with the side chain of Cys 132 $\alpha$ . This results in partial occupancy of the modelled sulfhydryl end of CoA in the electron density. The reason for having

this disulfide bond is not clear. One explanation is that it might inhibit the catalytic reaction, because the free thiol end of CoA would not be available to continue the third step in the proposed catalytic mechanism. However, since there is no evidence to support the idea that Cys 132 $\alpha$  can also form a disulfide bond with CoA in physiological conditions, the disulfide bond may only be formed when there is not enough reducing agent in the crystallization conditions.

**Table 4.1 The comparison of the interactions of CoA with GTPSCS and *E. coli* SCS.**

<b><i>E. coli</i> SCS in complex with CoA</b>			<b>GTPSCS in complex with CoA</b>		
CoA atom	<i>E. coli</i> SCS residue	Type of interaction	CoA atom	GTP SCS residue	Type of interaction
O7A	Thr 16 $\alpha$	Hydrophilic	O8A	Thr 24 $\alpha$	Hydrophilic
O1A and O4A	Ser 18 $\alpha$	Hydrophilic	O2A	Lys 26 $\alpha$	Hydrophilic
O4A	Gln 19 $\alpha$	Hydrophilic	O4A	Gln 27 $\alpha$	Hydrophilic
Adenine ring	Pro 40 $\alpha$	Hydrophobic	Adenine ring	Pro 48 $\alpha$	Hydrophobic
O7A	Lys 42 $\alpha$	Hydrophilic	O9A and O8A	Lys 50 $\alpha$	Hydrophilic
Adenine ring	Val 72 $\alpha$	Hydrophobic	Adenine ring	Val 80 $\alpha$	Hydrophobic
N4P	Ile 95 $\alpha$	Hydrophilic	-	-	-
O9P	Glu 97 $\alpha$	Hydrophilic	O9P	Glu 105 $\alpha$	Hydrophilic

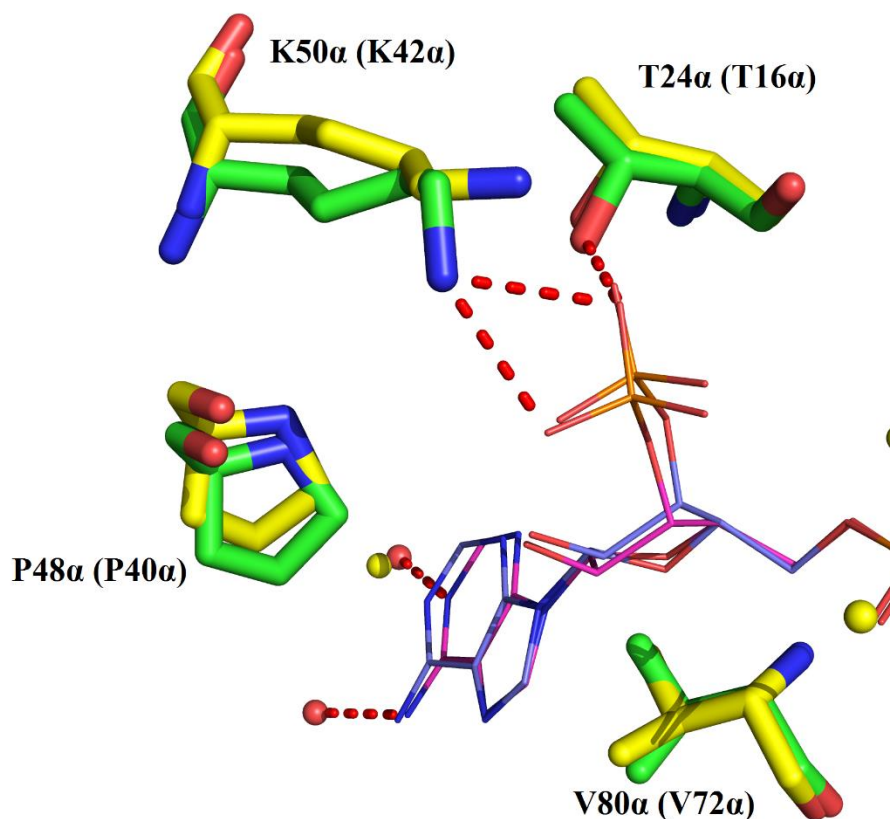


**Figure 4.1 Superposition of the N-terminal domains from  $\alpha$ -subunits of the GTPSCS/CoA complex and the *E. coli* SCS/CoA complex (PDB code 2SCU) in viewing 3'-phosphoadenosines of CoA. The carbon atoms are colored light blue for CoA bound to *E. coli* SCS, magenta for CoA bound to GTPSCS, yellow for *E. coli* SCS and green for GTPSCS. Residue labels for *E. coli* SCS are shown in parentheses and those for GTPSCS are shown outside the parentheses. Nitrogen atoms are blue, oxygen atoms are red, phosphorus atoms are orange, red spheres represent the water molecules in the GTPSCS/CoA complex, and yellow spheres represent the water molecules in the *E. coli* SCS/CoA complex. Red dashed lines indicate hydrogen bonds between CoA and GTPSCS.**



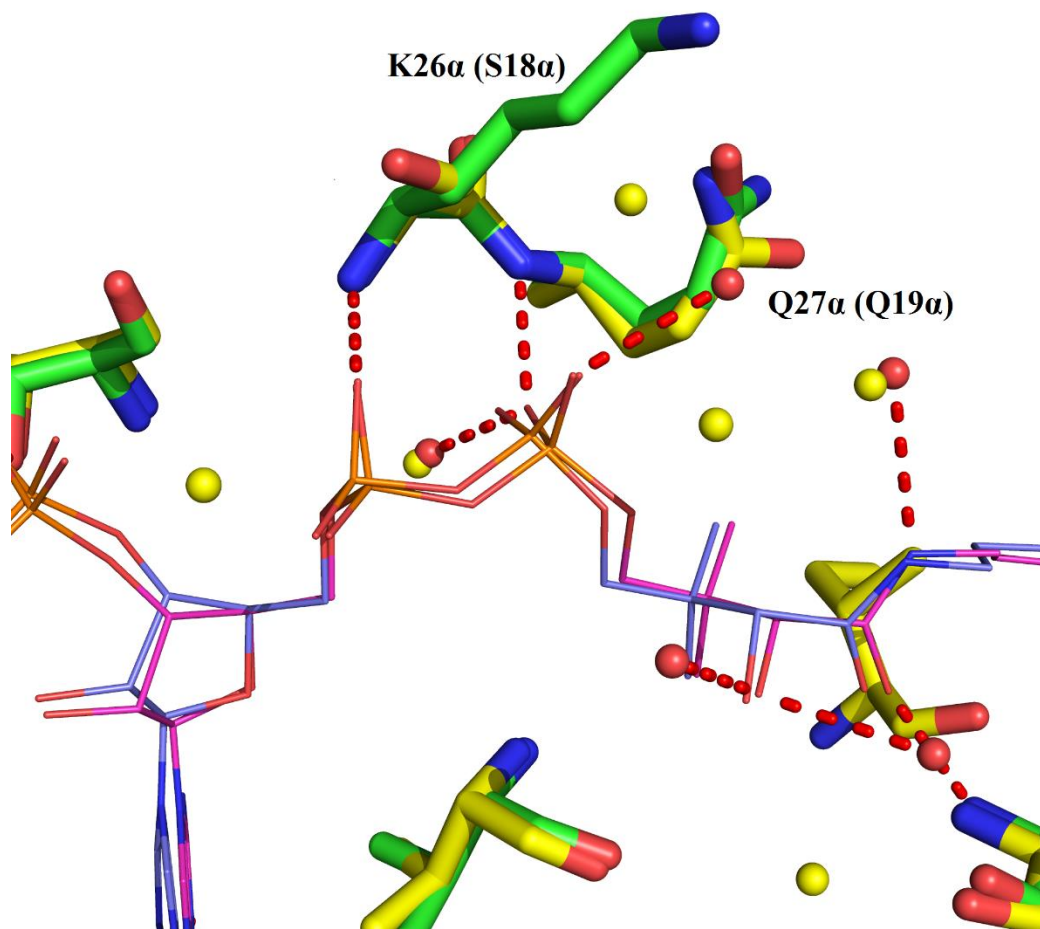


Figure 4.2 Superposition of the N-terminal domains from  $\alpha$ -subunits of the GTPSCS/CoA complex and the *E. coli* SCS/CoA complex (PDB code 2SCU) in viewing 5' diphosphates of CoA. The carbon atoms are colored light blue for CoA bound to *E. coli* SCS, magenta for CoA bound to GTPSCS, yellow for *E. coli* SCS and green for GTPSCS. Residue labels for *E. coli* SCS are shown in parentheses and those for GTPSCS are shown outside the parentheses. Nitrogen atoms are blue, oxygen atoms are red, phosphorus atoms are orange, red spheres represent the water molecules in the GTPSCS/CoA complex, and yellow spheres represent the water molecules in the *E. coli* SCS/CoA complex. Red dashed lines indicate hydrogen bonds between CoA and GTPSCS.

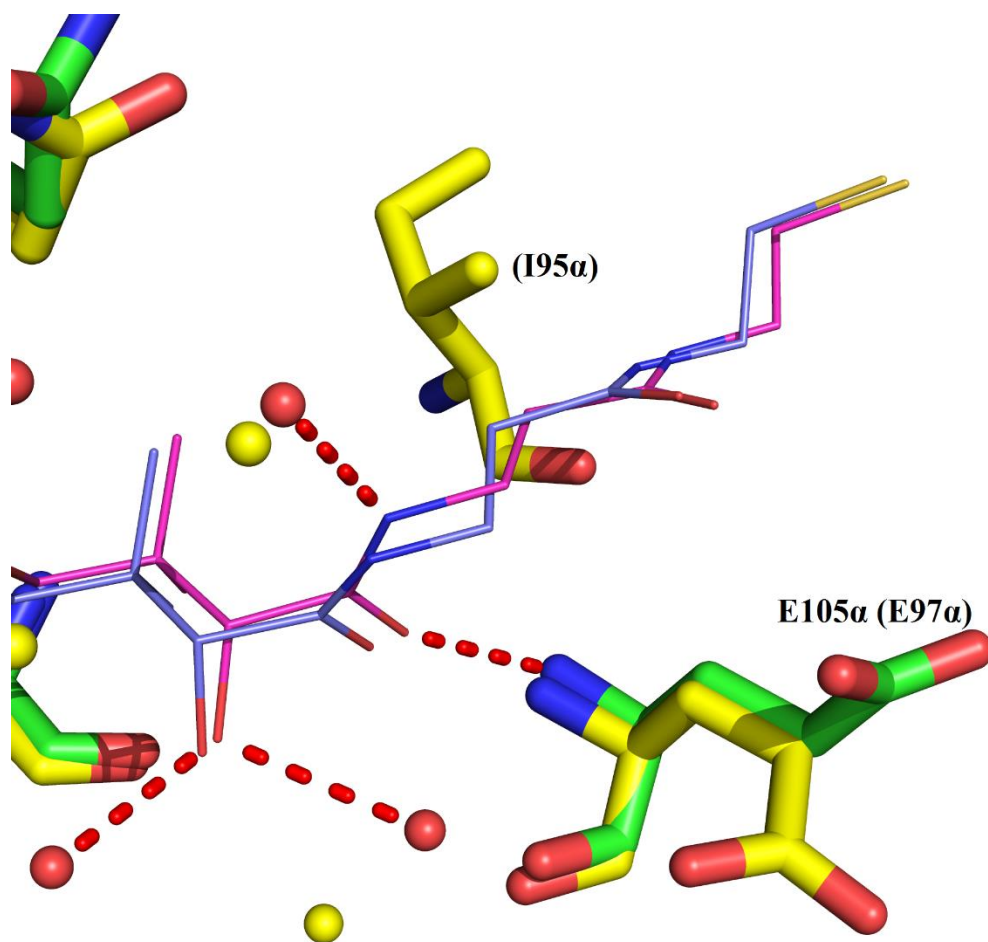
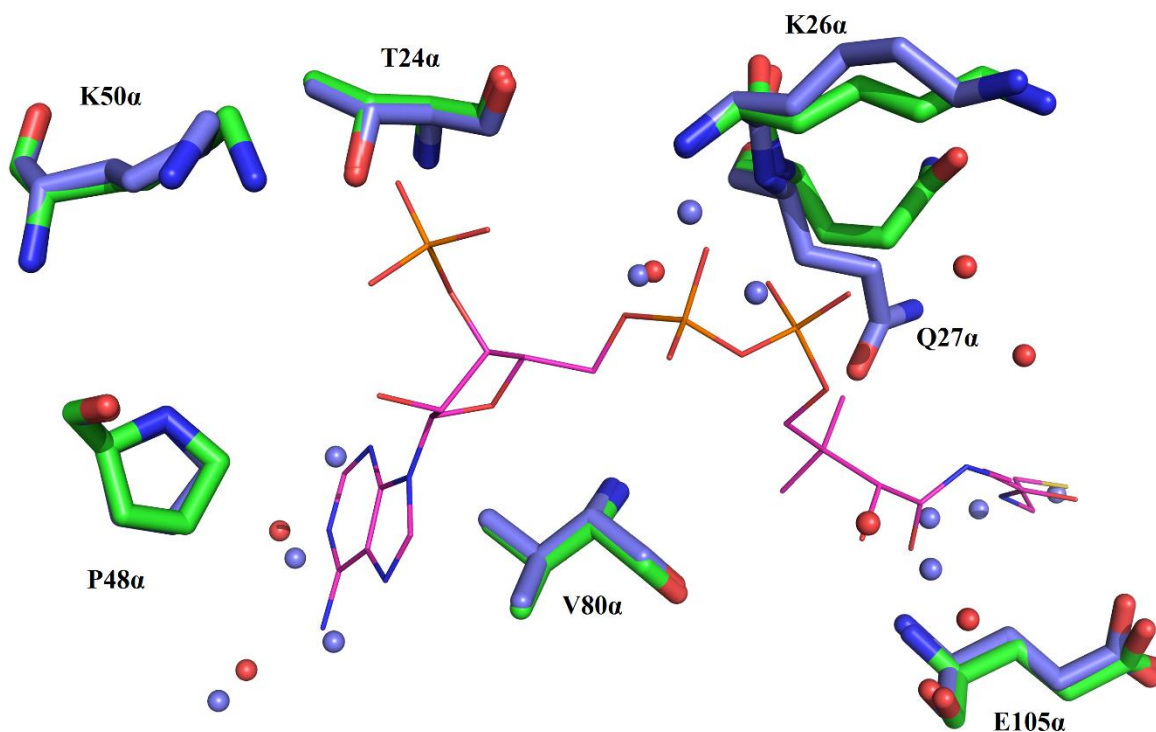


Figure 4.3 Superposition of the N-terminal domains from the  $\alpha$ -subunits of the GTPSCS/CoA complex and the *E. coli* SCS/CoA complex (PDB code 2SCU) in viewing pantetheine moiety of CoA. The carbon atoms are colored light blue for CoA bound to *E. coli* SCS, magenta for CoA bound to GTPSCS, yellow for *E. coli* SCS and green for GTPSCS. Residue labels for *E. coli* SCS are shown in parentheses and those for GTPSCS are shown outside the parentheses. Nitrogen atoms are blue, oxygen atoms are red, phosphorus atoms are orange, red spheres represent the water molecules in the GTPSCS/CoA complex, and yellow spheres represent the water molecules in the *E. coli* SCS/CoA complex. Red dashed lines indicate hydrogen bonds between CoA and GTPSCS.

Comparison of the structures of CoA-bound GTPSCS with apo GTPSCS can help to better understand how the conformation of the structure changes when the CoA molecule binds. Superposition of the N-terminal domain (residues 2-131) of the  $\alpha$ -subunit of the GTPSCS/CoA complex with that of dephosphorylated GTPSCS (PDB code 1EUC) shows r.m.s.d. 0.20 Å based on 130 C $\alpha$  atoms. The hydrophobic residues Pro 48 $\alpha$  and Val 80 $\alpha$  in the structure of 1EUC have almost identical conformations to the corresponding residues in the complex structure (Figure 4.4). The interaction between the 3' phosphate and the terminal nitrogen of Lys 50 $\alpha$  causes the slightly different side chain conformations (Figure 4.4). The most obvious difference that can be seen in the superposition is the conformational change in the side chains of residues Lys 26 $\alpha$  and Gln 27 $\alpha$  (Figure 4.4). However, CoA interacts with the backbone amide groups rather than the side chains. The only explanation for this visible change is that the side chain of Gln 27 $\alpha$  has to provide enough space for the CoA molecule to fit into the binding pocket. It is hard to interpret the conformational change of the Lys 26 $\alpha$  side chain. The other interesting discovery from this superposition is that some water molecules (shown by blue spheres in Figure 4.4) occupy the CoA binding site when CoA is absent. These water molecules are mainly located in positions corresponding to the adenine ring, the 5'-diphosphate and the sulfhydryl group at the end of CoA. They have very similar interactions with the protein residues that atoms of CoA have, which can be seen as the similar positions of these water molecules to the hydrogen-binding atoms of CoA. It is very possible that these water molecules stabilize the CoA-binding site residues in the absence of CoA. Therefore, it is proposed that when CoA binds to SCS, the water molecules in the CoA-binding site will be ejected and the side chain of Gln 27 $\alpha$  changes conformation to allow the pantetheine moiety of CoA to fit into the binding pocket.



**Figure 4.4 Superposition of the N-terminal domains (residues 2-131) from  $\alpha$ -subunits of GTPSCS/CoA complex and dephosphorylated GTPSCS (PDB code 1EUC). The superposition shows the conformational changes of side chains of the residues (shown as sticks) in the GTPSCS/CoA complex and 1EUC. The GTPSCS/CoA complex has green carbon atoms and 1EUC has light blue carbon atoms. CoA is shown in lines, with carbon atoms in magenta. Light blue spheres represent water molecules in 1EUC, and red spheres represent water molecules in the complex. Nitrogen atoms are blue, oxygen atoms are red and phosphorus atoms are orange.**

### 4.3 Succinate-binding site of SCS

#### 4.3.1 Comparison of the structure of succinate-bound GTPSCS with CoA-bound GTPSCS

Comparison of the structure of succinate- and CoA-bound GTPSCS (GTPSCS/succinate/CoA complex) with that of the CoA-bound GTPSCS can help to see the conformational changes in the succinate-binding domain when succinate binds. Superposition of the  $\alpha$ -subunits of these two complexes gives a r.m.s.d. 0.38 Å based on 303 C $\alpha$  atoms. Noticeable differences can be seen in the superposition of the C-terminal domains of the two structures (Figure 4.5). In general, the C-terminal domain of the GTPSCS/succinate/CoA complex moves towards the  $\alpha$ -subunit. Two  $\alpha$ -helices of the C-terminal domain adopt very different conformations. They move towards the  $\alpha$ -subunit when succinate binds, resulting in the obvious C-terminal domain motion. Hydrophobic residues (Phe 269 $\beta$ , Leu 296 $\beta$ , Phe 309 $\beta$ , Leu 311 $\beta$ , Ile 325 $\beta$  and Leu 352 $\beta$ ) located in the interface between the  $\beta$ -sheet and the  $\alpha$ -helices in the C-terminus of GTPSCS/succinate/CoA complex have different side chain conformations (Figure 4.6). These conformational changes may be necessary for the repositioning of the two succinate-binding loops. The first loop from Gly 328 $\beta$  to Val 330 $\beta$  in the GTPSCS/succinate/CoA complex was pushed closer to the active site and occludes the active site, so the C $\alpha$  atoms of Gly 328 $\beta$ , Ile 329 $\beta$  and Val 330 $\beta$  have distances of 3.7 Å, 5.3 Å and 5.7 Å from the corresponding residues in the superposition with CoA-bound GTPSCS (Figure 4.7). The conformational change of this succinate-binding loop allows interactions between succinate and GTPSCS. The second loop, which includes Gly 298 $\beta$ , was away from the position when succinate was absent. The C $\alpha$  atom of Gly 298 $\beta$  is about 4.6 Å away from the corresponding residue in the superposition with CoA complex (Figure 4.7). The conformational change of this loop is probably due to two reasons. First, it provides enough space for succinate to bind.

Second, it avoids steric clashes with the first loop. Because of the C-terminal domain motion, we can clearly find that the substrate succinate and the sulfydryl group end of CoA are buried in GTPSCS (Figure 4.8). These conformational changes indicate that the C-terminal domain has to adapt to accommodate the binding of succinate.

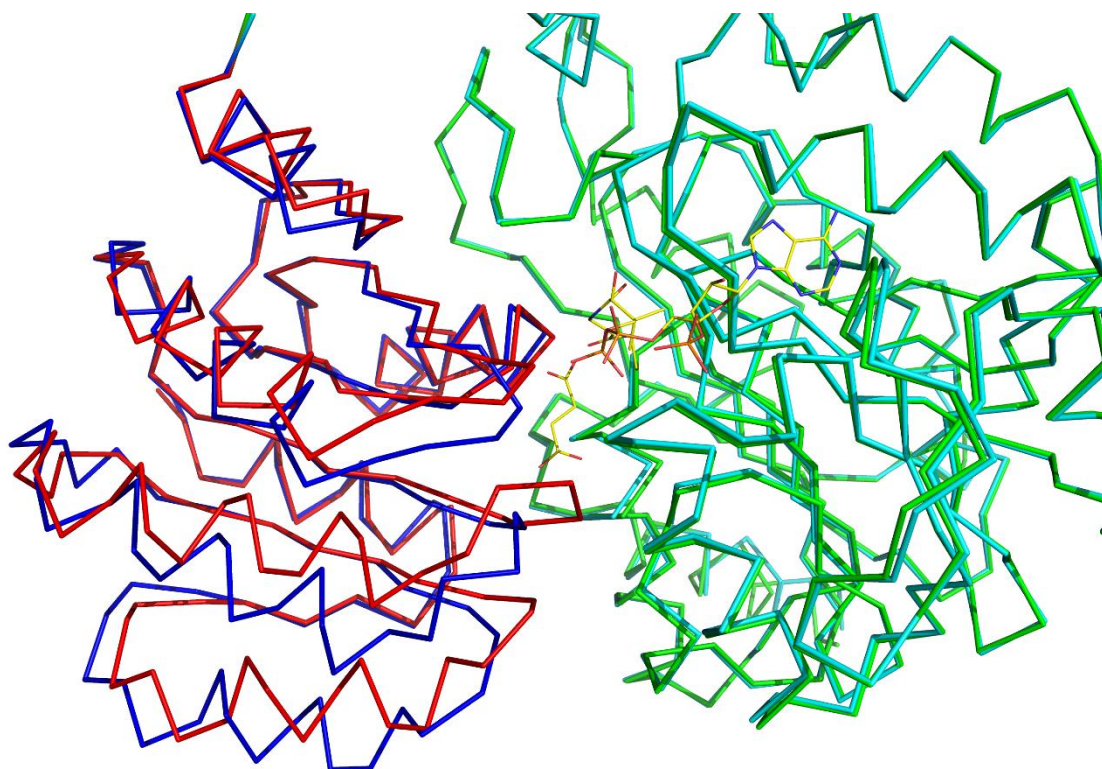


**Figure 4.5 Superposition of the GTPSCS/succinate/CoA complex and GTPSCS/CoA complex. The superposition is based on the  $\alpha$ -subunits (GTPSCS/CoA complex is in cyan and GTPSCS/succinate/CoA complex is in green) of these two structures. The C-terminal domain of the GTPSCS/CoA complex is displayed in blue, and of GTPSCS/succinate/CoA complex is displayed in red. Succinate and CoA are displayed as lines with yellow carbon atoms, blue nitrogen atoms, red oxygen atoms and orange phosphorus atoms.**

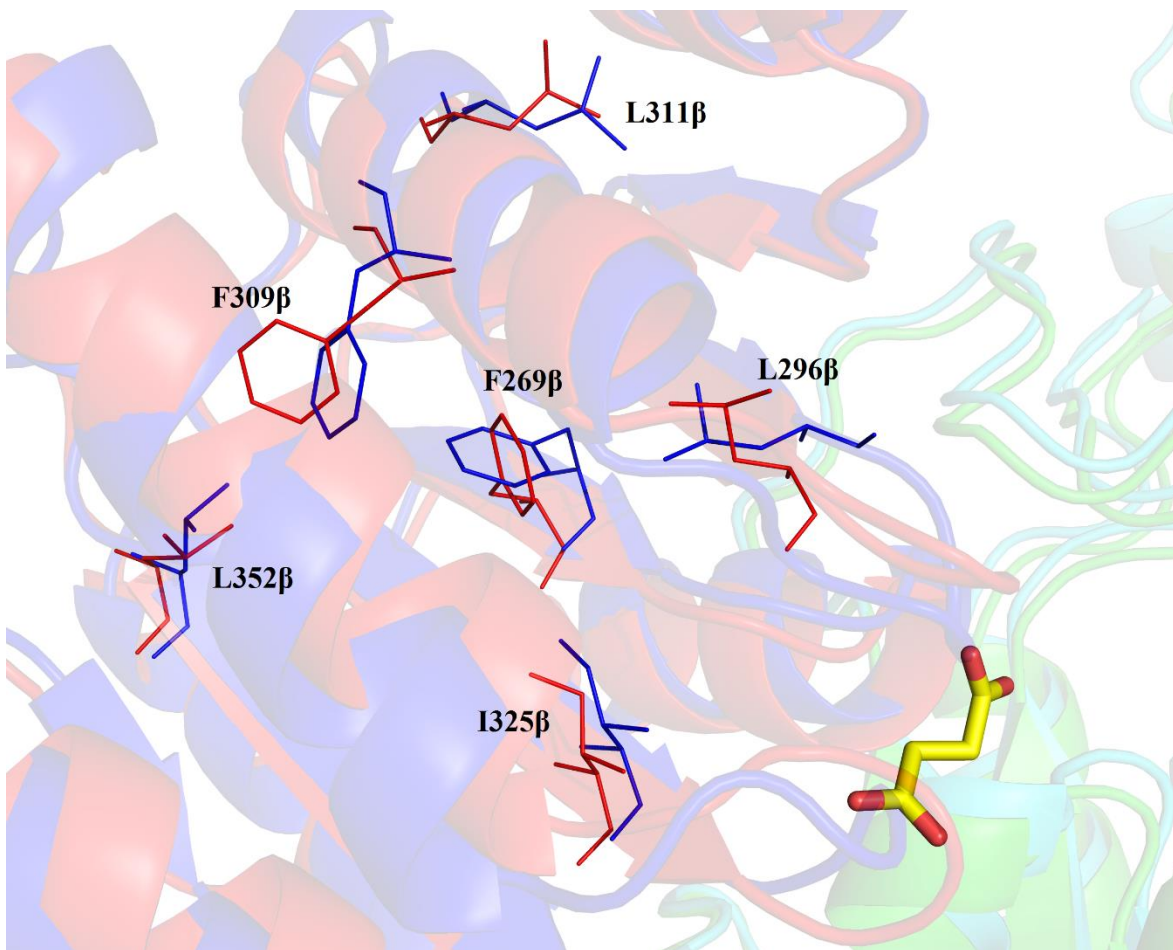


**Figure 4.6** Superposition of the succinate-binding domains of the GTPSCS/succinate/CoA complex and the GTPSCS/CoA complex. The superposition was based on 146  $C\alpha$  atoms with a r.m.s.d. of 1.35 Å. The C-terminal domain of GTPSCS/CoA complex is displayed in blue and that of the GTPSCS/succinate/CoA complex is displayed in red. The side chains of the hydrophobic residues are shown by lines. Succinate from the GTPSCS/succinate/CoA complex is shown in sticks with yellow carbon atoms and red oxygen atoms.

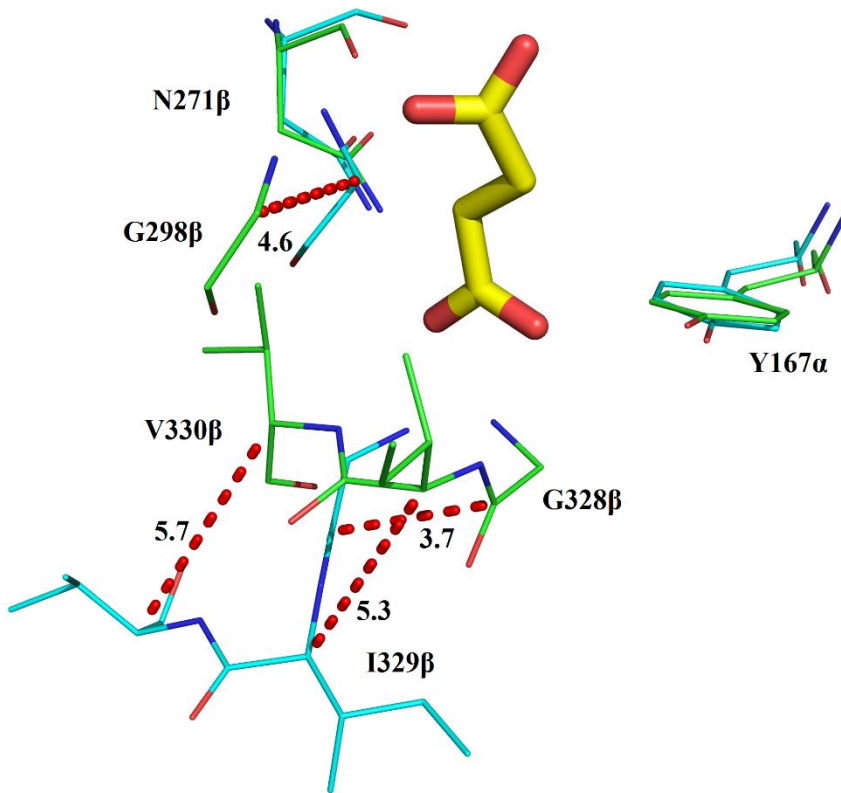


**Figure 4.7 Superposition of the succinate-binding sites of the GTPSCS/succinate/CoA complex and the GTPSCS/CoA complex. Protein residues are displayed by lines. Carbon atoms of the GTPSCS/succinate/CoA complex are displayed in green and that of the GTPSCS/CoA complex are displayed in cyan. In both structures, nitrogen atoms are blue, oxygen atoms are red. Succinate is displayed as sticks with yellow carbon atoms. The red dashed lines indicates the distance between succinate-binding site residues of the two structures.**



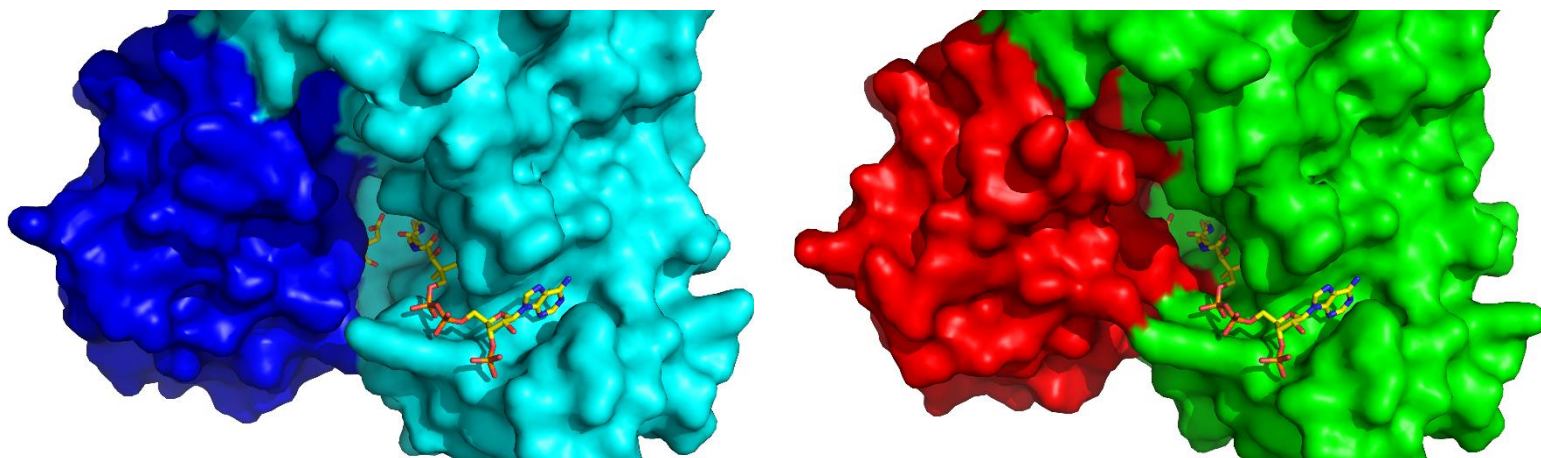


**Figure 4.8 Surface representations of the GTPSCS in complex with CoA (left) and the GTPSCS in complex with succinate and CoA (right). The solvent/protein contact surface is shown. The ligands succinate and CoA from the GTPSCS/succinate/CoA complex are shown as sticks in both structures (succinate and CoA were merged in to the surface structure of GTPSCS/CoA complex). The C-terminal domain of the GTPSCS/CoA complex is displayed in blue and that of the GTPSCS/succinate/CoA complex is displayed in red. For the ligands, carbon atoms are yellow, nitrogen atoms are blue, oxygen atoms are red, phosphorus atoms are orange.**

### ***4.3.2 The magnesium ion stabilizing succinate-bound GTPSCS***

Magnesium ions have been proposed to be a critical for the catalytic reaction<sup>4</sup>, and the structure of the GTPSCS/succinate/CoA complex shows why they are essential for succinate binding. My initial succinate-bound structure was crystallized using magnesium formate, PEG3350 and Hepes buffer (pH 7.0). From the  $F_o-F_c$  map in the X-ray diffraction data, electron density was seen between succinate and the active site residue His 259 $\alpha$ , even though the inorganic phosphate had already been fit into the model. It was impossible to put water molecules into the electron density, because the distances between water molecules were unrealistically small. Therefore, a metal ion was thought to be located between succinate and inorganic phosphate. A magnesium ion was selected, not only because magnesium formate was used in the crystallization, but also because this metal ion has an important role in the catalytic reaction. Surprisingly, the magnesium ion had octahedral coordination with one oxygen of inorganic phosphate, four water molecules and one oxygen of succinate. The positively charged magnesium ion plays an important biological role in stabilizing the negatively charged inorganic phosphate and succinate. In addition, this magnesium ion is postulated to serve the same role when the active site residue histidine in SCS is phosphorylated.

In order to support the idea that the magnesium ion is critical for succinate to bind to GTPSCS, two different crystals were grown using ammonium succinate, PEG 3350 and Hepes buffer (pH 7.0). Magnesium chloride was added to only one of the protein solutions. X-ray diffraction results showed that succinate only bound to GTPSCS when magnesium ions were present.

The succinate complex structure grown from ammonium succinate shows the same magnesium-binding site. The magnesium ion exists between the active site residue His 259 $\alpha$  and

succinate, forming an octahedral coordination with one oxygen of inorganic phosphate, four water molecules and one oxygen of succinate (Figure 4.9). The four water molecules play a role in the water-mediated interactions between residues Glu 105 $\alpha$ , Asn 131 $\alpha$ , Asn 271 $\beta$ , Asp 295 $\beta$  of GTPSCS and the magnesium ion. An alignment of 1000 sequences using Blast (NCBI) <sup>52</sup> shows that residues Glu 105 $\alpha$ , Asn 131 $\alpha$ , Asn 271 $\beta$ , Asp 295 $\beta$  (pig GTPSCS-numbering) are highly conserved among different species. This result indicates that the magnesium ion is indeed an essential factor for succinate to bind to SCS.

#### ***4.3.3 Analysis of succinate-binding sites of GTPSCS and ATPSCS***

According to the sequence alignments in Figure 1.4, the residues of the succinate-binding site in GTPSCS are slightly different from those of ATPSCS. Gly-Gly-Ile-Val in GTPSCS are replaced by Gly-Gly-Ile-Met in ATPSCS. An alignment of 100 sequences using Blast (NCBI) <sup>52</sup> shows that residues Gly 327 $\beta$ , Gly 328 $\beta$ , Ile 329 $\beta$  and Met 330 $\beta$  (human ATPSCS-numbering) are highly conserved among ATPSCSs. Although succinate interacts with Gly 328 $\beta$ , Ile 329 $\beta$  and Val 330 $\beta$  in GTPSCS, the interactions are with the amide groups of these residues. Val 330 $\beta$  in GTPSCS and Met 330 $\beta$  in ATPSCS are hydrophobic residues, and Tyr 167 $\alpha$ , Asn 271 $\beta$  and Gly 298 $\beta$  are conserved between GTPSCS and ATPSCS. Therefore, the succinate-binding site of ATPSCS should be Gly-Gly-Ile-Met. This single residue difference might lead to the different binding affinities of GTPSCS and ATPSCS for succinate observed by Johnson *et al* <sup>10</sup>.

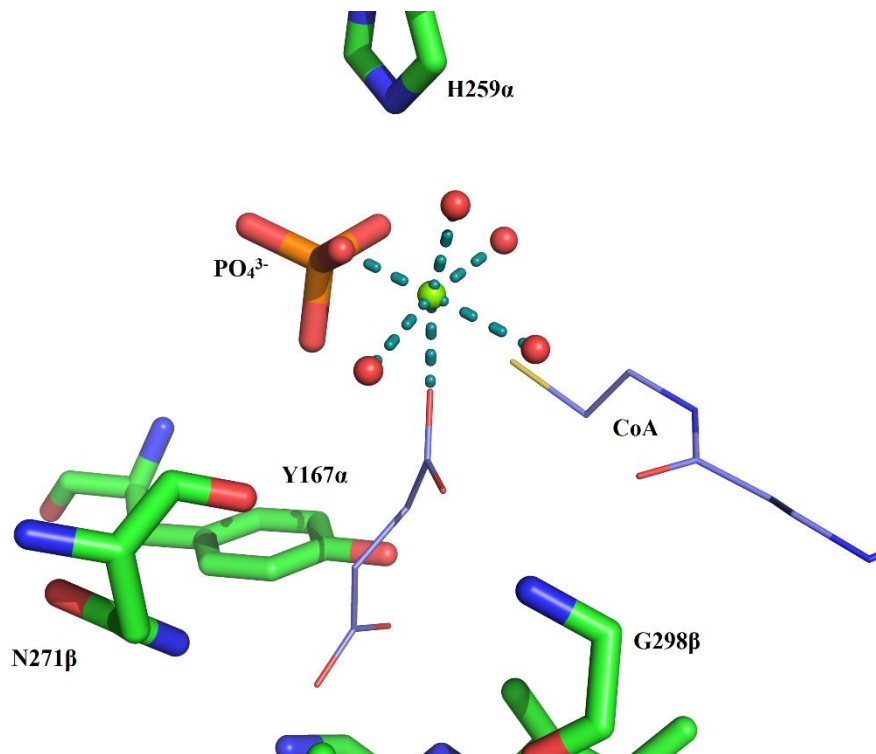


**Figure 4.9 Interactions of the magnesium ion with inorganic phosphate, water molecules and succinate in the GTPSCS/succinate/CoA complex. The interactions are indicated by deep teal dashed lines. Water molecules are red represented by spheres, and the magnesium ion is represented by a light green sphere. Carbon atoms are colored green for residues and light blue for succinate and CoA. Nitrogen atoms are blue, oxygen atoms are red, phosphorus atom is orange and sulfur atom is gold.**

#### ***4.3.4 Comparison of the structures of succinate-bound GTPSCS with citrate-bound hACLY***

The citrate binding site of hACLY was used to predict the succinate-binding site of GTPSCS. However, slight differences between the predicted and observed interactions of succinate were observed. Superposition of the succinate-binding domain of GTPSCS/succinate/CoA complex with the citrate-binding domain of citrate-bound ACLY (PDB code 3MWD) gives a r.m.s.d. 1.49 Å based on 117 C $\alpha$  atoms. The superposition shows a very similar localization of succinate and citrate in each protein (Figure 4.10). The succinate-binding site of GTPSCS is located in almost the same position as predicted, except for the orientation of the non-reactive carboxyl group of succinate. This non-reactive carboxyl group is rotated more than 45 degrees when compared with the prediction. Because of this conformational change, the non-reactive carboxyl group of succinate interacts with the amide groups of Gly 328 $\beta$ , Ile 329 $\beta$  and Val 330 $\beta$  instead of only Gly 328 $\beta$  and Val 330 $\beta$ . Surprisingly, the residue Gly 298 $\beta$  in GTPSCS superposes well with Gly 309 in ACLY. In GTPSCS, Gly 298 $\beta$  is the only residue directly interacting with the reactive carboxyl group of succinate. But in ACLY, Gly 309 stabilizes the hydroxyl group of citrate. There is no indication that Gly 298 $\beta$  in GTPSCS would form an interaction with CoA even though a relatively short distance ( $\sim 3.5$  Å) is observed between CoA and Gly 298 $\beta$ . Therefore, Gly 298 $\beta$  might only be a residue transiently stabilizing the reactive carboxyl group of succinate before succinate attacks the phosphohistidine.

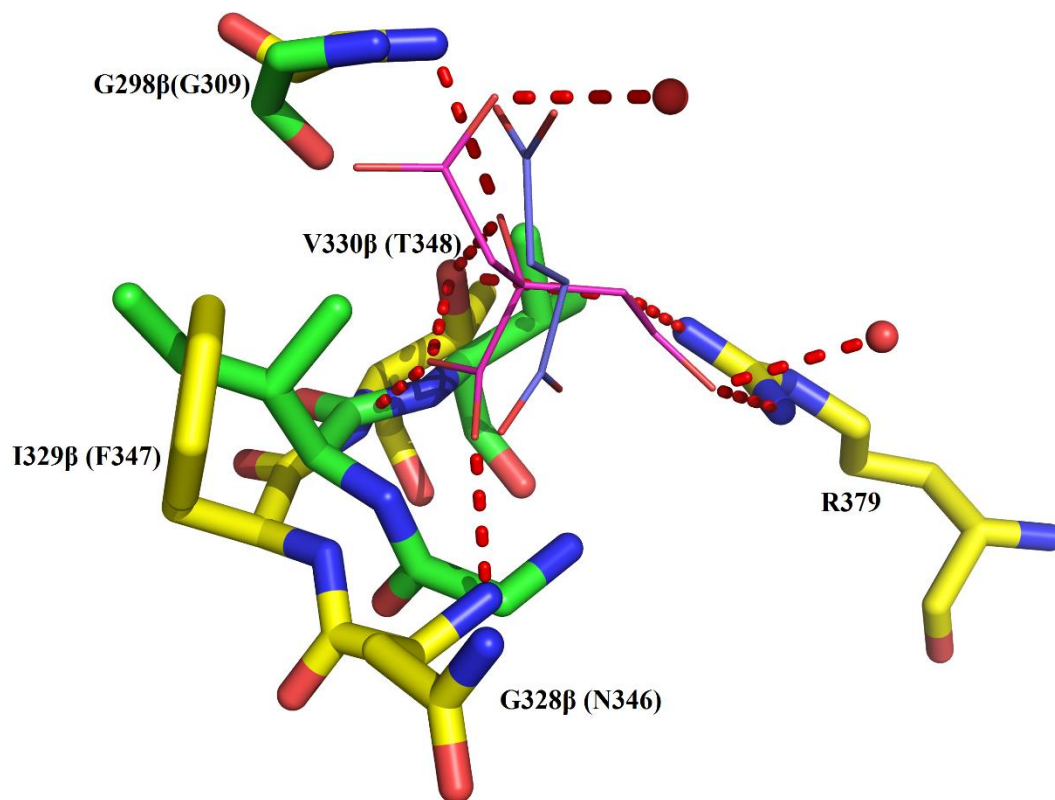


**Figure 4.10 Superposition of the succinate-binding domain of succinate-bound GTPSCS with the citrate-binding domain of citrate-bound ACLY (PDB code 3MWD). Protein residues are shown as sticks and ligands are shown as lines. GTPSCS has green carbon atoms and ACLY has yellow carbon atoms. Succinate has light blue carbon atoms and citrate has magenta carbon atoms. Residue labels are shown outside the parentheses for GTPSCS, and inside the parentheses for ACLY. Nitrogen atoms are colored blue, oxygen atoms are colored red. The red spheres represent water molecules in the ACLY structure. Red dashed lines are hydrogen bonds between citrate and ACLY or water molecules.**

#### 4.4 Verification of the proposed catalytic mechanism based on analysis of the structure

Comparison of the structure of GTPSCS/succinate/CoA complex with phosphorylated GTPSCS can give a better understanding of the proposed catalytic mechanism. Superposition of the C-terminal domain of the  $\alpha$ -subunit of the succinate-bound structure with that of phosphorylated GTPSCS (PDB code 2FP4) gives a r.m.s.d. 0.39 Å based on 174 C $\alpha$  atoms. This high structure similarity between two  $\alpha$ -subunits indicates a similar position of active site histidine residues existed in both structures. Therefore, the phosphorylated active site residue His 259 $\alpha$  from the structure of phosphorylated GTPSCS can be merged with the structure of GTPSCS/succinate/CoA complex (Figure 4.11). This helps in analysis of the proposed second step in the catalytic reaction. The terminal oxygen atoms of the reactive carboxyl group of succinate are 3.6 Å and 5.5 Å from the phosphorus atom of phosphorylated His 259 $\alpha$ . It is likely that one of the oxygen atoms in the reactive carboxyl group would maintain the interactions with the magnesium ion, and the other oxygen atom would approach the phosphorylated His 259 $\alpha$  to attack the phosphorus atom. However, the non-reactive carboxyl group of succinate would still interact with GTPSCS, so this requires that the reactive carboxyl group rotate. In Figure 4.11, the reactive carboxyl group of succinate has been rotated to a position close to the phosphorylated His 259 $\alpha$  (~3.8 Å from one terminal oxygen atom of succinate to the phosphorus atom), while the other terminal oxygen atom is still stabilized by the magnesium ion. The discovery of the succinate-binding site of GTPSCS does support the view that the succinyl-phosphate complex can be formed in the second step of the catalytic reaction.

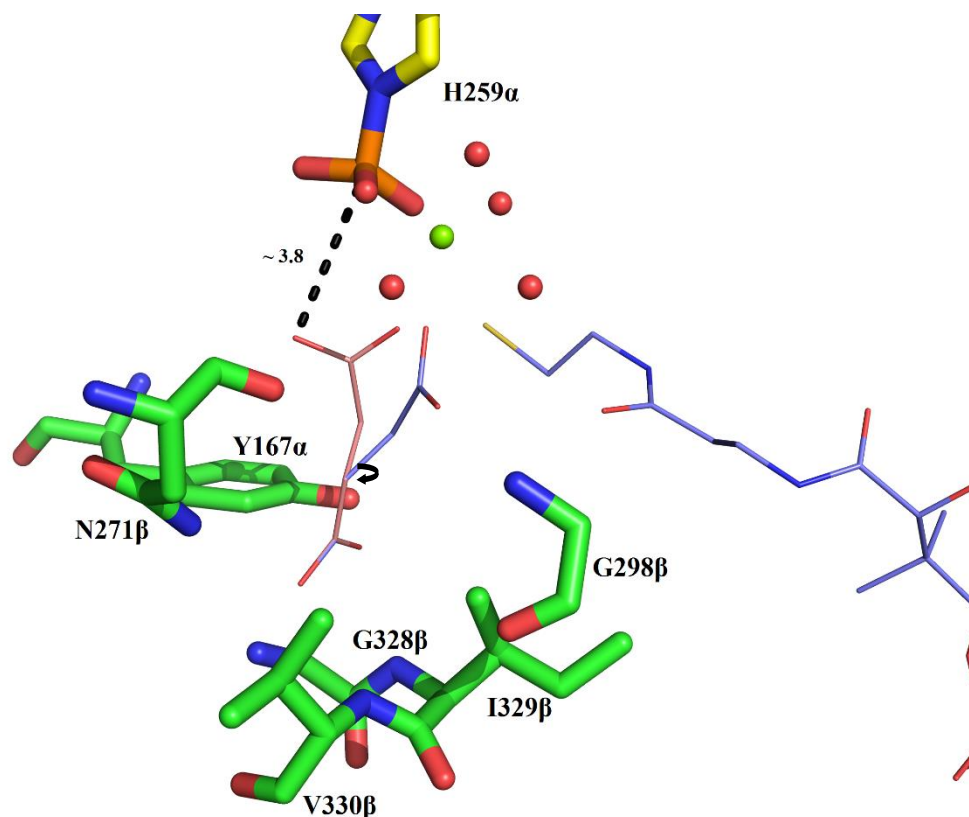


**Figure 4.11 Superposition of the C-terminal domains from  $\alpha$ -subunits of the GTPSCS/succinate/CoA complex and phosphorylated GTPSCS (PDB code 2FP4). Phosphorylated His 259 $\alpha$  (carbon atoms are in yellow) from 2FP4 has been merged with the structure of GTPSCS/succinate/CoA complex. Two orientations of succinate are shown in the figure. The one with light blue carbon atoms is from the succinate complex, while the one with pink carbon atoms was obtained by rotating about the carbon-carbon bonds of the original succinate. The carbon atoms of residues are green. Nitrogen atoms are blue, oxygen atoms are red, phosphorus atoms are orange and the sulfur atom is gold. The red spheres represent water molecules and green sphere is the magnesium ion. Black dashed lines indicate the distance between the phosphorus atom of phosphorylated His 259 $\alpha$  and the terminal oxygen of the reactive carboxyl group on succinate.**



#### 4.5 The formate inhibition on GTPSCS

The crystal of succinate-bound GTPSCS that grew from magnesium formate showed partial occupancy of succinate and disorder of some parts of the structure. Enzyme kinetic assays were done in order to know whether formate competes with succinate to bind to GTPSCS and inhibits GTPSCS. A competitive inhibitor will compete with the substrate to bind to enzyme, resulting in an increasing value of  $K_m$  for the substrate but no change for the  $V_{max}$ . The overlap of  $V_{max}$  s at the 95% confidence interval indicates the same maximum velocity at three different concentrations of formate. However, the apparent  $K_m$ s do not overlap. The  $K_m$  values increase as the concentration of formate increases. The increasing values of  $K_m$  and constant value of  $V_{max}$  at 0 mM, 100 mM and 200 mM formate indicate formate is a competitive inhibitor. In order to know the inhibition constant  $K_i$ , a plot of apparent  $K_m$  as a function of formate concentration was drawn. A line of best fit cannot go through all three points, and leads to a positive x-intercept value. Copeland suggests that the concentration of the inhibitor should be chosen to have 30% to 75% inhibition of the enzyme at the substrate concentration equal to  $K_m$ . This leads to significant inhibition while allowing accurate measurement of the initial velocity<sup>63</sup>. For the kinetic assay, 0 mM, 100 mM and 200 mM have been selected as the concentrations of formate to study the inhibition, because 140 mM magnesium formate had been used to grow the crystal of the succinate-bound GTPSCS. Therefore, formate concentrations of 100 mM and 200 mM were selected in order to support the idea that the competition between formate and succinate led to the unsatisfactory structure. In the assay, when the succinate concentration was 0.39 mM, the velocities were 1.9  $\mu\text{mol}/\text{min}$ , 0.6  $\mu\text{mol}/\text{min}$  and 0.3  $\mu\text{mol}/\text{min}$  at 0 mM, 100 mM and 200 mM formate, respectively. 100 mM formate yields almost 30% inhibition, 200 mM has far more

inhibition on the enzyme, suggesting that too high an inhibitor concentration was selected. This is probably the reason for not being able to obtain a positive value for the inhibition constant  $K_i$ .

## Chapter Five: Conclusions and future studies

### 5.1 Conclusions

The main goal of this research was to discover the succinate-binding site of SCS in order to further understand the proposed catalytic mechanism. To discover the substrate-binding site, co-crystallization of pure SCS with succinate was required. GTPSCS of high purity was obtained through three different steps of column purification, using Ni-NTA affinity column, Superdex-200 pg column and Hitrap Blue High Performance affinity column. SDS-PAGE gels, enzyme assays and 280 nm absorbance were used to detect the purity, activity and existence of GTPSCS. The CoA-binding site of GTPSCS was determined first and this model was used to solve the structure of GTPSCS in complex with succinate and CoA. A crystal of CoA-bound GTPSCS diffracted to 2.1 Å, and this structure shows that the CoA-binding site is located in the N-terminal domain of the  $\alpha$ -subunit. Vapour diffusion using hanging drops was used to co-crystallize GTPSCS with succinate and CoA. Two different salts, magnesium formate and ammonium succinate, were used to obtain crystals of the complex. Crystals of high quality diffracted to 1.95 Å and 2.2 Å for the magnesium formate and ammonium succinate crystals, respectively. Both conditions showed the same succinate-binding site, located in the C-terminal domain of the  $\beta$ -subunit. However, the crystal grown from magnesium formate did not show good electron density in the  $F_o-F_c$  map for succinate, suggesting partial occupancy of succinate in the GTPSCS. The discontinuous electron density in some parts of the C-terminal domain of the  $\beta$ -subunit could not be fitted with a model, indicating disorder in these parts. In order to know whether formate competes with succinate and inhibits GTPSCS, enzyme kinetic assays have been conducted, and the results showed that formate is a competitive inhibitor for GTPSCS. The other crystal grown for ammonium succinate showed relatively good electron density in the  $F_o-F_c$

map for succinate (Figure 3.14), so this structure was used to determine the succinate-binding site of GTPSCS. The crystals grown from two different salts both revealed a magnesium ion forming octahedral coordination with one oxygen of inorganic phosphate, four water molecules and one oxygen of succinate. The GTPSCS/succinate/CoA structure shows that the succinate-binding site is close to the active site residue His 259 $\alpha$  and CoA. This discovery supports the idea that succinyl-phosphate will be formed in the second step of the catalytic reaction, and its formation is followed by attack by the free thiol of CoA in order to produce succinyl-CoA.

## 5.2 Future studies

Although the succinate-binding site has been revealed and a short distance has been observed between succinate and His 259 $\alpha$ , whether succinyl-phosphate is formed in the second step of the reaction is still not known. Further experiments co-crystallizing GTPSCS in complex with succinate and GTP are required to determine whether the enzyme-bound succinyl-phosphate intermediate exists. The crystallization conditions for growing succinate-bound GTPSCS are already known from my study, therefore, the crystals of GTPSCS in complex with succinate and GTP will be grown using similar conditions as were used for growing the crystals of GTPSCS/succinate/CoA complex. The only difference is adding GTP to the protein solution instead of using CoA. The crystal of succinate- and GTP-bound GTPSCS could reveal succinyl-phosphate bound to the enzyme, proving that succinyl-phosphate is an intermediate in the reaction mechanism.

In addition, my research offers insight on how to stabilize the phosphohistidine loop in ACLY. Residues Thr 750 to Gln 767, which form the phosphohistidine loop in ACLY, were not modelled in the structure of truncated hACLY (PDB code 3MWD). However, superposition of

GTPSCS with truncated hACLY shows where the phosphohistidine loop would be expected to lie in ACLY (Figure 5.1). It was proposed that disulfide bonds between cysteine residues prevented the phosphohistidine loop of ACLY to adopt a stable conformation, so it was disordered in the crystal structure<sup>48</sup>. We propose that a magnesium ion, which stabilizes succinate and the phosphate in GTPSCS, would stabilize citrate and the phosphohistidine loop in ACLY. The structural superposition in Figure 5.1 shows that the positively charged magnesium ion can stabilize both negatively charged inorganic phosphate and citrate, and the inorganic phosphate stabilizes the active site residue histidine. This phosphate-mediate interaction between magnesium ion and the active site histidine would probably stabilize the phosphohistidine loop in ACLY. Therefore, future work includes crystallizing the N-terminal portion of a mutant form of hACLY, in which the cysteine residues have been mutated to prevent formation of the disulfide bonds, in the presence of citrate and magnesium ions.

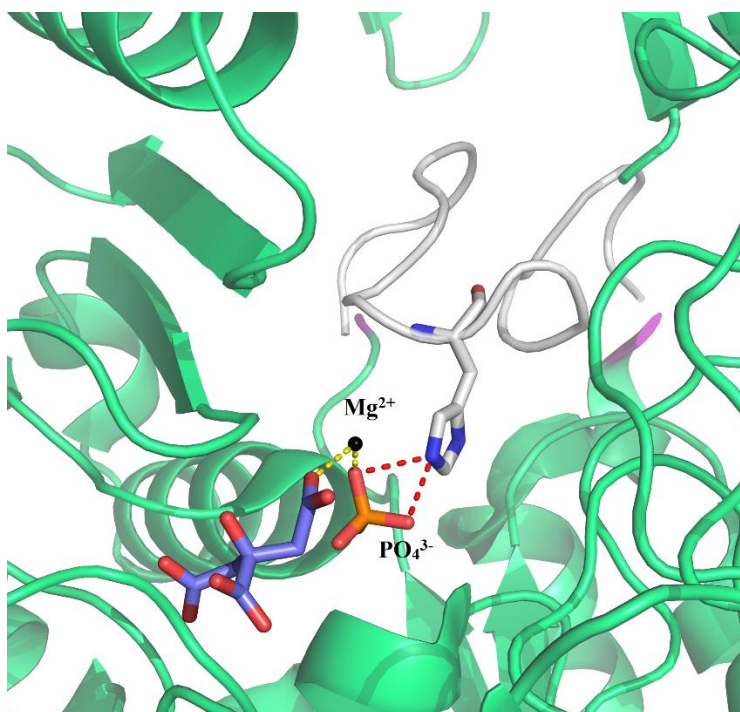


**Figure 5.1** The proposed site of phosphohistidine loop in ACLY. The succinate-binding domain of the GTPSCS/succinate/CoA complex and the citrate-binding domain of hACLY (PDB code 3MWD) are superposed. The hACLY is displayed as ribbons in light green. The missing phosphohistidine loop in hACLY is substituted by the phosphohistidine loop (A251 $\alpha$ -K268 $\alpha$ ) from the GTPSCS/succinate/CoA complex. The phosphohistidine loop (A251 $\alpha$ -K268 $\alpha$ ) in GTPSCS/succinate/CoA complex is drawn in white and His 259 $\alpha$  is displayed as sticks. The missing phosphohistidine loop in hACLY is from Thr 750 to Gln 767 (highlighted in purple). Carbon atoms of the citrate are in light blue. Nitrogen atoms are blue, phosphorus atom is orange and oxygen atoms are red. Black sphere represents the magnesium ion and the inorganic phosphate displays as sticks both from the GTPSCS/succinate/CoA complex. Yellow dashed lines indicate the interactions between magnesium ion and citrate or phosphate. Red dashed lines indicate the interactions between phosphate and active site histidine at the proposed site.

## References

1. Sanadi, D. R., Gibson, D. M., Ayengar, P., and Jacob, M. (1956) Alpha-ketoglutaric dehydrogenase. V. guanosine diphosphate in coupled phosphorylation. *J. Biol. Chem.* 218, 505-520.
2. Ottaway, J. H., McClellan, J. A., and Saunderson, C. L. (1981) Succinic thiokinase and metabolic control. *Int. J. Biochem.* 13, 401-410.
3. Bishop, D. F., Tchaikovskii, V., Hoffbrand, A. V., Fraser, M. E., and Margolis, S. (2012) X-linked sideroblastic anemia due to carboxyl-terminal ALAS2 mutations that cause loss of binding to the beta-subunit of succinyl-CoA synthetase (SUCLA2). *J. Biol. Chem.* 287, 28943-28955.
4. Robinson, J. L., Benson, R. W., and Boyer, P. D. (1969) Dephosphorylation of succinyl coenzyme A synthetase as related to enzyme specificity and catalytic intermediates. *Biochemistry.* 8, 2503-2508.
5. Cha, S., and Parks, R. E., Jr. (1964) Succinic thiokinase. ii. kinetic studies: Initial velocity, product inhibition, and effect of arsenate. *J. Biol. Chem.* 239, 1968-1977.
6. Leitzmann, C., Wu, J. Y., and Boyer, P. D. (1970) Subunits, composition, and related properties of succinyl coenzyme A synthetase. *Biochemistry (N. Y.).* 9, 2338-2346.
7. Buck, D., Spencer, M. E., and Guest, J. R. (1986) Cloning and expression of the succinyl-CoA synthetase genes of escherichia coli K12. *J. Gen. Microbiol.* 132, 1753-1762.
8. Joyce, M. A., Hayakawa, K., Wolodko, W. T., and Fraser, M. E. (2012) Biochemical and structural characterization of the GTP-preferring succinyl-CoA synthetase from thermus aquaticus. *Acta Crystallogr. D Biol. Crystallogr.* 68, 751-762.
9. Kaufman, S., and Alivisatos, S. G. (1955) Purification and properties of the phosphorylating enzyme from spinach. *J. Biol. Chem.* 216, 141-152.
10. Johnson, J. D., Muhonen, W. W., and Lambeth, D. O. (1998) Characterization of the ATP- and GTP-specific succinyl-CoA synthetases in pigeon. the enzymes incorporate the same alpha-subunit. *J. Biol. Chem.* 273, 27573-27579.
11. Baccanari, D. P., and Cha, S. (1973) Succinate thiokinase. VI. multiple interconvertible forms of the enzyme. *J. Biol. Chem.* 248, 15-24.
12. Lambeth, D. O., Tews, K. N., Adkins, S., Frohlich, D., and Milavetz, B. I. (2004) Expression of two succinyl-CoA synthetases with different nucleotide specificities in mammalian tissues. *J. Biol. Chem.* 279, 36621-36624.

13. Wolodko, W. T., James, M. N., and Bridger, W. A. (1984) Crystallization of succinyl-CoA synthetase from escherichia coli. *J. Biol. Chem.* 259, 5316-5320.
14. Henning, W. D., Upton, C., McFadden, G., Majumdar, R., and Bridger, W. A. (1988) Cloning and sequencing of the cytoplasmic precursor to the alpha subunit of rat liver mitochondrial succinyl-CoA synthetase. *Proc. Natl. Acad. Sci. U. S. A.* 85, 1432-1436.
15. Bailey, D. L., Wolodko, W. T., and Bridger, W. A. (1993) Cloning, characterization, and expression of the beta subunit of pig heart succinyl-CoA synthetase. *Protein Sci.* 2, 1255-1262.
16. Furuyama, K., and Sassa, S. (2000) Interaction between succinyl CoA synthetase and the heme-biosynthetic enzyme ALAS-E is disrupted in sideroblastic anemia. *J. Clin. Invest.* 105, 757-764.
17. Elpeleg, O., Miller, C., Hershkovitz, E., Bitner-Glindzicz, M., Bondi-Rubinstein, G., Rahman, S., Pagnamenta, A., Eshhar, S., and Saada, A. (2005) Deficiency of the ADP-forming succinyl-CoA synthase activity is associated with encephalomyopathy and mitochondrial DNA depletion. *The American Journal of Human Genetics.* 76, 1081-1086.
18. Carrozzo, R., Dionisi-Vici, C., Steuerwald, U., Luciola, S., Deodato, F., Di Giandomenico, S., Bertini, E., Franke, B., Kluijtmans, L. A., Meschini, M. C., Rizzo, C., Piemonte, F., Rodenburg, R., Santer, R., Santorelli, F. M., van Rooij, A., Vermunt-de Koning, D., Morava, E., and Wevers, R. A. (2007) SUCLA2 mutations are associated with mild methylmalonic aciduria, leigh-like encephalomyopathy, dystonia and deafness. *Brain.* 130, 862-874.
19. Navarro-Sastre, A., Montoya, J., Unceta, M., Martinez, M. J., Briones, P., Ribes, A., Tort, F., Garcia-Villoria, J., Pons, M. R., Nascimento, A., Colomer, J., Campistol, J., Yoldi, M. E., and López-Gallardo, E. (2012) Mitochondrial DNA depletion syndrome: New descriptions and the use of citrate synthase as a helpful tool to better characterise the patients. *Mol. Genet. Metab.* 107, 409-415.
20. Jaber, E., Chitsazian, F., Ali Shahidi, G., Rohani, M., Sina, F., Safari, I., Malakouti Nejad, M., Houshmand, M., Klotzle, B., and Elahi, E. (2013) The novel mutation p.Asp251Asn in the beta-subunit of succinate-CoA ligase causes encephalomyopathy and elevated succinylcarnitine. *J. Hum. Genet.* 58, 526-530.
21. Ostergaard, E., Hansen, F. J., Sorensen, N., Duno, M., Vissing, J., Larsen, P. L., Faeroe, O., Thorgrímsson, S., Wibrand, F., Christensen, E., and Schwartz, M. (2007) Mitochondrial encephalomyopathy with elevated methylmalonic acid is caused by SUCLA2 mutations. *Brain.* 130, 853-861.
22. Morava, E., Steuerwald, U., Carrozzo, R., Kluijtmans, L. A., Joensen, F., Santer, R., Dionisi-Vici, C., and Wevers, R. A. (2009) Dystonia and deafness due to SUCLA2 defect; clinical course and biochemical markers in 16 children. *Mitochondrion.* 9, 438-442.



23. Nogueira, C., Meschini, M. C., Nesti, C., Garcia, P., Diogo, L., Valongo, C., Costa, R., Videira, A., Vilarinho, L., and Santorelli, F. M. (2014) A novel SUCLA2 mutation in a portuguese child associated with "mild" methylmalonic aciduria. *J. Child Neurol.*
24. Lamperti, C., Fang, M., Invernizzi, F., Liu, X., Wang, H., Zhang, Q., Carrara, F., Moroni, I., Zeviani, M., Zhang, J., and Ghezzi, D. (2012) A novel homozygous mutation in SUCLA2 gene identified by exome sequencing. *Mol. Genet. Metab.* 107, 403-408.
25. Ostergaard, E., Christensen, E., Kristensen, E., Mogensen, B., Duno, M., Shoubridge, E. A., and Wibrand, F. (2007) Deficiency of the a subunit of Succinate–Coenzyme A ligase causes fatal infantile lactic acidosis with mitochondrial DNA depletion. *The American Journal of Human Genetics.* 81, 383-387.
26. Ostergaard, E., Schwartz, M., Batbayli, M., Christensen, E., Hjalmarson, O., Kollberg, G., and Holme, E. (2010) A novel missense mutation in SUCLG1 associated with mitochondrial DNA depletion, encephalomyopathic form, with methylmalonic aciduria. *Eur. J. Pediatr.* 169, 201-205.
27. Rivera, H., Merinero, B., Martinez-Pardo, M., Arroyo, I., Ruiz-Sala, P., Bornstein, B., Serra-Suhe, C., Gallardo, E., Marti, R., Moran, M. J., Ugalde, C., Perez-Jurado, L. A., Andreu, A. L., Garesse, R., Ugarte, M., Arenas, J., and Martin, M. A. (2010) Marked mitochondrial DNA depletion associated with a novel SUCLG1 gene mutation resulting in lethal neonatal acidosis, multi-organ failure, and interrupted aortic arch. *Mitochondrion.* 10, 362-368.
28. Randolph, L. M., Jackson, H. A., Wang, J., Shimada, H., Sanchez-Lara, P. A., Wong, D. A., Wong, L. J., and Boles, R. G. (2011) Fatal infantile lactic acidosis and a novel homozygous mutation in the SUCLG1 gene: A mitochondrial DNA depletion disorder. *Mol. Genet. Metab.* 102, 149-152.
29. Sakamoto, O., Ohura, T., Murayama, K., Ohtake, A., Harashima, H., Abukawa, D., Takeyama, J., Haginoya, K., Miyabayashi, S., and Kure, S. (2011) Neonatal lactic acidosis with methylmalonic aciduria due to novel mutations in the SUCLG1 gene. *Pediatr. Int.* 53, 921-925.
30. Valayannopoulos, V., Haudry, C., Serre, V., Barth, M., Boddaert, N., Arnoux, J. B., Cormier-Daire, V., Rio, M., Rabier, D., Vassault, A., Munnich, A., Bonnefont, J. P., de Lonlay, P., Rotig, A., and Lebre, A. S. (2010) New SUCLG1 patients expanding the phenotypic spectrum of this rare cause of mild methylmalonic aciduria. *Mitochondrion.* 10, 335-341.
31. Honzik, T., Tesarova, M., Magner, M., Mayr, J., Jesina, P., Vesela, K., Wenchich, L., Szentivanyi, K., Hansikova, H., Sperl, W., and Zeman, J. (2012) Neonatal onset of mitochondrial disorders in 129 patients: Clinical and laboratory characteristics and a new approach to diagnosis. *J. Inherit. Metab. Dis.* 35, 749-759.

32. Rouzier, C., Le Guedard-Mereuze, S., Fragaki, K., Serre, V., Miro, J., Tuffery-Giraud, S., Chaussonot, A., Bannwarth, S., Caruba, C., Ostergaard, E., Pellissier, J. F., Richelme, C., Espil, C., Chabrol, B., and Paquis-Flucklinger, V. (2010) The severity of phenotype linked to SUCLG1 mutations could be correlated with residual amount of SUCLG1 protein. *J. Med. Genet.* 47, 670-676.
33. Schlattner, U., Tokarska-Schlattner, M., Ramirez, S., Tyurina, Y. Y., Amoscato, A. A., Mohammadyani, D., Huang, Z., Jiang, J., Yanamala, N., Seffouh, A., Boissan, M., Epand, R. F., Epand, R. M., Klein-Seetharaman, J., Lacombe, M. L., and Kagan, V. E. (2013) Dual function of mitochondrial Nm23-H4 protein in phosphotransfer and intermembrane lipid transfer: A cardiolipin-dependent switch. *J. Biol. Chem.* 288, 111-121.
34. Stark, R., and Kibbey, R. G. (2014) The mitochondrial isoform of phosphoenolpyruvate carboxykinase (PEPCK-M) and glucose homeostasis: Has it been overlooked? *Biochim. Biophys. Acta.* 1840, 1313-1330.
35. Kibbey, R. G., Pongratz, R. L., Romanelli, A. J., Wollheim, C. B., Cline, G. W., and Shulman, G. I. (2007) Mitochondrial GTP regulates glucose-stimulated insulin secretion. *Cell Metabolism.* 5, 253-264.
36. Wolodko, W. T., Fraser, M. E., James, M. N., and Bridger, W. A. (1994) The crystal structure of succinyl-CoA synthetase from escherichia coli at 2.5-Å resolution. *J. Biol. Chem.* 269, 10883-10890.
37. Cha, S., Cha, C. J., and Parks, R. E., Jr. (1965) Succinic thiokinase. 3. the occurrence of a nonphosphorylated high energy intermediate of the enzyme. *J. Biol. Chem.* 240, 3700-3702.
38. Kaufman, S., Gilvarg, C., Cori, O., and Ochoa, S. (1953) Enzymatic oxidation of alpha-ketoglutarate and coupled phosphorylation. *J. Biol. Chem.* 203, 869-888.
39. Kreil, G., and Boyer, P. D. (1964) Detection of bound phosphohistidine in E. coli succinate thiokinase. *Biochem. Biophys. Res. Commun.* 16, 551-555.
40. Pearson, P. H., and Bridger, W. A. (1975) Catalysis of a step of the overall reaction by the alpha subunit of escherichia coli succinyl coenzyme A synthetase. *J. Biol. Chem.* 250, 8524-8529.
41. Bridger, W. A. (1971) Evidence for two types of subunits in succinyl coenzyme A synthetase. *Biochem. Biophys. Res. Commun.* 42, 948-954.
42. Buck, D., Spencer, M. E., and Guest, J. R. (1985) Primary structure of the succinyl-CoA synthetase of escherichia coli. *Biochemistry.* 24, 6245-6252.

43. Wang, T., Jurasek, L., and Bridger, W. A. (1972) Succinyl coenzyme A synthetase of escherichia coli. sequence of a peptide containing the active-site phosphohistidine residue. *Biochemistry*. 11, 2067-2070.
44. Joyce, M. A., Fraser, M. E., James, M. N., Bridger, W. A., and Wolodko, W. T. (2000) ADP-binding site of escherichia coli succinyl-CoA synthetase revealed by x-ray crystallography. *Biochemistry*. 39, 17-25.
45. Fraser, M. E., Hayakawa, K., Hume, M. S., Ryan, D. G., and Brownie, E. R. (2006) Interactions of GTP with the ATP-grasp domain of GTP-specific succinyl-CoA synthetase. *J. Biol. Chem.* 281, 11058-11065.
46. Fraser, M. E., James, M. N., Bridger, W. A., and Wolodko, W. T. (1999) A detailed structural description of escherichia coli succinyl-CoA synthetase. *J. Mol. Biol.* 285, 1633-1653.
47. Nishimura, J. S., and Meister, A. (1965) Evidence for succinyl phosphate as an enzyme-bound intermediate in the reaction catalyzed by succinyl coenzyme A synthetase. *Biochemistry (N. Y.)*. 4, 1457-1462.
48. Sun, T., Hayakawa, K., Bateman, K. S., and Fraser, M. E. (2010) Identification of the citrate-binding site of human ATP-citrate lyase using X-ray crystallography. *J. Biol. Chem.* 285, 27418-27428.
49. Sanchez, L. B., Galperin, M. Y., and Muller, M. (2000) Acetyl-CoA synthetase from the amitochondriate eukaryote giardia lamblia belongs to the newly recognized superfamily of acyl-CoA synthetases (nucleoside diphosphate-forming). *J. Biol. Chem.* 275, 5794-5803.
50. Srere, P. A., and Lipmann, F. (1953) An enzymatic reaction between citrate, adenosine triphosphate and coenzyme A1. *J. Am. Chem. Soc.* 75, 4874-4874.
51. Wells, T. N. (1991) ATP-citrate lyase from rat liver. characterisation of the citryl-enzyme complexes. *European journal of biochemistry / FEBS*. 199, 163-168.
52. Altschul, S. F., Gish, W., Miller, W., Myers, E. W., and Lipman, D. J. (1990) Basic local alignment search tool. *J. Mol. Biol.* 215, 403-410.
53. Joyce, M. A., Fraser, M. E., Brownie, E. R., James, M. N., Bridger, W. A., and Wolodko, W. T. (1999) Probing the nucleotide-binding site of escherichia coli succinyl-CoA synthetase. *Biochemistry*. 38, 7273-7283.
54. Murakami, Y., and Nishimura, J. S. (1974) Porcine heart succinate thiokinase reactivity of sulfhydryl groups, cross-linking and immunochemical properties of the enzyme. *Biochimica et Biophysica Acta (BBA) - Protein Structure*. 336, 252-263.

55. Deng J, Davies D.R, Wisedchaisri G, Wu M, Hol W.G.J, and Mehlin C. (2004) An improved protocol for rapid freezing of protein samples for long-term storage. *Acta Crystallographica Section D*. 60, 203-204.
56. Palmer, J. M., and Wedding, R. T. (1966) Purification and properties of succinyl-CoA synthetase from jerusalem artichoke mitochondria. *Biochimica et Biophysica Acta (BBA) - Enzymology and Biological Oxidation*. 113, 167-174.
57. Battye, T. G. G., Kontogiannis, L., Johnson, O., Powell, H. R., and Leslie, A. G. W. (2011) iMOSFLM: A new graphical interface for diffraction-image processing with MOSFLM. *Acta crystallographica. Section D, Biological crystallography*. 67, 271-281.
58. Collaborative Computational Project, Number 4. (1994) The CCP4 suite: Programs for protein crystallography. *Acta crystallographica. Section D, Biological crystallography*. 50, 760-763.
59. Adams, P. D., Grosse-Kunstleve, R. W., McCoy, A. J., Moriarty, N. W., Oeffner, R., Read, R. J., Richardson, D. C., Richardson, J. S., Terwilliger, T. C., Zwart, P. H., Afonine, P. V., Bunkóczi, G., Chen, V. B., Davis, I. W., Echols, N., Headd, J. J., Hung, L., and Kapral, G. J. (2010) PHENIX: A comprehensive python-based system for macromolecular structure solution. *Acta crystallographica. Section D, Biological crystallography*. 66, 213-221.
60. Emsley, P., and Cowtan, K. (2004) Coot: Model-building tools for molecular graphics. *Acta crystallographica. Section D, Biological crystallography*. 60, 2126-2132.
61. Davis, I. W., Richardson, J. S., Richardson, D. C., Leaver-Fay, A., Chen, V. B., Block, J. N., Kapral, G. J., Wang, X., Murray, L. W., Arendall, 3., W Bryan, and Snoeyink, J. (2007) MolProbity: All-atom contacts and structure validation for proteins and nucleic acids. *Nucleic Acids Res*. 35, W375-W383.
62. Mann, C. J., Hardies, S. C., and Nishimura, J. S. (1989) Site-directed mutagenesis of escherichia coli succinyl-CoA synthetase. beta-Cys325 is a nonessential active site residue. *J. Biol. Chem*. 264, 1457-1460.
63. Copeland, R. A. (2000) *Enzymes: A Practical Introduction to Structure, Mechanism, and Data Analysis*. J. Wiley, New York.